NOTICE

The quality of this microform is heavily dependent upon the quality of the original thesis submitted for microfilming. Every effort has been made to ensure the highest quality of reproduction possible.

If pages are missing, contact the university which granted the degree.

Some pages may have indistinct print especially if the original pages were typed with a poor typewriter ribbon or if the university sent us an inferior photocopy.

Reproduction in full or in part of this microform is governed by the Canadian Copyright Act, R.S.C. 1970, c. C-30, and subsequent amendments.

AVIS

La qualité de cette microforme dépend grandement de la qualité de la thèse soumise au microfilmage. Nous avons tout fait pour assurer une qualité supérieure de reproduction.

S'il manque des pages, veuillez communiquer avec l'université qui a conféré le grade.

La qualité d'impression de certaines pages peut laisser à désirer, surtout si les pages originales ont été dactylographiées à l'aide d'un ruban usé ou si l'université nous a fait parvenir une photocopie de qualité inférieure.

La reproduction, même partielle, de cette microforme est soumise à la Loi canadienne sur le droit d'auteur, SRC 1970, c. C-30, et ses amendements subséquents.

ISBN 0-315-53288-2

Differentially Coherent Trellis Coded Modulation with Subset Dilation

by

Stephen John Spenler, B.A.Sc.

A thesis submitted to the
School of Graduate Studies and Research
in partial fulfilment of the requirements
for the degree

Master of Applied Science

Ottawa-Carleton Institute for Electrical Engineering
Department of Electrical Engineering
Faculty of Engineering
University of Ottawa
July 1989

Abstract

This thesis introduces a new family of coded channel constellations – collectively known as Differentially Coherent Trellis-coded M-M-PSK (DTC-M-M-PSK) – which combine the advantages of Phase Shift Keying (PSK), trellis coding and differential detection. It is of particular interest for mobile and fading channels which have traditionally employed differentially coherent detection and PSK signal constellations to combat the effects of Doppler, shadowing and fading. DTC-M-M-PSK involves a radial expansion of part of the coded signal constellation in a manner which increases the trellis free distance beyond that possible with Ungerboeck coding alone. A number of promising DTC-M-M-PSK codes have been evaluated using analytical techniques. One of these codes has been further characterised for a Gaussian channel using a Monte Carlo simulation package.

Acknowledgements

I would like to thank my two thesis supervisors – Dr. A. Yongacoglu of the University of Ottawa and Dr. D.D. Falconer of Carleton University – for creating an environment in which interesting research could occur. This thesis would not have been completed without their combined support.

I am grateful for the many stimulating discussions – both technical and otherwise – with other faculty and my fellow graduate students in the Digital Communications and Signal Processing Group (Rooms B-408 and B-417). I also want to thank Nick Peereboom for his advice and encouragement. I wish both he and the other graduate students success in their studies.

I would also like to acknowledge the NSERC and TRIO funding which made this research possible. I trust the ideas and results contained in this thesis will be of benefit to other researchers who follow.

Contents

1 Introduction 12

1.1 Thesis Scope 12

1.2 Trellis Coded Modulation 12

1.3 Differential Detection 14

1.4 Differentially Coherent M-M-PSK 15

1.5 Thesis Organization 18

2 Differentially Coherent TC-2M-PSK 19

2.1 Introduction 19

2.2 Trellis Coding for PSK Constellations 20

2.2.1 Coding Gain for TC-(8,4)-16-PSK 29

2.3 Differential Detection 33

2.4 Development of a Noise Model 38

2.4.1 Differential Demodulation 38

2.4.2 Effects of Noise 42

2.5 Performance of Trellis-coded PSK 46

2.6 Limitations of DTC-2M-PSK 50

3 Differentially Coherent Trellis-Coded M-M-PSK 52

3.1 Introduction 52

3.2 Variations on TC-2M-PSK 53

3.3 Rationale for the M-M-PSK Constellation Format 55

3.4 Differential Encoding 60

3.5 DTC-M-M-PSK Noise Model 70

3.5.1 Differential Demodulation 70
3.5.2 Effects of Noise 71
3.6 Modified Viterbi Decoder Trellis Structure 75
3.7 Asymptotic Coding Gain 78
3.7.1 4-state Trellis 80
3.7.2 8-state Trellises 87
3.7.3 16-state Trellises 91
3.7.4 Summary 91

4 DTC-M-M-PSK Simulation Results **95**
4.1 Introduction 95
4.2 Simulation Software 96
4.2.1 Data Sequence Generator 96
4.2.2 Convolutional Encoder 96
4.2.3 Differential Encoder 96
4.2.4 Signal Mapper 99
4.2.5 AWGN Channel 99
4.2.6 Differential Demodulator 99
4.2.7 Viterbi Decoder 99
4.2.8 Convolutional Decoder 100
4.2.9 Error Analysis 100
4.3 Simulation Results 100
4.3.1 Differentially Coherent Uncoded 8-PSK (D8PSK) 101
4.3.2 DTC-(8,4)-16-PSK 101
4.3.3 DTC-(16,4)-16-PSK 107
4.3.4 DTC-(8,4)-8-8-PSK 107
4.4 Summary 113

5 Conclusions and Recommendations **118**
5.1 Summary 118
5.2 Conclusions for DTC-M-M-PSK 119

5.3 Recommendations for Further Research 120

A Tabulated Simulation Results **121**

Bibliography **127**

List of Figures

1.1 Transmit Constellation for DTC-16-PSK 16

1.2 Transmit Constellation for DTC-8-8-PSK 17

2.1 Basic TCM Modulator 21

2.2 Ungerboeck's 4-state Trellis Diagram 22

2.3 Ungerboeck's 8-state Trellis Diagram 23

2.4 Ungerboeck's 16-state Trellis Diagram 24

2.5 TCM Subset Partitioning Tree for 16-PSK 26

2.6 Effects of Error Path Distances on Symbol Error Rate Calculations 28

2.7 16-PSK Constellation 30

2.8 Differentially Coherent TCM Modulator and Demodulator 34

2.9 Differential Encoding/Decoding of Signal Constellations 36

2.10 Differential Demodulator 40

2.11 Comparison of Asymptotic and Simulated Performance for TC-(4,2)-8-PSK 48

3.1 Distance Parameters for TC-16-PSK 54

3.2 Effect of Amplitude and Phase Offsets on D-level Subsets 58

3.3 Effect of Phase-Difference Encoding on the DTC-8-8-PSK Product Constellation 62

3.4 Subset Partitioning Tree for the 8-8-PSK Transmit Constellation 63

3.5 Subset Partitioning Tree for the 8-8-PSK Product Constellation 65

3.6 TCM Intrasubset Distances for DTC-8-8-PSK 66

3.7 Determination of Pairwise Decision Thresholds 74

3.8 Superstate Diagrams for DTC-2M-PSK and DTC-M-M-PSK 76

3.9 Viterbi Decoder Trellis for DTC-(8,4)-M-M-PSK 79
3.10 Standard (4,2)-trellis 81
3.11 Viterbi Decoder Trellis used with DTC-(4,2)-M-M-PSK 82

4.1 Organization of the Simulation Software 97
4.2 Random Data Sequence Generator 98
4.3 Trellis for D8PSK 102
4.4 Constellation for D8PSK 103
4.5 Simulation results for D8PSK 104
4.6 Transmit trellis for all Type-(8,4) Trellis Codes 105
4.7 Convolutional Encoder for all Type-(8,4) Trellis Codes 106
4.8 Transmit Constellation for DTC-(8,4)-16-PSK 108
4.9 Simulation results for DTC-(8,4)-16-PSK 109
4.10 Simulation results for DTC-(16,4)-16-PSK 110
4.11 Transmit Constellation for DTC-(8,4)-8-8-PSK 111
4.12 Product Constellation for DTC-(8,4)-8-8-PSK 112
4.13 Viterbi decoder trellis for DTC-(8,4)-8-8-PSK 114
4.14 Simulation results for DTC-(8,4)-8-8-PSK 115
4.15 Simulation of DTC-(8,4)-8-8-PSK for $r_B \leq 1.638$ 116
4.16 Simulation of DTC-(8,4)-8-8-PSK for $r_B \geq 1.638$ 117

List of Tables

2.1 Asymptotic Coding Gains for Ungerboeck PSK codes 47

2.2 Asymptotic Coding Gains for Ungerboeck QASK codes 49

3.1 Optimum TCM Intrasubset Distances for M-M-PSK using Phase Difference Encoding 69

3.2 Contender Path Weights for DTC-(4,2)-4-4-PSK at various values of r_B . . 83

3.3 Contender Path Weights for DTC-(4,2)-16-16-PSK at various values of r_B . 85

3.4 Contender Path Weights for DTC-(4,2)-M-M-PSK at optimum values of r_B 86

3.5 Contender Path Weights for DTC-(8,2)-M-M-PSK at optimum values of r_B 88

3.6 Contender Path Weights for DTC-(8,4)-M-M-PSK at optimum values of r_B 90

3.7 Contender Path Weights for DTC-(16,2)-M-M-PSK at optimum values of r_B 92

3.8 Contender Path Weights for DTC-(16,4)-M-M-PSK at optimum values of r_B 93

A.1 Simulation Data for DTC-(8,4)-16-PSK 122

A.2 Simulation Data for DTC-(16,4)-16-PSK 123

A.3 Simulation Data for DTC-(8,4)-8-8-PSK at $r_B = 1.3$ 124

A.4 Simulation Data for DTC-(8,4)-8-8-PSK at $r_B = 1.6$ 125

A.5 Simulation Data for DTC-(8,4)-8-8-PSK at $r_B = 2.0$ 126

Acronyms and Definitions

AWGN	Additive White Gaussian Noise Channel
BER	Bit Error Rate
BPSK	Binary Phase Shift Keying
DTC-M-M-PSK	Differentially coherent Trellis-coded M-M-PSK
DTC-2M-PSK	Differentially coherent TC-2M-PSK
M-M-PSK	Constellation containing two M-PSK rings which may have different amplitudes and a phase offset
MPSK	PSK with M constellation points
Product Constellation	Set of equivalent baseband symbols at the output of the receiver's differential detector (before Viterbi decoding)
PSK	Phase Shift Keying
QPSK	Quaternary Phase Shift Keying
SER	Symbol Error Rate
SNR	Signal to Noise Ratio
TCM	Trellis Coded Modulation
TCM Constellation	Set of equivalent baseband symbols at the output of the transmitter's signal mapper
TC-2M-PSK	Trellis coded PSK constellation with $2M$ points
TDMA	Time Division Multiple Access
Transmit Constellation	Set of equivalent baseband symbols transmitted over the channel (after differential encoding)

Nomenclature

A_n	Uncoded data symbols
B_n	Convolutional Encoder output symbols
$B0$	Level 1 transmit constellation subset containing M points at amplitude r_A
$B0'$	Level 1 product constellation subset containing M points – can only occur if the preceding product constellation subset was of type $B0$
$B0''$	Level 1 product constellation subset containing M points – can only occur if the preceding product constellation subset was of type $B1$
$B1$	Level 1 transmit constellation subset containing M points at amplitude r_B ($r_B \geq r_A$)
$B1'$	Level 1 product constellation subset containing M points – can only occur if the preceding product constellation subset was of type $B0$
$B1''$	Level 1 product constellation subset containing M points – can only occur if the preceding product constellation subset was of type $B1$
C_n	TCM constellation point – equivalent baseband complex representation (before differential encoding)
D_n	Transmit constellation point – equivalent baseband complex representation (after differential encoding)
$D(t)$	Equivalent baseband complex coded transmit waveform associated with D_n
$\hat{D}(t)$	Estimate of $D(t)$

$d^2(\cdot,\cdot)$	Squared Euclidean distance measure
d_{free}	Smallest Euclidean distance between any correct code sequence and any error sequence
d_i	Euclidean weight of the i^{th} error path
E_n	Product constellation point (after differential demodulation)
e_n	Hamming error sequence between the correct code sequence and the incorrect code sequence
k	Index
M	Number of symbols in the uncoded alphabet
m	Number of bits per uncoded symbol
N	Number of states in the TCM encoder trellis
N_{free}	Multiplicity of the free distance error path – average number of error paths at distance d_{free} for all possible correct paths.
N_i	Multiplicity of the i^{th} error path
n	Discrete time index
$n(t)$	Additive White Gaussian noise
$n_P(t)$	Demodulator output noise (Product Space)
$n_R(t)$	Bandpass filtered noise
P_b	Probability of a bit error
P_e	Probability of a symbol error
$p(t)$	Differential demodulator LPF output (Product space)
$p_I(t)$	In-phase component of $p(t)$
$p_Q(t)$	Quadrature component of $p(t)$
$Q(\cdot)$	Gaussian error probability function

r_A	Amplitude of transmit constellation subset $B0$ (smaller subset)
r_B	Amplitude of transmit constellation subset $B1$ (larger subset)
$r_m(t)$	Amplitude of the m^{th} constellation point
$s(t)$	Transmitter output
$\hat{s}_h(t)$	Hilbert transform of $s(t)$
W	Path weight in Euclidean space
w_n	Metric correction factor associated with E_n
y_n	Correct code sequence
y'_n	An incorrect sequence which remerges with the correct sequence
Δ_i	Minimum Euclidean distance between any pair of points in an i^{th} level constellation subset
Δ'_i	Minimum distance from an i^{th} level M-M-PSK constellation subset of type $B0'$ to the reference i^{th} level subset of type $B0'$
Δ''_i	Minimum distance from an i^{th} level M-M-PSK constellation subset of type $B0''$ to the reference i^{th} level subset of type $B0'$
λ	Arbitrary phase offset
μ_{E_n}	Metric associated with Product constellation point E_n
$\rho_N(k)$	Correlation coefficient of $n(t)$ and $n(t-kT)$
$\rho_{N_P}(k)$	Correlation coefficient of $n_P(t)$ and $n_P(t-kT)$
σ_N^2	Channel Noise Power (in the bandwidth of interest)

$\sigma^2_{N_R}$	Power of $n_R(t)$
$\sigma^2_{N_P}$	Noise power at demodulator output
θ_m	Phase of the m^{th} constellation point
$\xi(\cdot)$	Function mapping a convolutional code from Hamming space to Euclidean space
$\oplus$	Modulo-2 addition
$(\cdot)^*$	Complex conjugate operator

Chapter 1

Introduction

1.1 Thesis Scope

This thesis describes a novel modulation technique – called DTC-M-M-PSK – which can improve the error performance of differentially coherent trellis coded modulation systems. DTC-M-M-PSK combines the advantages of Phase Shift Keying, trellis coding and differential detection.

It draws upon the work of Ungerboeck, Divsalar and Simon, Wilson, Proakis and others to present the strengths and weaknesses of these techniques when they are used in isolation.

With this as a foundation, we describe how these three well established techniques complement each other when applied to the new DTC-M-M-PSK family of channel constellations.

An analytical framework is then developed to permit easy evaluation of specific DTC-M-M-PSK codes for the asymptotic case of high SNR on an Additive White Gaussian Noise (AWGN) channel.

Simulation results are then presented which validate the asymptotic analysis for the most promising DTC-M-M-PSK code.

This thesis concludes with an analysis of the potential applications of these codes and recommendations for further research.

1.2 Trellis Coded Modulation

The origin of Trellis Coded Modulation is widely attributed to the work of G. Ungerboeck as presented at a conference in 1976 [43] and later published in 1982 [1]. However the concept

of combining channel coding and modulator signal constellation design was first proposed in a paper by J.L. Massey [41] [23] in a 1974 conference publication.

Prior to the early 1980's only BPSK and QPSK were considered for widespread use over satellite [28] and mobile channels. Higher PSK signal constellations, such as 8-PSK, were not yet cost effective. For BPSK the transmission channel is binary; for QPSK, each of the orthogonal channel components is binary. Consequently channel coding techniques were developed to optimise performance on these binary signalling channels. In this case, maximizing the distance between constellation points in signal space was reduced to the identical problem of maximizing Hamming distance between code symbols at the modulator input [1] [2] [13].

However, advances in technology and the need for greater bandwidth efficiency have made larger signal constellations more common – and more cost effective. For these modulation types, additional channel coding gains can be realized beyond those resulting from the maximization of Hamming distance [1] [12].

For modulation types in which each quadrature channel transmits more than one bit per signalling period, there is no longer a linear relationship between the Hamming distance of the code vectors and the Euclidean distances in the coded constellation. It is no longer possible to design the channel coder and the signal constellation in isolation and still achieve optimum performance.

It was this realization that led G. Ungerboeck [1] to investigate techniques for designing channel coders and signal constellations as a matched set to achieve maximum Euclidean distance. Initially he developed a number of TCM designs that, while simple to implement, yielded coding gains of 3dB or greater when compared with uncoded modulation.

The classical approach to channel coding had been to introduce redundant bits into the data stream to provide error detection or correction capability at the receiver. In some cases the constellation size was increased to maintain a constant channel rate but the signal mapping was not adjusted to optimize performance with the specific convolutional encoder. In most cases the signal space constellation was not changed. With reference to the uncoded system, this required either a reduction in the input data rate or an increase in the transmission signalling rate. The channel bandwidth of the signal was increased when

normalized with respect to the input data rate.

For TCM, performance gains are achieved without this bandwidth penalty. Rather than increasing the signalling rate and channel bandwidth – a precious commodity in satellite and mobile communications – the size of the signal constellation is increased.

Since the start of TCM research it has found applications in a wide variety of communication channels. TCM forms the basis for a new generation of voiceband 9.6 kbps and 14.4 kbps modems as specified in CCITT Recommendations V.32 [26] [38] and V.33 [39], respectively. One-dimensional TCM is under consideration for digital subscriber loop applications – particularly broadband ISDN as reported by Joshi and Falconer [37] and Falconer et al [36]. TCM is already in use for 64 kbps satellite terminals [7]. Development is underway for TCM satellite terminals with data rates of 120 Mbps and higher [4] [5]. The application of TCM to fading channels is also gaining prominence [20] [21] [22] [44]. Despins [23] provides an overview of research in this area.

The new TCM technique described in this thesis achieves significant performance increases when compared with other TCM schemes involving PSK constellations and differential detection. Consequently it is most applicable to mobile and satellite channels. Mobile channels often use differential detection to combat the effects of fading and shadowing. Satellite channels are usually peak power limited and involve non-linear amplification. Consequently constellations with a low peak-to-average energy ratio or a constant signal envelope are preferable.

1.3 Differential Detection

Differential detection – also referred to as differentially coherent detection – offers several advantages over coherent detection. Since carrier recovery is not necessary, it typically can be implemented with a receiver which is less complex than that required for coherent detection. It is also less sensitive to carrier frequency offsets and Doppler effects. In slow fading environments, differential detection can outperform coherent detection [25]. In TDMA burst applications, differential detection eliminates the need for long burst acquisition training sequences. On the basis of these advantages, Divsalar and Simon [9] [35] indicate that differentially coherent trellis coded PSK is appropriate for many fading mobile channels.

Differential detection is usually implemented by multiplying the receive signal by a delayed version of itself. This highlights its chief limitation. The signal is demodulated using a noisy signal rather than a low noise carrier estimate. Consequently the noise at the output of the differential detector is approximately double the input noise power. As a result, differential detection is always accompanied by a performance loss which is 2.3dB for 4-PSK at high SNR and approaches 3.0dB for denser PSK constellations [14] [32].

Although differential detection has traditionally been applied only to PSK-type modulation formats, we shall explore its implementation on a family of transmit constellations which deviate from PSK. Despite their higher peak-to-average energy ratio, these constellations have shown promise in terms of bit error rate performance on mobile channels employing differential detection. Non-PSK constellations are also beginning to gain acceptance in satellite applications as the need for greater bandwidth efficiency increases [6] [28]. For example, for coded transmission rates of 4 bits/symbol period, a choice is currently being made between 16-QASK and 16-PSK [6]. The former has better power efficiency but its performance gains over 8-PSK are discounted when compared with 16-PSK on a peak energy basis. Wilson et al [13] consider Trellis-coded 16-PSK to be preferable to TC-16-QASK over non-linear satellite channels because of its constant amplitude properties. However Lyons et al [6] contend that TC-16-QASK is preferable provided pre-warping is used to provide some compensation for channel non-linearities.

Trellis-coded 16-PSK would appear to also have the advantage of being differentially encodeable. To date all literature on differential detection is based on a process of mapping phase differences between consecutive PSK channel symbols onto the transmitted channel symbol. However this thesis will also examine alternative differential encoding strategies which make use of both the differential demodulator and the TCM Viterbi decoder to extract the information relevant to the transmitted sequence.

1.4 Differentially Coherent M-M-PSK

Differentially coherent M-M-PSK improves the error performance of DTC-2M-PSK by dilating one of the two major constellation subsets.

Figures 1.1 and 1.2 show the constellations used for DTC-16-PSK and DTC-8-8-PSK.

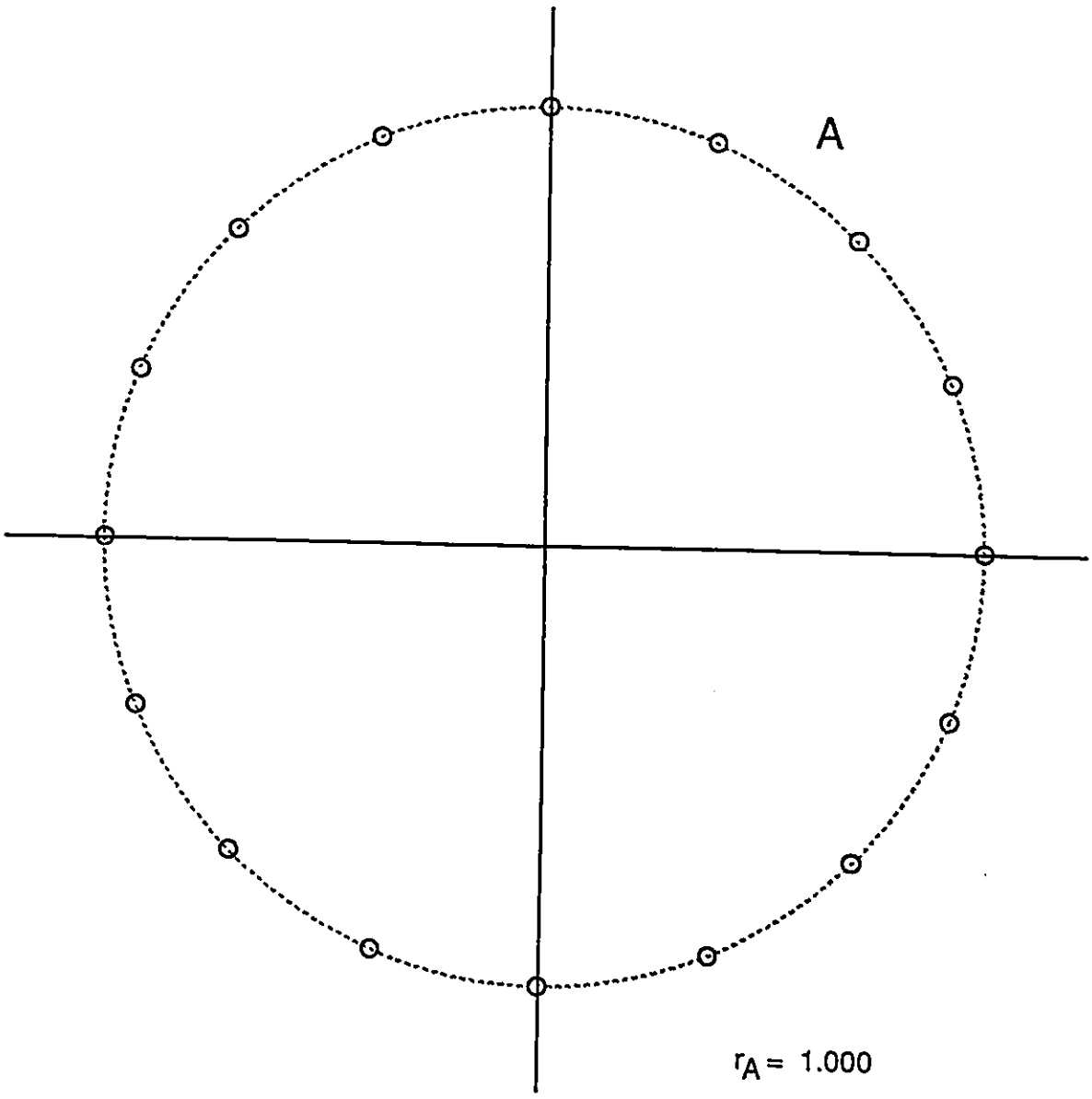

Figure 1.1: Transmit Constellation for DTC-16-PSK

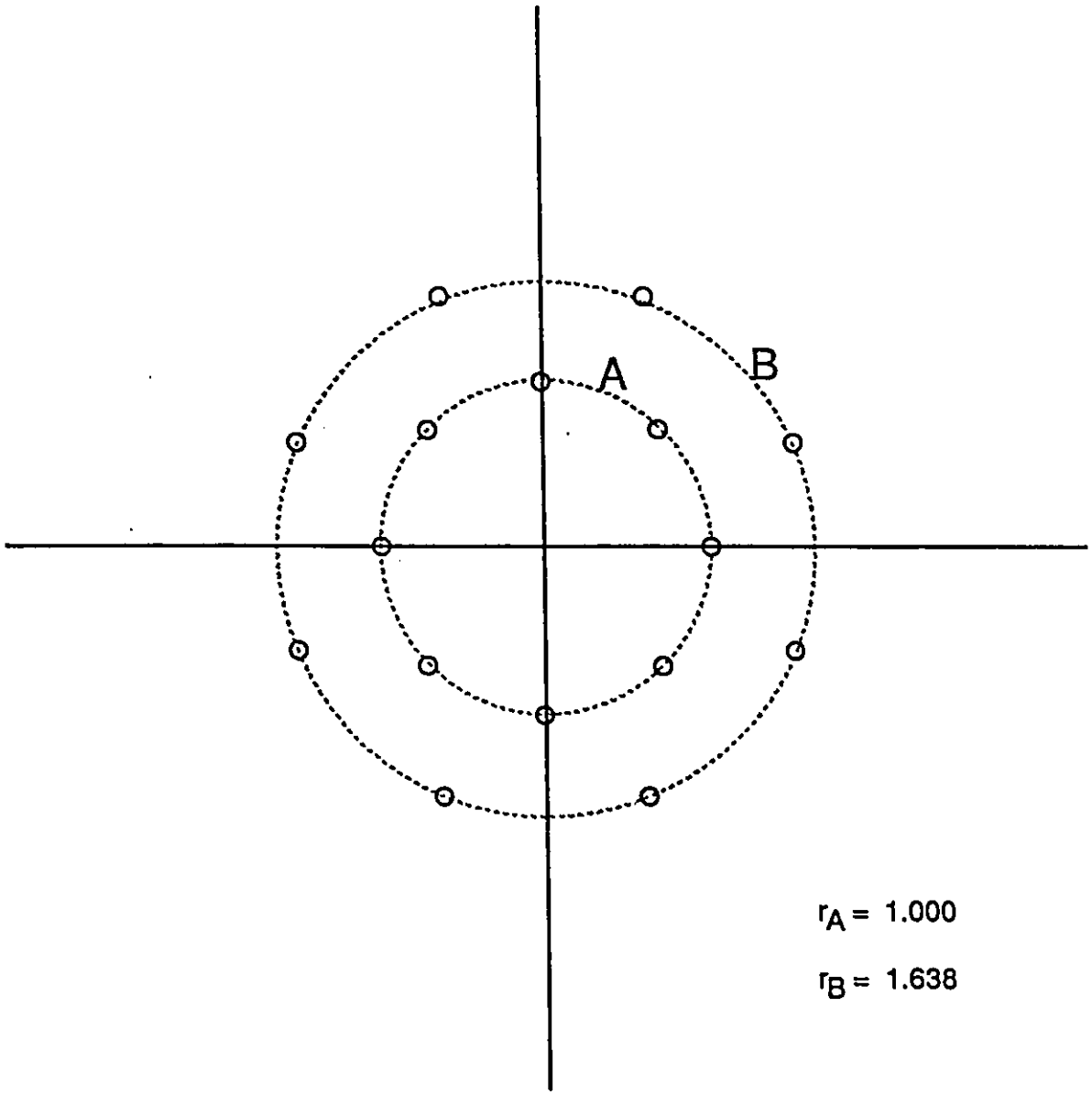

Figure 1.2: Transmit Constellation for DTC-8-8-PSK

The latter constellation clearly has a higher average energy. However when used with differential detection and trellis coding, its increased distance properties can be exploited to overcome this energy penalty and provide additional coding gain.

These dilated constellations still retain many of the desirable characteristics of conventional PSK constellations. Usually when differential detection is performed on a non-PSK constellation the receiver must evaluate up to $4M^2$ product constellation points, rather than the $2M$ points which occur for coded 2M-PSK. However with DTC-M-M-PSK the product space constellation merely increases to $3M$ points.

1.5 Thesis Organization

The thesis consists of five chapters with the material organized as follows.

This initial chapter has presented an overview of the research area covered by the thesis and has presented the rationale for the development of the DTC-M-M-PSK family of constellations.

Chapter 2 presents background material on Trellis Coded Modulation (TCM) and differential detection as applied to PSK constellations. A noise model is presented to support the performance analysis of these codes for the asymptotic case of high SNR. Performance results are then evaluated for DTC-2M-PSK and other similar codes presented in the literature.

Chapter 3 introduces the DTC-M-M-PSK family of trellis coded constellations. Adaptations are made to the noise model developed earlier in Chapter 2. On this basis, BER performance comparisons are made for a wide variety of DTC-M-M-PSK constellations for the asymptotic case of high SNR on an AWGN channel.

Chapter 4 describes the simulations performed on a specific DTC-M-M-PSK code – DTC-(8,4)-8-8-PSK. The results are presented and compared with the analytical model from Chapter 3.

Chapter 5 summarizes the development of the DTC-M-M-PSK constellations and analyzes their potential applications. It concludes with a discussion of areas for future research.

Tabular results for the simulations described in Chapter 4 are included in Appendix A.

Chapter 2

Differentially Coherent TC-2M-PSK

2.1 Introduction

This chapter describes trellis coding in greater detail and applies it to the specific case of differential detection and PSK constellations. On the basis of this background material we will introduce the new family of DTC-M-M-PSK codes in Chapter 3.

We begin by describing the design approach for trellis codes. The concepts of "mapping by set partitioning" and "trellis free distance" are introduced. We then apply these techniques to a specific trellis code – 8-state 16-PSK – and provide an explanation for its 3.54dB asymptotic gain over uncoded 8-PSK.

Next differentially coherent detection is described in greater detail and applied to trelliscoded PSK. We consider only the standard phase difference encoding technique. However it is treated in a manner that will be readily applicable to the M-M-PSK constellations introduced in Chapter 3.

We then proceed to develop a noise model for differentially coherent trellis codes. It is then applied to PSK trellis codes to demonstrate that the same Viterbi decoder trellis and branch metrics are optimum for both coherent TC-PSK and its differentially coherent counterpart.

We conclude with a discussion of some of the advantages and limitations of differentially coherent 2M-PSK.

2.2 Trellis Coding for PSK Constellations

Trellis coding can be implemented as an additional stage preceding a conventional modulator. This is shown in Figure 2.1.

This configuration consists of a rate $m/(m+1)$ convolutional encoder followed by a signal mapper. The convolutional encoder permits additional signal constellation points to be used to provide redundancy. The signal mapper ensures that the encoder output symbols are allocated to these constellation points in a manner which optimizes the Euclidean distance between sequences of channel symbols.

In theory – using a rate $m/(m+n)$ encoder – as n approaches infinity, trellis coding gains of 7-8dB [2] can be achieved with a signal set size 2^n times that of the uncoded signal set. However Ungerboeck has shown that most of the coding gain is achieved by a simple doubling of the constellation size. In terms of modem complexity, increasing n beyond a value of 1 is generally not worth the diminishing returns in performance [1].

Trellis coded modulation derives its name from the trellis diagram representation of how sequences of constellation points are chosen for a given uncoded data sequence. A typical trellis diagram is shown in Figure 2.2. This 4-state trellis was used by Ungerboeck [1] to obtain a 3dB gain for trellis-coded 8-PSK over uncoded 4-PSK. Ungerboeck's 8- and 16-state trellises are shown in Figures 2.3 and 2.4, respectively. The trellis representation facilitates the design of TCM codes with good Euclidean distance properties.

The concept of set partitioning is an essential part of TCM code design. To achieve coding gains beyond that of conventional channel coding with MLSE decoding, it is necessary to increase the Euclidean distance between the constellation points that are possible in a given signalling interval.

Ungerboeck's set partitioning strategy ensures that the lower bound on the distance between two code vectors in Euclidean space increases monotonically with Hamming distance. To achieve this binary-to-Euclidean-space mapping, it is first necessary to form a tree of signal constellations as shown in Figure 2.5. At any level in the set partitioning tree except the top level, pairs of constellations are formed from the signal points of the constellations at the next higher level. Each constellation contains half the points of the

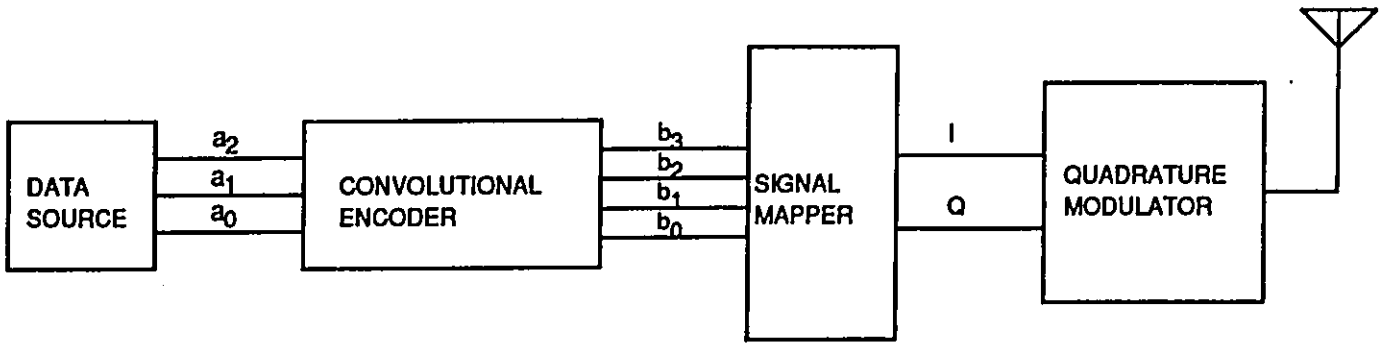

Figure 2.1: Basic TCM Modulator

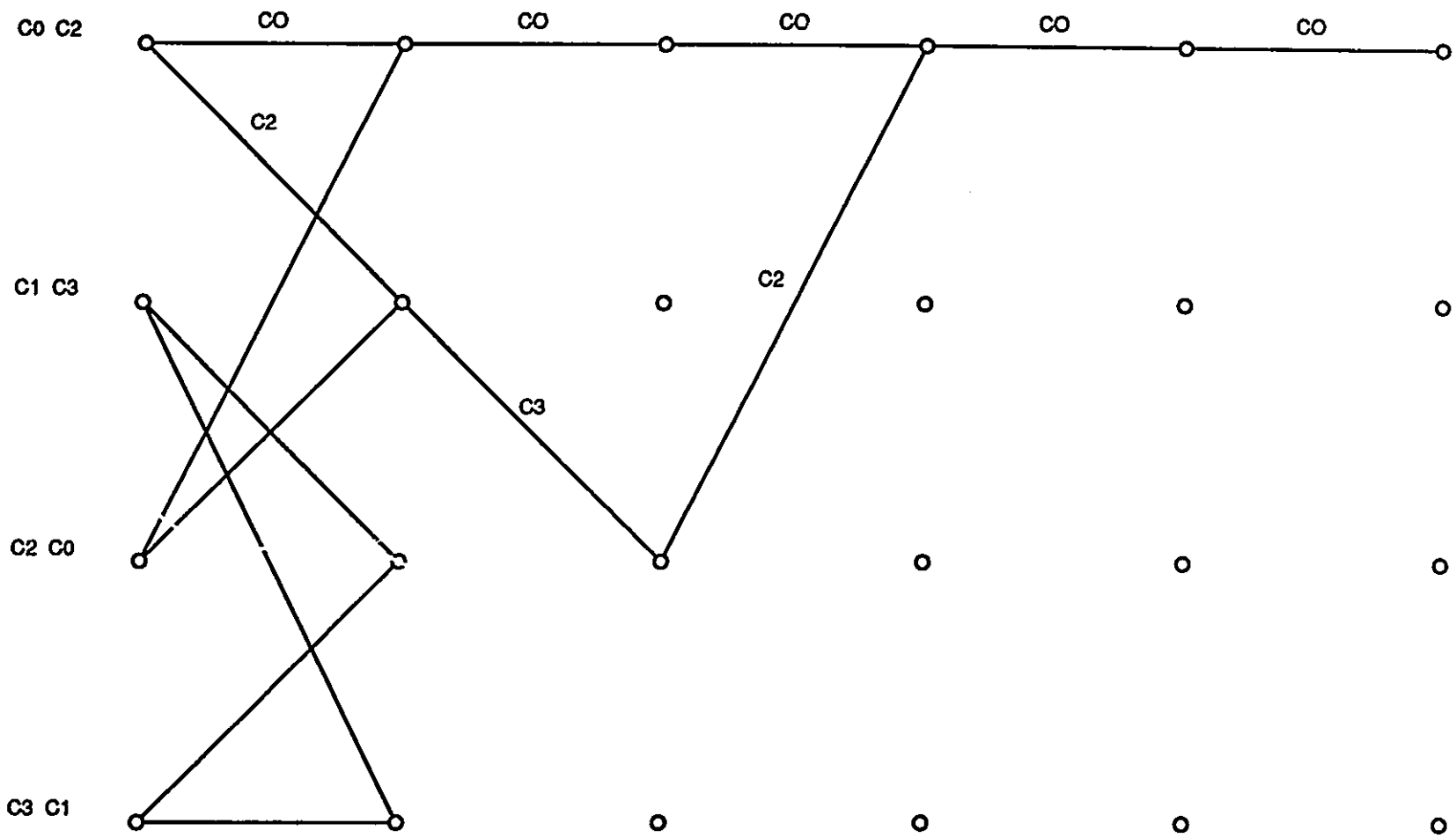

Figure 2.2: Ungerboeck's 4-state Trellis Diagram

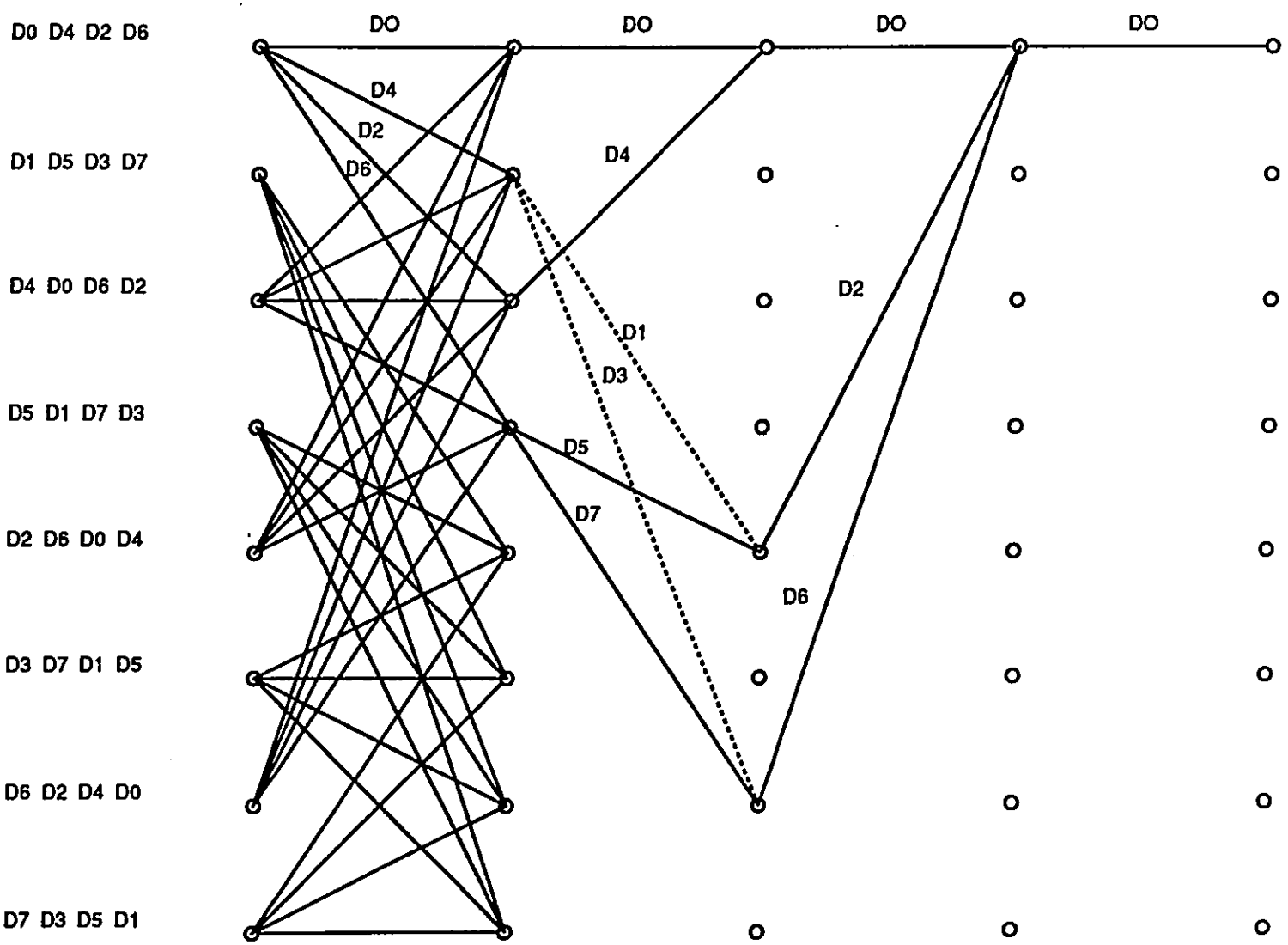

Figure 2.3: Ungerboeck's 8-state Trellis Diagram

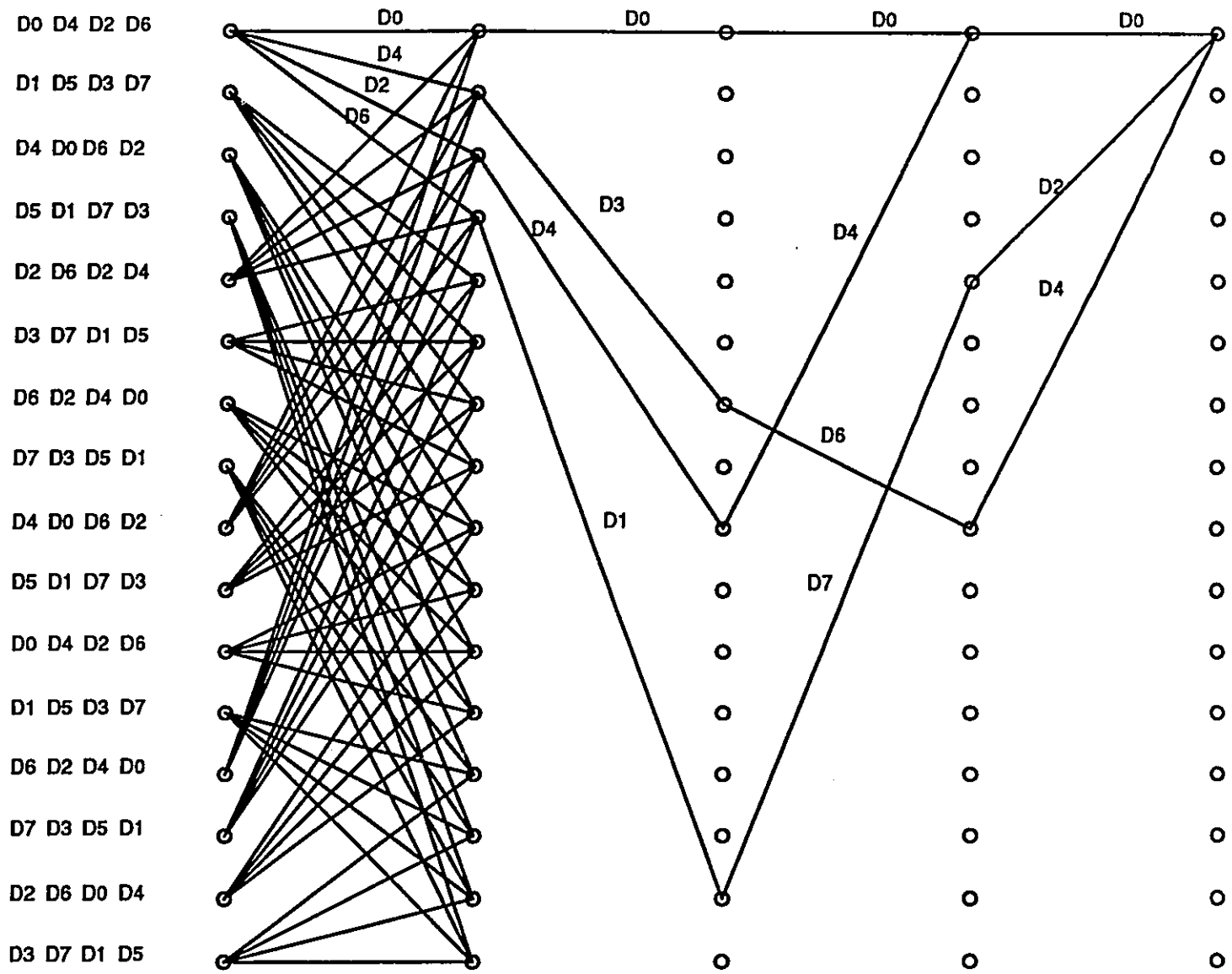

Figure 2.4: Ungerboeck's 16-state Trellis Diagram

larger constellation. The points are partitioned into these two subsets in a manner which maximizes the minimum distance between points in any given subset.

If, as in Figure 2.5, the number of levels in the tree equals the number of bits in the encoder output symbol, then it is easy to map each code word to a constellation point. Starting at the top of the tree, partitioning proceeds using the left or right branch depending on whether the code's least significant bit is a zero or a one, respectively. The next branch is chosen in a similar manner based on the state of the next least significant bit of the code word. When all codeword bits are exhausted, the constellation subset will contain only one point.

For most signal constellations, all subsets at a given level in the tree will have the same intra-subset minimum distance. This is denoted as Δ_i for the i^{th} level in the tree. As noted by Ungerboeck, the minimum distance between codes is lower bounded by the Δ_i value for the constellation subset which contains both code vectors [1].

For sequence coding, the free distance of the code is equal to

$$d^2_{free} = \min\{d^2[\xi(y_n), \xi(y_n{}')]\} \tag{2.1}$$

for all code sequences $y_n \neq y_n{}'$, where $\xi(\cdot)$ maps code words to Euclidean vectors [1].

Since convolutional codes are linear codes, $y_n{}'$ may be written as

$$y_n{}' = y_n \oplus e_n \tag{2.2}$$

where e_n is also a code word. Using Ungerboeck's method of mapping codewords to Euclidean vectors it can be shown that

$$d^2[\xi(y_n), \xi(y_n{}')] = d^2[\xi(e_n), \xi(0)] = \mathbf{w}^2[\xi(\mathrm{e_n})] \tag{2.3}$$

where $w(\cdot)$ is the weight, or Euclidean distance from the zero code vector.

From the tree in Figure 2.5 it can also be shown that $w[\xi(e_n)]$ is lower bounded by the intra-subset minimum distance for the constellation subset containing both this code vector and the zero code vector. This distance is Δ_i where i is the number of trailing zeros in the error vector.

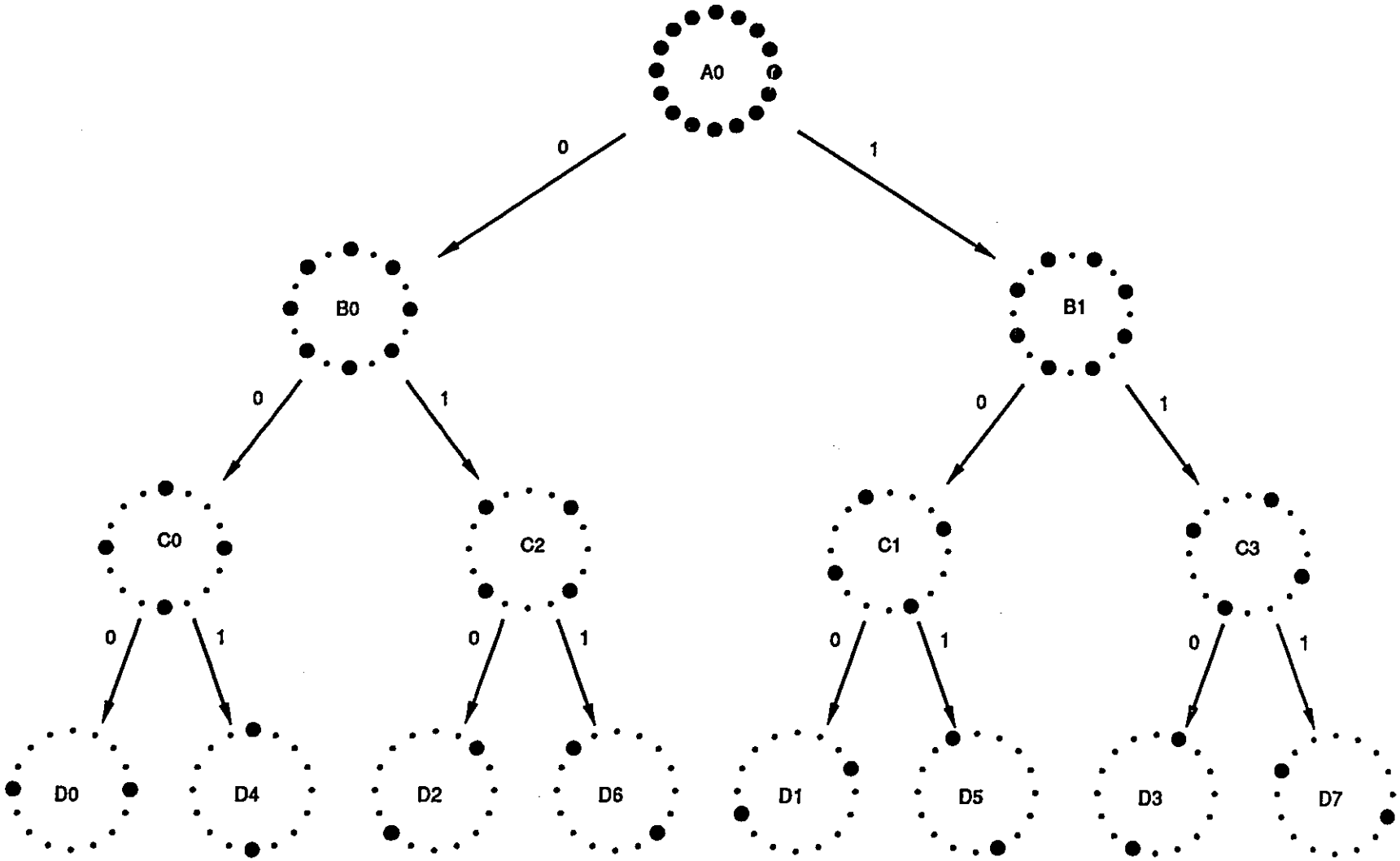

Figure 2.5: TCM Subset Partitioning Tree for 16-PSK

Consequently we can obtain a lower bound for d^2_{free} which can be written in the following form:

$$d^2_{free} = \min\{w^2[\xi(e_n)]\} \tag{2.4}$$

where

$$w^2[t(e_n)] \leq (a_0\,\Delta_0^2 + a_1\,\Delta_1^2 + a_2\,\Delta_2^2 + a_3\Delta_3^2, ...) \text{ for all } n \tag{2.5}$$

where $\{a_i\}$ are integers with values dependent on the specific trellis code.

For this lower bound on d_{free} we obtain the following upper bound for the probability of error at high SNR:

$$P_e \leq N_{free} \cdot Q(\frac{d_{free}}{2\sigma_N}) \tag{2.6}$$

where N_{free} is the multiplicity of the minimum weight error path, σ_N is the standard deviation of the post-detection noise, and $Q(\cdot)$ is the Gaussian error integral defined as:

$$Q(x) = \frac{1}{\sqrt{2\pi}} \int_x^\infty e^{-y^2/2} \cdot dy \tag{2.7}$$

At high SNR only the minimum weight error path is of significance. At low SNR, however, the bound on P_e could be better expressed as:

$$P_e \leq N_{free} \cdot Q(\frac{d_{free}}{2\sigma_N}) + \sum_{i=2}^{\infty}[N_i \cdot Q(\frac{d_i}{2\sigma_N})] \tag{2.8}$$

where d_i and N_i are the weight and multiplicity of other error paths of greater weight than $d_1 = d_{free}$. Because of the exponential nature of the Q-function, the additional terms will be much smaller than the first when σ_N is small. Figure 2.6 illustrates the relative importance of the first four terms in equation (2.8) for low SNR.

At high SNR the first term is even more predominant. Consequently at high SNR only the minimum weight error path need be considered.

In general a newly designed trellis code must be compared with other codes to evaluate its importance. For this purpose it is common practice to assume high SNR and neglect the multiplicity of the error paths. The ratio of coding gains for the two modulation types can then be estimated as follows:

$$G_{Sys1/Sys2} = \frac{d^2_{free_1}}{d^2_{free_2}} \cdot \frac{E_{ave,2}}{E_{ave,1}} \tag{2.9}$$

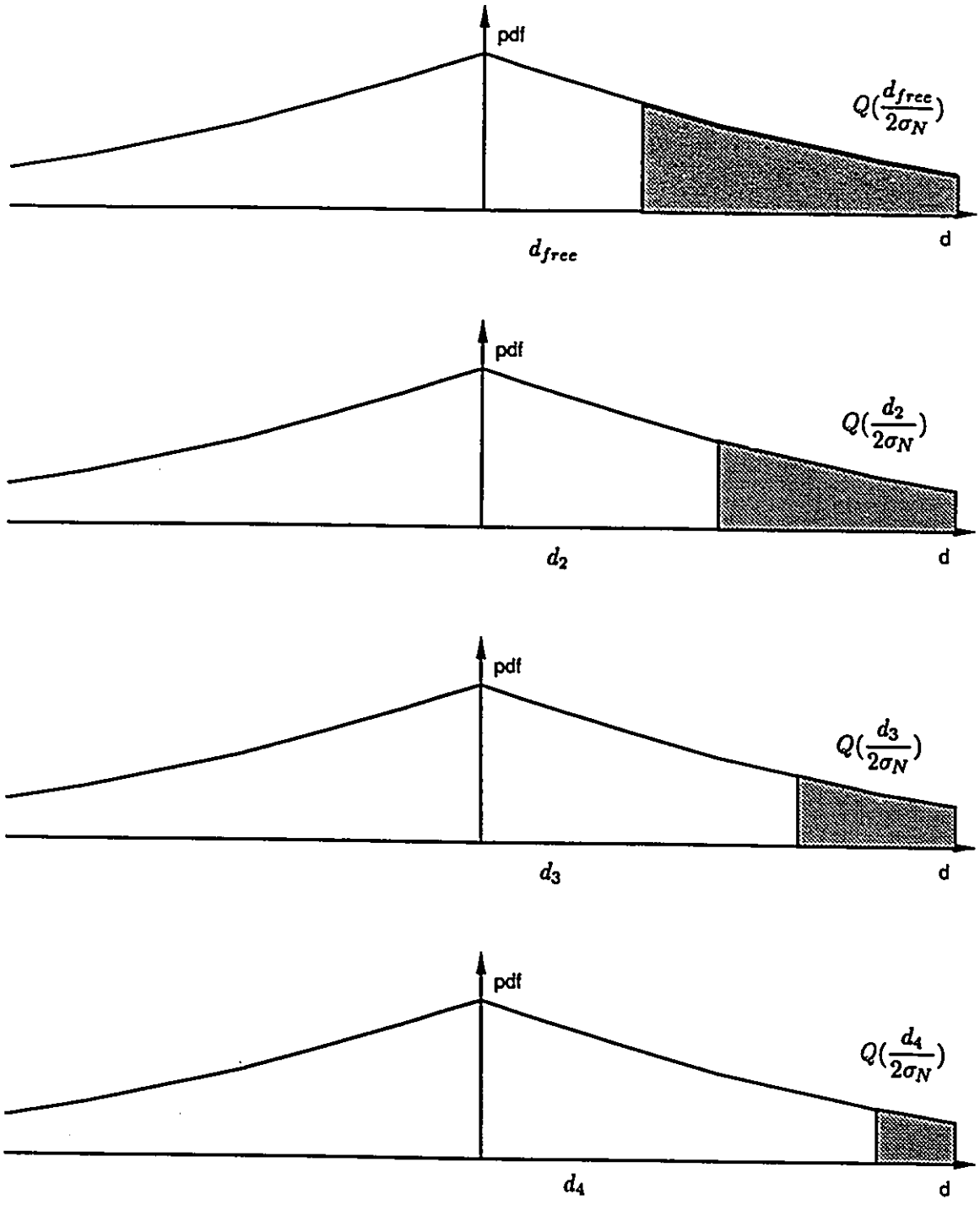

Figure 2.6: Effects of Error Path Distances on Symbol Error Rate Calculations

where E_{ave} is the overage energy of the applicable constellation.

When a gain is predicted for a specific trellis code on the basis of the above analytical method, it is then necessary to perform simulations to determine the effect of the multiplicity of the shortest error path and the effect of other error paths which become significant at low SNR.

2.2.1 Coding Gain for TC-(8,4)-16-PSK

Now let us consider the specific case of the 16-PSK constellation, shown in Figure 2.7 using the 8-state trellis shown earlier in Figure 2.3. We will provide a detailed explanation of the gain that can be achieved. Later in Chapter 3 we will demonstrate how this code can be modified to incorporate differential detection in a manner which avoids part of the usual 2.8dB loss associated with differential 16-PSK.

For trellis-coded 16-PSK, the constellation set partitioning tree is as shown in Figure 2.5. For a code with 4 sets of branches per state – such as those using the (8,4)-trellis – partitioning ends at the D-level. Since the coded constellation contains 16 points, each D-level subset contains a pair of points. If the same trellis was used for an 8-point constellation each D-level subset would contain a single point. However Ungerboeck's technique for determining a free distance bound is sufficiently general that it can be applied to subsets which contain single points or a number of points.

At the C-level, each 16-PSK constellation subset contains 4 points. These subsets have been selected such that the C-level intra-subset distance, Δ_2, is identical and maximum for each C-level subset. At the B level, each subset contains 8 points. These two subsets have been selected such that the intra-subset distance, Δ_1, is identical and maximum for both subsets.

Now we will make use of these Δ-parameters to obtain a free distance measure for the trellis shown in Figure 2.3. On this diagram the names of the appropriate D-level subsets are listed to the left of each trellis state. When the code sequence is at a specific state in the trellis it must transmit a constellation point from one of the listed constellation subsets in order to proceed to the next trellis state. The specific choice of subset will identify the next state in the trellis path.

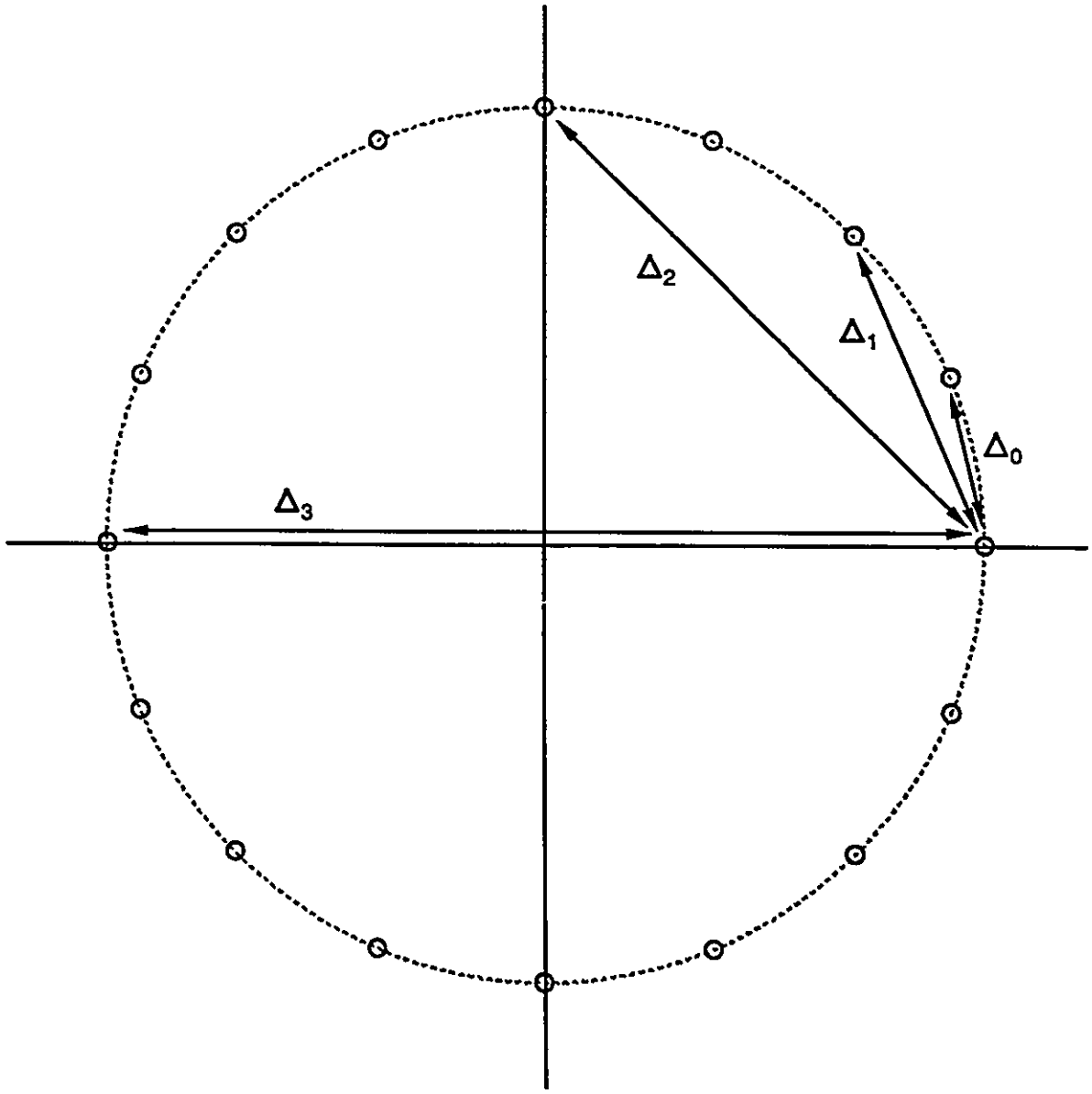

Figure 2.7: 16-PSK Constellation

We follow Ungerboeck's labelling convention whereby the leftmost subset label applies to the topmost trellis branch emanating from a specific state. The remaining subset labels are applied in sequence to the remaining branches leaving that state. This notation permits accurate labelling of more complicated trellises.

As mentioned earlier, Ungerboeck codes are linear. Consequently, when evaluating code performance we can consider the all-zero code word to be the correct code word without loss of generality. This corresponds to the all-D0 path along the top of the trellis diagram.

Figure 2.3 shows a few of the shorter error paths for this specific trellis and the all-zero correct path. Each error path starts from the all-D0 path, diverges, and remerges several symbol periods later. As explained earlier, for high SNR we need only consider the error path with the lowest weight; this weight is defined as the trellis free distance, d_{free}. We will show that the two paths labelled D6-D5-D2 and D6-D7-D6 have the lowest weight.

Figure 2.3 also shows another pair of length 3 paths – labelled D4-D1-D2 and D4-D3-D6. It will be shown that this pair of paths has a larger Euclidean weight when compared to the first pair.

In determining d_{free}, we will primarily consider the D6-D7-D6 error path. When appropriate, the D6-D5-D2 will be considered in more detail as well. The Euclidean squared distance from this error path to the correct path will be the summation of the squared distances between their respective signal constellation points in each symbol period. We need only consider the three symbol periods in which the paths differ since in all other symbol periods the two paths have no Euclidean separation.

In the first symbol period the correct path corresponds to either point from the D0 subset, and the error path corresponds to either point from the D6 subset. The minimum distance between any possible pair of correct path and error path points is lower bounded by Δ_1^2, the minimum intra-subset distance for the constellation subset which contains both the D0 and D6 subset.

During the second symbol period we must consider the distance between points in either the D5 or D7 subsets and the correct path subset, D0. For either comparison we must identify the lowest constellation subset which contains both constellation points. In either case this is the A0 subset – the overall 16-PSK constellation.

Consequently we can state that the Euclidean squared distance in this symbol period is lower bounded by Δ_0^2 – the intra-subset squared distance for the 16-PSK constellation. In actual fact the points in the D7 subset are closer to the correct path than are points in the D5 subset. For the D5 branch the distance to the correct path is greater than Δ_0^2. However Ungerboeck's technique applies a lower bound of Δ_0^2 to both branches.

If we consider now the third symbol period, for either error path the subset they have in common with the correct D0 subset is B0. Consequently the Euclidean squared distance is lower bounded by Δ_1^2.

Combining the results above we obtain the following lower bound for the weight of this error path:

$$\begin{aligned} W_{D6-D7-D6} &= \Delta_1^2 + \Delta_0^2 + \Delta_1^2 \\ &= 0.5858 + 0.1522 + 0.5858 \\ &= 1.3238 \end{aligned} \tag{2.10}$$

If we now perform the same analysis on the other two error paths – identified by the dashed lines in Figure 2.3 – we will obtain the following lower bound for both path weights:

$$\begin{aligned} W_{D4-D1-D2} &= \Delta_2^2 + \Delta_0^2 + \Delta_1^2 \\ &= 2.000 + 0.1522 + 0.5858 \\ &= 2.7380 \end{aligned} \tag{2.11}$$

These path weights are much larger than $W_{D6-D7-D6}$ because they include the Δ_2 parameter which is much larger than either Δ_0 or Δ_1.

For the sake of completeness, we will also consider another error path that is not immediately obvious from Figure 2.3. Up to this point we have considered the correct path to consist of a sequence of any symbols from the D0 subset. However this subset contains two symbols. Only one of these symbols can be the correct symbol; if the other symbol occurs, it too is an error. This is known as the "parallel" error path. It is only present in trellis codes in which subsets at the lowest partitioning level contain more than one constellation point.

The weight of this path is easily evaluated as follows:

$$\begin{aligned} W_{D0} &= \Delta_3^2 \\ &= 4.000 \end{aligned} \tag{2.12}$$

Ungerboeck's set partitioning algorithm ensures that such parallel paths have the greatest possible Euclidean separation. In most cases – TC-(8,4)-16-PSK included – the parallel error path has a minimal impact on the trellis free distance.

Now the trellis free distance is defined as the minimum weight for any error path. Consequently

$$\begin{aligned} d_{free}^2 &= W_{D6-D7-D6} \\ &= 1.3238 \end{aligned} \tag{2.13}$$

We must now compare this with the free distance of the corresponding uncoded constellation – 8-PSK. In this case, if we assume an average constellation energy of 1, $d_{free}^2 = \Delta_{0,8-PSK}^2 = 0.5858$. The above coding gain for TC-(8,4)-16-PSK was also based on an average constellation energy of 1. Consequently, using equation (2.9) we obtain:

$$\begin{aligned} G_{TC-16PSK/8-PSK} &= (\frac{1.3238}{0.5858}) \cdot (\frac{1}{1}) \\ &= 2.260 \\ &= 3.54\text{dB} \end{aligned} \tag{2.14}$$

In a later section we will use this result to obtain a coding gain for the same trellis code using differentially coherent detection.

2.3 Differential Detection

This section will examine the current method used to apply differential encoding to TCM using PSK transmit constellations. This will provide the groundwork for Chapter 3 where we will then consider a deviation from this approach that can be used with other non-PSK transmit constellations. Figure 2.8 is a block diagram of a TCM modulator and demodulator which includes differential encoding and decoding.

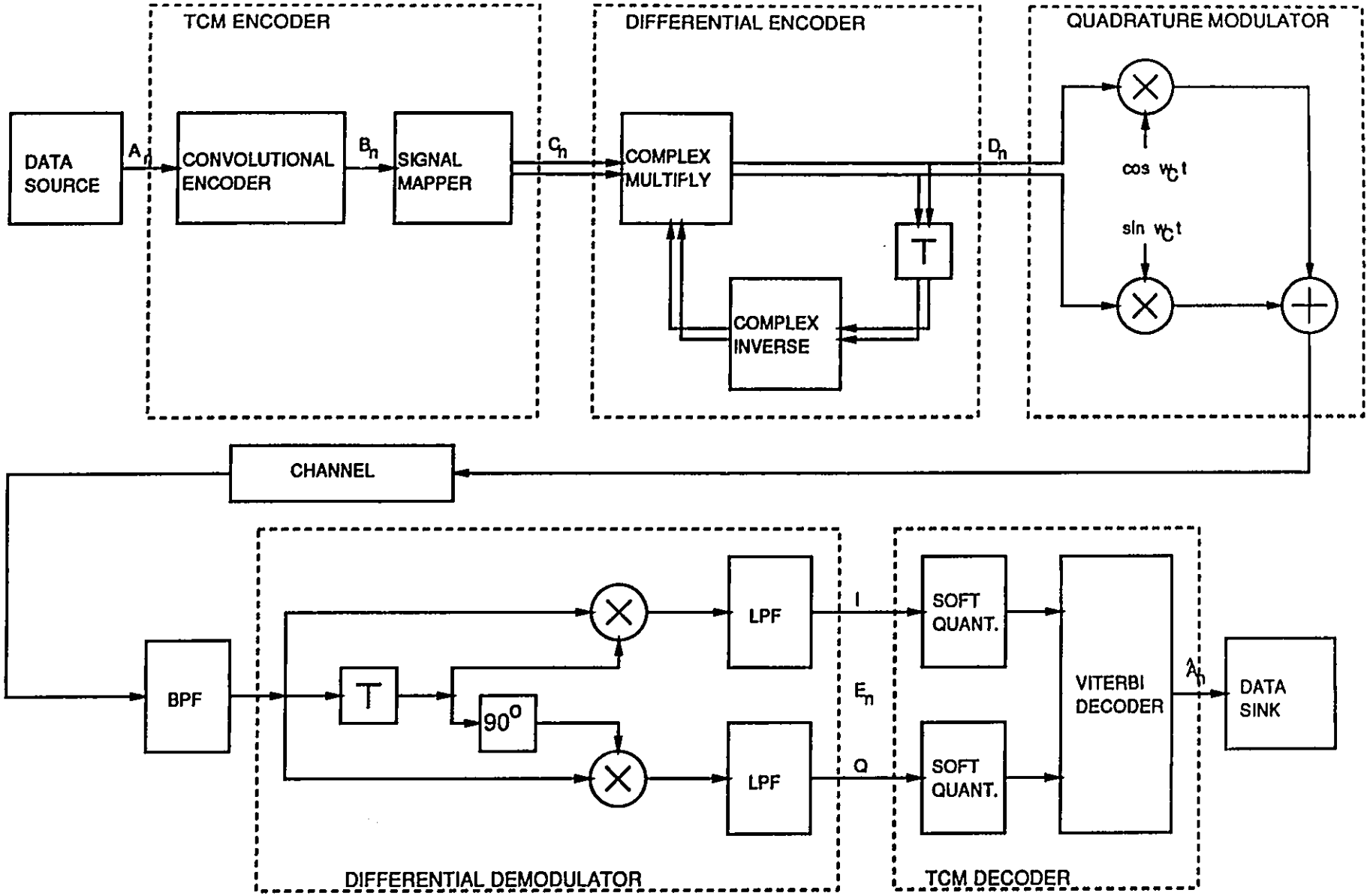

Figure 2.8: Differentially Coherent TCM Modulator and Demodulator

Consistent with Makrakis et al [15] the differential encoder is treated as a distinct entity which operates on channel symbols produced by the trellis encoder. Similarly the differential decoder is treated as a separate entity located before the TCM Viterbi decoder. In Chapter 3 we will explore the advantages of combining the differential decoder and the TCM Viterbi decoder operations.

Referring once again to the TCM modulator and demodulator shown in Figure 2.9, we will define the signal at three specific points. This will facilitate our discussions about differentially coherent TCM.

The equivalent baseband representation of the signal immediately following the signal mapper is defined as a point C_n from the "TCM constellation". For coherent TCM this is the only constellation that need be considered.

At the output of the differential encoder we define the signal to be a point, D_n, from the "transmit constellation". This is the signal that will actually be modulated and transmitted through the channel to the receiver.

In a practical differential TC-PSK modulator it is unlikely that a signal such as C_n could be identified. In all likelihood the differential encoding would be performed by modulo-(2M) subtraction on consecutive convolutional encoder outputs. The resultant transmit symbols would then be mapped directly to the transmit constellation point, D_n. However for discussion purposes it is convenient to show the modulator in a form which clearly identifies the TCM constellation points.

The signal at the input of the TCM receiver still corresponds to the transmit constellation – albeit with additional narrowband channel noise. However, after differential demodulation – essentially a complex multiplication – we define the signal to be a point, E_n, from the "product constellation".

For DTC-2M-PSK, the product constellation and the original TCM constellation are identical. However when discussing differentially coherent TC-M-M-PSK in Chapter 3, the distinction between the original TCM constellation and the product constellation will become important.

PSK signal constellations have certain properties which facilitate differential encoding. These are highlighted in Figure 2.9. The constellation points can be represented as unique

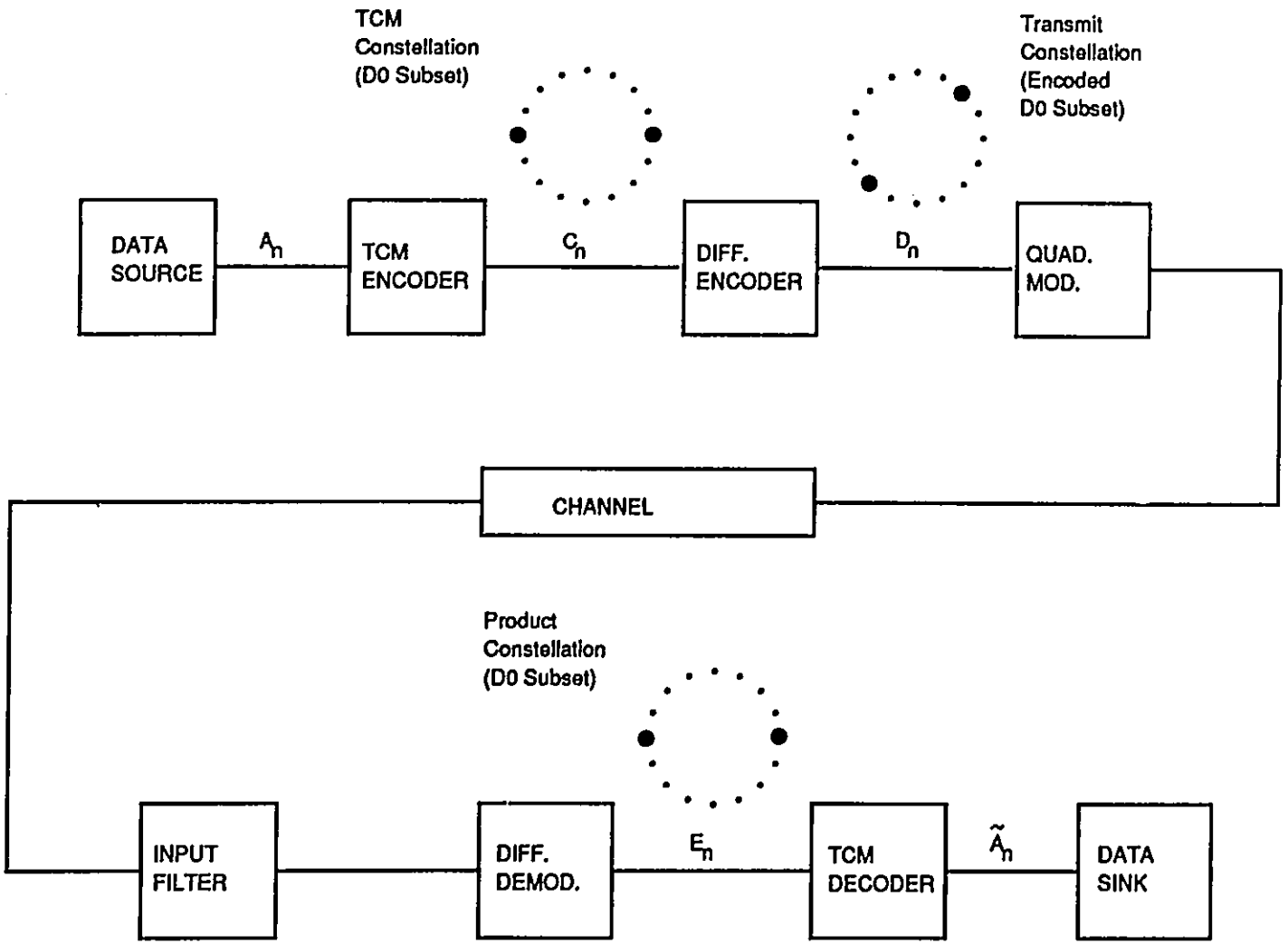

Figure 2.9: Differential Encoding/Decoding of Signal Constellations

equally-spaced numerical values corresponding to their phases. The amplitudes of all constellation points are identical and contain no information.

The multiplication of any two complex constellation points leads to a set of product constellation points which also form an M-PSK constellation. Each product point contains the sum of the phases of the two points which produced it.

If the original M-PSK constellation contains a point with 0 phase or $\frac{\pi}{M}$ phase, then each point in the constellation has a multiplicative inverse. Thus if one constellation point is multiplied by the complex inverse of another constellation point, the resultant point will contain their phase difference.

The current transmitted constellation point, D_n, can be formed as

$$\begin{aligned} D_n &= C_n \cdot \frac{1}{D_{n-1}^*} \\ &= C_n \cdot \frac{D_{n-1}}{|D_{n-1}|^2} \end{aligned} \tag{2.15}$$

where C_n is the current TCM constellation point.

At the receiver C_n can be estimated as follows:

$$\hat{C}_n = \hat{D}_n \cdot \hat{D}_{n-1}^* \tag{2.16}$$

The differential detector shown in Figure 2.8 performs this complex multiplication while translating the signal from the carrier frequency to baseband. In this manner, an estimate of the transmitter's TCM constellation is recreated for use by the Viterbi decoder [16].

For 16-PSK, this encoding scheme ensures that both the transmit constellation and the differentially decoded product constellation are identical. Although the differential decoder lowers the SNR of the received signal, it still produces a 16-PSK constellation for use by the Viterbi decoder.

Before applying differential detection to our earlier coding gain predictions for TC-(8,4)-16-PSK, we will first develop a model to explain the effects of differential detection on the Viterbi decoder used in the reception of TCM signals.

2.4 Development of a Noise Model

In this section we present an analytical model to explain the performance differences between coherent and differentially coherent trellis-coded PSK. We will expand upon this model in Chapter 3 to determine the changes that are necessary to make a DTC-2M-PSK Viterbi decoder work with the new DTC-M-M-PSK codes.

2.4.1 Differential Demodulation

We will start with the general equivalent baseband representation for the uncoded PSK signal set as provided by Proakis [14]:

$$s_m(t) = Re\{u(t) \exp\ \mathrm{j}[2\pi f_c t + \frac{2\pi}{M}(m-1) + \lambda]\},\ \text{for } m = 1, 2, ...M \qquad (2.17)$$

where $u(t)$ is the baseband equivalent representation for the transmitter pulse shape and λ is an arbitrary phase offset. The corresponding transmitter output for a coded 2M-PSK signal would be

$$s_m(t) = Re\{r_m(t) \exp\ \mathrm{j}[2\pi f_c t + \theta_m + \lambda]\},\ \text{for } m = 1, 2, ...(2M) \qquad (2.18)$$

where the parameter $r_m(t)$ is the envelope for individual channel symbols. Although these are all the same value for 2M-PSK, this notation will facilitate the introduction of M-M-PSK channel symbols in Chapter 3.

These $(2M)$ waveforms are based on the 2M-PSK constellation points $D_m(t) = r_m(t)\mathrm{e}^{\,\mathrm{j}\theta_m}$. Thus $D_m(t)$ is the complex representation of the m^{th} 2M-PSK constellation point. When it is more convenient, the amplitude ($r_m(t)$) and the phase (θ_m) will be used instead.

The above equation could also be expressed as:

$$s_m(t) = Re\{D_m(t) \exp\ \mathrm{j}[2\pi f_c t + \lambda]\},\ \text{for } m = 1, 2, ...(2M) \qquad (2.19)$$

where the θ_m parameter is included within $D_m(t)$.

When the amplitude function, $r_m(t)$, has a constant value for each signalling interval the above equation can be written as:

$$s_m(t) = A_{c,m} \cos(2\pi f_c t) - A_{s,m} \sin(2\pi f_c t),\ \text{for } m = 1, 2, ...(2M) \qquad (2.20)$$

This is equation (4.2.90) from Proakis [14]. For 2M-PSK we have:

$$A_{c,m} = r_m \cos(\theta_m + \lambda), \text{ for } m = 1, 2, ...(2M) \tag{2.21}$$

$$A_{s,m} = r_m \sin(\theta_m + \lambda), \text{ for } m = 1, 2, ...(2M) \tag{2.22}$$

Consider now the receiver shown in Figure 2.10. We will assume no ISI and no carrier phase jitter. Consequently the received signal $y(t)$ is equal to the transmitted signal plus bandlimited noise. Dropping the subscript to obtain the general case, we have:

$$y(t) = s(t) + n(t) \tag{2.23}$$

The differential demodulator uses a delayed version of this signal to produce the in-phase and quadrature estimates of the product space signal. After the low pass filtering these two branches represent the complex signal:

$$p(t) = p_I(t) + \mathrm{j} \cdot p_Q(t) \tag{2.24}$$

where $p_I(t)$ and $p_Q(t)$ are the in-phase and quadrature components of the signal, respectively.

Since this is the signal that will be processed by the Viterbi decoder, it is necessary to determine the effects of signal statistics and noise statistics on $p(t)$. Let us first examine $p_I(t)$ and $p_Q(t)$ for the case of no noise.

$$\begin{aligned}
p_I(t) &= [s(t) \cdot s(t-T)]_{LPF} \\
&= \{[A_c(t)\cos(2\pi f_c t) - A_s(t)\sin(2\pi f_c t)] \times \\
&\quad [A_c(t-T)\cos(2\pi f_c(t-T)) - \\
&\quad A_s(t-T)\sin(2\pi f_c(t-T))]\}_{LPF} \\
&= \frac{1}{2}[A_c(t)A_c(t-T) + A_s(t)A_s(t-T)]\cos(2\pi f_c T) + \\
&\quad \frac{1}{2}[A_s(t)A_c(t-T) - A_c(t)A_s(t-T)]\sin(2\pi f_c T)
\end{aligned} \tag{2.25}$$

Let us denote $s_h(t)$ to be the Hilbert transform of $s(t)$. Then for $p_Q(t)$ we have:

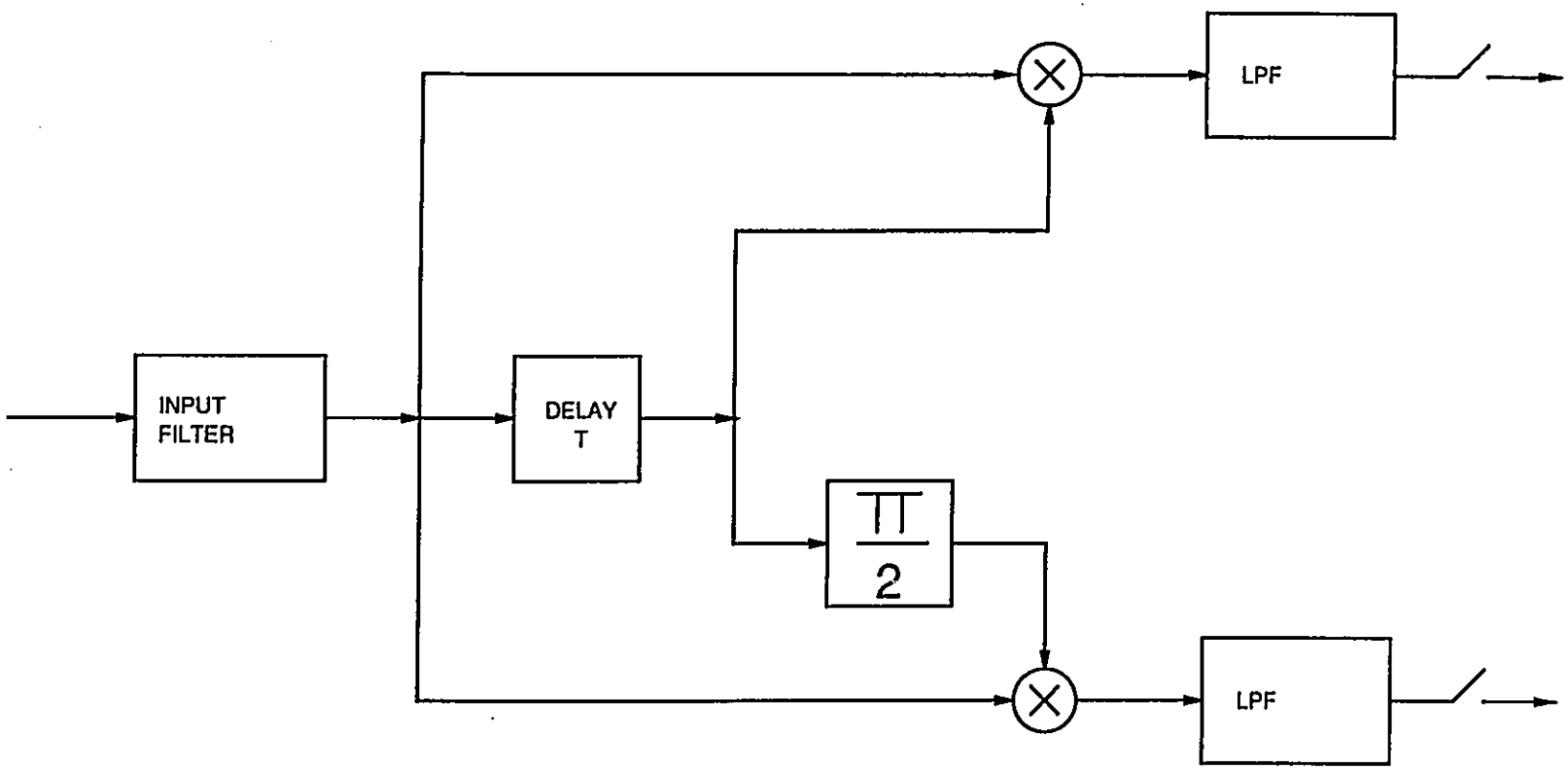

Figure 2.10: Differential Demodulator

$$
\begin{aligned}
p_Q(t) &= [s(t) \cdot s_h(t-T)]_{LPF} \\
&= \{[A_c(t)\cos(2\pi f_c t) - A_s(t)\sin(2\pi f_c t)] \times \\
&\quad [A_c(t-T)\sin(2\pi f_c(t-T)) + \\
&\quad A_s(t-T)\cos(2\pi f_c(t-T))]\}_{LPF} \\
&= \frac{1}{2}[A_c(t)A_s(t-T) + A_s(t)A_c(t-T)]\cos(2\pi f_c T) + \\
&\quad \frac{1}{2}[A_c(t)A_c(t-T) - A_s(t)A_s(t-T)]\sin(2\pi f_c T)
\end{aligned}
\tag{2.26}
$$

Now if we chose a sampling rate of $T = \frac{k}{f_c}$, where k is some integer, $\cos(2\pi f_c T) = 1$ and $\sin(2\pi f_c T) = 0$. This leads to

$$p_{I,n} = \frac{1}{2}[A_{c,n}A_{c,n-1} + A_{s,n}A_{s,n-1}] \tag{2.27}$$

$$p_{Q,n} = \frac{1}{2}[A_{c,n}A_{s,n-1} - A_{s,n}A_{c,n-1}] \tag{2.28}$$

If we then make use of the above definitions for A_c and A_s from equations (2.21) and (2.22) respectively, we obtain:

$$p_{I,n} = r_n \cdot r_{n-1}\cos(\theta_n - \theta_{n-1}) \tag{2.29}$$

$$p_{Q,n} = r_n \cdot r_{n-1}\sin(\theta_n - \theta_{n-1}) \tag{2.30}$$

Combining $p_{I,n}$ and $p_{Q,n}$ to obtain p_n we get:

$$
\begin{aligned}
p_n &= r_n \cdot r_{n-1}[\cos(\theta_n - \theta_{n-1}) + \mathrm{j} \cdot \sin(\theta_n - \theta_{n-1})] \\
&= D_n \cdot D_{n-1}^* \\
&= E_n
\end{aligned}
\tag{2.31}
$$

where E_n is the 2M-PSK product constellation point at the n^{th} time instant in the absence of noise. For PSK constellations the differential demodulator reverses the phase difference encoding performed by the modulator such that

$$E_n = C_n \tag{2.32}$$

where C_n is the original TCM constellation point. In Chapter 3 we will re-evaluate this phenomenon using a non-PSK transmit constellation.

2.4.2 Effects of Noise

In this section we develop a model for the noise that will be present in 2M-PSK product space. The objective is to define the assumptions which are necessary to easily evaluate the effects of DTC-2M-PSK on path distances in a Viterbi decoder trellis.

After differential demodulation the product space points are represented as $p(t) = \tilde{D}(t) \cdot \tilde{D}^*(t-T)$ where $\tilde{D}(t)$ is what the receiver perceives as the transmitted constellation point $D(t)$.

In actual fact

$$\tilde{D}(t) = D(t) + n_R(t) \tag{2.33}$$

where $n(t)$ is channel noise which passes through the receiver's bandpass input filter – possibly matched to the transmitter's pulse shaping – to produce $n_R(t)$. Consequently

$$\begin{aligned} p(t) &= [D(t) + n_R(t)] \cdot [D^*(t-T) + n_R^*(t-T)] \\ &= D(t) \cdot D^*(t-T) + D(t) \cdot n_R^*(t-T) + n_R(t) \cdot D^*(t-T) + n_R(t) \cdot n_R^*(t-T) \end{aligned} \tag{2.34}$$

Now after sampling we obtain

$$p_n = E_n + n_{P_n} \tag{2.35}$$

where

$$E_n = D(t) \cdot D^*(t-T) \mid_{t=nT} \tag{2.36}$$

and

$$n_{P_n} = [D(t) \cdot n_R^*(t-T) + n_R(t) \cdot D^*(t-T) + n_R(t) \cdot n_R^*(t-T)] \mid_{t=nT} \tag{2.37}$$

The n_{P_n} values are the noise samples associated with these product constellation points. This expression can be further simplified to

$$n_{P_n} = D_n \cdot n_{R_{n-1}}^* + D_{n-1}^* \cdot n_{R_n} + n_{R_n} \cdot n_{R_{n-1}}^* \tag{2.38}$$

where D_n and D^*_{n-1} are the transmit constellation points. Since we are dealing with PSK constellations, each of these complex values have unit amplitude.

To facilitate the calculation of trellis free distances, it is helpful to further simplify the noise model for $n_R(t)$ – the noise prior to differential demodulation. The first assumption we will make is that subsequent noise samples are independent. This assumption may not be completely valid when the effect of the receiver bandpass filtering is considered.

However Lucky et al [32] indicate that although receiver filters cause some spreading of the noise autocorrelation function, its value is still very close to zero at $t = kT(k \neq 0)$ – provided the overall response is Nyquist and the filtering is equally split between the transmitter and receiver. Park [33] has further analyzed the effects of receiver filters on the performance of DPSK. Both of these sources support the premise that – even after filtering – noise samples which are one sample apart are independent. Grami et al [34] concur by showing that the noise autocorrelation function will be zero at other sampling instants provided the square of the receive filter frequency response is Nyquist.

This assumption can be summarized as follows:

$$E\{n_R(t), n_R(t-kT)\} = \rho_{n_R}(k) \approx 0, \text{ for } k \geq 1 \tag{2.39}$$

Statistics of n_P

The expectation of n_P can be evaluated as follows:

$$\begin{aligned} E\{n_P\} &= E\{D_n n^*_{n-1} + D^*_{n-1} n_n + n_n n^*_{n-1}\} \\ &= D_n \cdot E\{n^*_{n-1}\} + D^*_{n-1} \cdot E\{n_n\} + E\{n_n\} \cdot E\{n^*_{n-1}\} \\ &= 0 \end{aligned} \tag{2.40}$$

The variance of n_P can be evaluated as follows:

$$\begin{aligned} \sigma^2_{N_P} &= \frac{1}{2} \cdot E\{|n_P|^2\} \\ &= \frac{1}{2} \cdot E\{n_P \cdot n^*_P\} \\ &= \frac{1}{2} \cdot E\{[D_n n^*_{n-1} + D^*_{n-1} n_n + n_n n^*_{n-1}] \cdot [D^*_n n_{n-1} + D_{n-1} n^*_n + n^*_n n_{n-1}]\} \\ &= \frac{1}{2}[D_n D^*_n \cdot E\{n^*_{n-1} n_{n-1}\} + D^*_{n-1} D_{n-1} \cdot E\{n_n n^*_n\} + E\{n_n n^*_n\} \cdot E\{n^*_{n-1} n_{n-1}\}] \\ &= \sigma^2_N[|D_n|^2 + |D_{n-1}|^2 + \sigma^2_N] \end{aligned} \tag{2.41}$$

The autocorrelation of n_P is:

$$\begin{aligned} R_{N_P}(1) &= E\{n_{P_n} \cdot n^*_{P_{n-1}}\} \\ &= E\{[D_n n^*_{n-1} + D^*_{n-1} n_n + n_n n^*_{n-1}] \cdot \\ &\quad [D^*_{n-1} n_{n-2} + D_{n-2} n^*_{n-1} + n^*_{n-1} n_{n-2}]\} \\ &= D_n D_{n-2} \cdot E\{n^*_{n-1} n^*_{n-1}\} \\ &= D_n D_{n-2} \cdot [\frac{1}{2}\sigma_{Re\{n\}} - \frac{1}{2}\sigma_{Im\{n\}} - \mathrm{j}E\{Re\{n\}\} \cdot E\{Im\{n\}\}] \cdot \sigma_{Re\{n\},Im\{n\}} \\ &= 0 \end{aligned} \tag{2.42}$$

This can be stated as:

$$\rho_{N_P}(1) = 0 \tag{2.43}$$

Although $\rho_{N_P}(1) = 0$ can be shown that

$$\rho_{Re\{n_P\},Re\{n_P\}}(1) = \frac{1}{2} \cdot Re\{D_n D^*_{n-2}\} \cdot \sigma_N^2 \tag{2.44}$$

$$\rho_{Re\{n_P\},Im\{n_P\}}(1) = \frac{1}{2} \cdot Im\{D_n D^*_{n-2}\} \cdot \sigma_N^2 \tag{2.45}$$

$$\rho_{Im\{n_P\},Re\{n_P\}}(1) = \frac{1}{2} \cdot Im\{D_n D^*_{n-2}\} \cdot \sigma_N^2 \tag{2.46}$$

$$\rho_{Im\{n_P\},Im\{n_P\}}(1) = \frac{1}{2} \cdot Re\{D_n D^*_{n-2}\} \cdot \sigma_N^2 \tag{2.47}$$

In a similar fashion it can be shown that for $k \geq 2$

$$\rho_{N_P}(k) = 0 \tag{2.48}$$

It is also easy to show that for a time separation of 2 symbol periods or greater ($k \geq 2$) there is no correlation between the various real and imaginary components of n_P.

Application of the Noise Model to Trellis Metrics

Before applying the above results to trellis branch metrics we will make one further assumption. Our objective is to facilitate the evaluation of trellis free distances for a variety of 2M-PSK constellations and trellises. Consistent with the literature, we seek a performance measure for the asymptotic case of high SNR. These results will be used to select a candidate constellation and trellis that will then undergo simulation to determine its performance over the entire range of practical SNR values.

For the high SNR case we discount the $Noise \times Noise$ term in equation (2.38) and approximate n_P as follows:

$$n_P \approx D_n n_{n-1}^* + D_{n-1}^* n_n \tag{2.49}$$

This simplifies equation (2.41) to produce the following noise variance:

$$\begin{aligned} \sigma_{N_P}^2 &\approx \sigma_N^2[|D_n|^2 + |D_{n-1}|^2] \\ &\approx \sigma_N^2[r_n^2 + r_{n-1}^2] \end{aligned} \tag{2.50}$$

Since $r_n^2 = 1$ and $r_{n-1}^2 = 1$ this can be written as

$$\sigma_{N_P}^2 = 2 \cdot \sigma_N^2 \tag{2.51}$$

Consequently for high SNR and differential detection, the symbol error probability can be estimated as follows:

$$\begin{aligned} P_e &= N_{free} \cdot Q(\frac{d_{free,coh}}{2\sigma_{N_P}}) \\ &= N_{free} \cdot Q(\frac{d_{free,coh}}{2\sqrt{2}\sigma_N}) \end{aligned} \tag{2.52}$$

For the purposes of comparison with other trellis codes – both coherent and differentially coherent – we instead express it as

$$P_e = N_{free} \cdot Q(\frac{d_{free,dd}}{2\sigma_N}) \tag{2.53}$$

where

$$d_{free,dd} \equiv \frac{d_{free,coh}}{\sqrt{2}} \tag{2.54}$$

Throughout this thesis we will use d_{free} to mean $d_{free,coh}$ or $d_{free,dd}$, depending on whether coherent or differential detection applies.

In terms of Viterbi decoder branch metrics, we obtain the following expression for the differential detection case:

$$\begin{aligned} \mu_{E_n,dd} &= \frac{1}{2} \cdot d^2(E_n, p_n) \\ &= \frac{1}{2} \cdot \mu_{E_n,coh} \end{aligned} \tag{2.55}$$

In view of the simple scaling factor between the metrics for the coherent and differentially coherent case, we can use the same Viterbi decoder in either situation. In Chapter 3 we will find that such is not the case for the new family of DTC-M-M-PSK codes.

Application of the Noise Model to DTC-(8,4)-16-PSK

Earlier in section 2.14 we obtained the following lower bound on the free distance for coherent TC-(8,4)-8-PSK:

$$d^2_{free,coh} = 1.3238 \tag{2.56}$$

In view of the above analysis, we can state that the lower bound on the trellis free distance in the differentially coherent case is

$$\begin{aligned} d^2_{free,dd} &= \frac{d^2_{free,coh}}{2} \\ &= 0.6619 \end{aligned} \tag{2.57}$$

This free distance for DTC-(8,4)-16-PSK will be used again in Chapter 3 when we compare it against its DTC-M-M-PSK counterpart.

2.5 Performance of Trellis-coded PSK

In this section we will consider some of the performance gains that have been achieved to date using various combinations of trellis coding, differential detection and PSK constellations.

Table 2.1 shows the asymptotic coding gains predicted for PSK trellis codes developed by Ungerboeck [3]. Although the asymptotic coding gain increases with the number of states in the trellis, most of the gain over uncoded transmission or traditional channel coding is achieved using relatively few trellis states. The results for 4-, 8- and 16-states correspond to the trellises shown earlier in Figures 2.2, 2.3 and 2.4, respectively.

It is worth noting that at practical bit error rates the actual coding gain may be significantly less than that for asymptotically high SNR. Figure 2.11 shows a comparison by Ungerboeck [2] between the simulated performance of his 4-state 8-PSK and the asymptotic prediction. At an error rate of 10^{-3} the simulation showed a coding gain of only 2.2 dB compared to the asymptotic value of 3 dB.

Table 2.2 shows Ungerboeck coding gains for QASK modulation formats. For each trellis size, QASK shows a higher coding gain than PSK. This can be attributed to the better utilization of the two-dimensional constellation in the case of QASK. As the size of a PSK

TABLE II
CODES FOR PHASE MODULATION
8-PSK: $\{\Delta_i, 0 \le i \le 2\} = 2\sin(\pi/8), \sqrt{2}, 2$;
16-PSK: $\{\Delta_i, 0 \le i \le 3\} = 2\sin(\pi/16), 2\sin(\pi/8), \sqrt{2}, 2$.

No. of states 2^ν	$\bar{m}$	Parity-check coefficients $\underline{h}^2$	$\underline{h}^1$	$\underline{h}^0$	d^2_{free}/Δ_0^2	Asympt. coding gain [dB] $G_{8PSK/4PSK}$ (m=2)	$G_{16PSK/8PSK}$ (m=3)	N_{free} (m→∞)
4	1	—	2	5	4.000*	3.01	—	1
8	2	04	02	11	4.586	3.60	—	2
16	2	16	04	23	5.172	4.13	—	≈2.3
32	2	34	16	45	5.758	4.59	—	4
64	2	066	030	103	6.343	5.01	—	≈5.3
128	2	122	054	277	6.586	5.17	—	≈0.5
256	2	130	072	435	7.515	5.75	—	≈1.5
4	1	—	2	5	1.324	—	3.54	4
8	1	—	04	13	1.476	—	4.01	4
16	1	—	04	23	1.628	—	4.44	8
32	1	—	10	45	1.910	—	5.13	8
64	1	—	024	103	2.000*	—	5.33	2
128	1	—	024	203	2.000*	—	5.33	2
256	2	374	176	427	2.085	—	5.51	≈8.0

Table 2.1: Asymptotic Coding Gains for Ungerboeck PSK codes (reproduced from Ungerboeck [3])

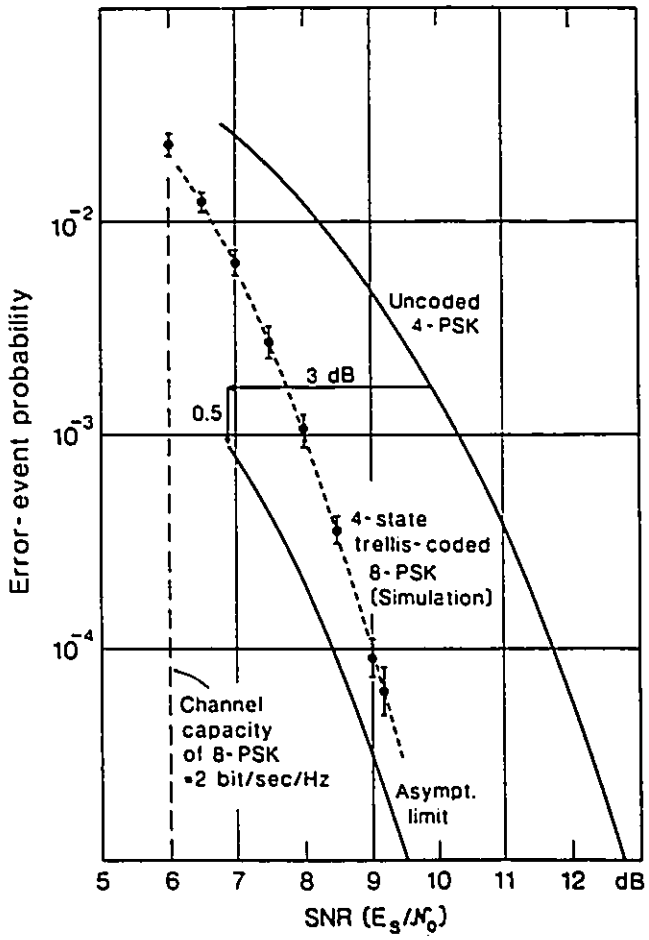

Figure 2.11: Comparison of Asymptotic and Simulated Performance for TC-(4,2)-8-PSK (reproduced from Ungerboeck [2])

TABLE III
CODES FOR TWO-DIMENSIONAL MODULATION WITH "Z_2" SIGNALS,
$\{\Delta_i, 0 \le i \le 3\} = \Delta_0, \sqrt{2}\,\Delta_0, \sqrt{4}\,\Delta_0, \sqrt{8}\,\Delta_0$.

No. of states 2^ν	$\tilde{m}$	Parity-check coefficients $\underline{h}^2$	$\underline{h}^1$	$\underline{h}^0$	d^2_{free}/Δ_0^2	Asympt. coding gain [dB] $G_{16QA/8PSK}$ (m=3)	$G_{32CR/16QA}$ (m=4)	$G_{64QA/32CR}$ (m=5)	$G_{C/U}$ (m→∞)	N_{free} (m→∞)
4	1	—	2	5	4.0*	4.36	3.01	2.80	3.01	4
8	2	04	02	11	5.0	5.33	3.98	3.77	3.98	16
16	2	16	04	23	6.0	6.12	4.77	4.56	4.77	56
32	2	10	06	41	6.0	6.12	4.77	4.56	4.77	16
64	2	064	016	101	7.0	6.79	5.44	5.23	5.44	56
128	2	042	014	203	8.0	7.37	6.02	5.81	6.02	344
256	2	304	056	401	8.0	7.37	6.02	5.81	6.02	44
512	2	0510	0346	1001	8.0*	7.37	6.02	5.81	6.02	4

Table 2.2: Asymptotic Coding Gains for Ungerboeck QASK codes (reproduced from Ungerboeck [3])

constellation is increased, the sequence of TCM Δ-parameters begins to approximate that of one-dimensional modulation. Consequently, based on information theory, one would expect the codes with less dimensionality – TC-2M-PSK – to have lower performance. In Chapter 3 we will evaluate a modification to TC-2M-PSK which increases both its dimensionality and performance.

Wilson et al [13] have further analyzed trellis coded performance using PSK constellations. Their results show that on an AWGN channel, PSK constellations can achieve their highest asymptotic coding gains using trellises with only two sets of branches per state. They predict that this trend will continue until the trellis contains 128-states or more.

McLane et al [25] have considered the application of trellis coded PSK to mobile channels with multipath fading, shadowing and Doppler carrier shifts. In contrast to Wilson's results for the AWGN channel, best performance was achieved using trellises employing a maximum number of branches per state. Although these codes are not optimum for an ideal Gaussian channel, they prove to be more robust in a practical mobile communications environment. The codes considered in this thesis are all of this type.

Divsalar and Simon [21] [22] have also considered trellis-coded PSK for satellite and mobile applications. Their work with Yuen [31] on asymmetric trellis-coded PSK is of particular interest because of its relationship to the DTC-M-M-PSK codes that will be introduced in Chapter 3.

2.6 Limitations of DTC-2M-PSK

In spite of the significant coding gains that were achieved when trellis-coding was first applied to PSK signals, a number of drawbacks do exist, particularly when differential detection is also used.

With recent technological advances, larger constellation sizes are being employed to achieve existing channel performance using less bandwidth. At present many satellite and mobile applications utilize 4-PSK or 8-PSK. The use of 16-point constellations may soon become widespread.

However as PSK constellation sizes increase they behave more and more like one-dimensional modulation. The uncoded 16-point PSK constellation is often regarded as

inferior to other less restrictive two-dimensional modulation formats. For example, on an average energy basis it is inferior to uncoded 16-QASK.

When trellis coding is applied to these constellations, the performance discrepancy increases. The reason becomes apparent when their TCM Δ-sequences are considered. For QASK the sequence of Δ-parameters, normalized with respect to Δ_0, is $\{1, \sqrt{2}, \sqrt{4}, \sqrt{8}\}$. The corresponding sequences for one dimensional 16-level PAM and 16-PSK are $\{1, 2, 4, 8\}$ and $\{1, 2.00, 206.34, 291.81\}$, respectively.

As the PSK constellation size is increased, the initial parameters in its Δ-sequence approach that of one dimensional modulation. Now the average constellation is related to the largest Δ-parameter in the sequence; in the case of a 16-point constellation this is Δ_3. Because QASK has a more gradual increase in its Δ-parameters, for the same average constellation energy it has larger low-order Δ-parameters. For most trellis codes, only Δ_0 and Δ_1 appear in the expression for trellis free distance. Consequently QASK trellis codes will in general outperform those of PSK and PAM when compared on an average energy basis.

Two chief advantages for PSK constellations are its improved resilience to non-linear channel characteristics and the simplicity with which differentially coherent detection can be implemented. However in view of its greater power efficiency, it would appear that there may be reason to consider the use of coherent trellis-coded 16-QASK instead of differentially coherent trellis-coded 16-PSK – even on non-linear channels. For some communication systems, the reduction in required transmitter power may be worth the additional receiver complexity and the losses associated with non-linear channel distortion.

In the next chapter we will consider a third alternative which retains many of the advantages of 16-PSK while achieving a differential detection performance that is more competitive when compared to other truly two-dimensional modulation schemes.

Chapter 3

Differentially Coherent Trellis-Coded M-M-PSK

3.1 Introduction

This chapter presents a new modulation type for use with differentially coherent trellis coding. Earlier chapters have laid the groundwork by identifying the advantages of trellis coding, differential demodulation, and PSK signal constellations. We will now define a modulation format which seeks to optimize the use of these three techniques.

This new modulation type is called Differentially Coherent Trellis-coded M-M-PSK (DTC-M-M-PSK). It enables an M symbol alphabet to be differentially encoded using a signal constellation which consists of two M-PSK sub-constellations – each with a different amplitude. It will be shown that such a transmit constellation can achieve larger path distances in a modified Viterbi decoder trellis compared to those possible with DTC-2M-PSK.

The DTC-2M-PSK noise model from Chapter 2 will be expanded to handle the case of DTC-M-M-PSK. With 2M-PSK, all signal points have the same amplitude – both in the transmit and product constellations. For M-M-PSK, signal points occur at 2 amplitudes in the transmit constellation and 3 amplitudes in the product constellation. During differential demodulation the noise and signal components from subsequent symbol periods will be multiplied together and the result is a noise power that is generally larger than that present with 2M-PSK.

After the above issues have been examined on an individual basis, we will then consider

their combined effect on the performance of a number of specific trellis codes.

3.2 Variations on TC-2M-PSK

Before dealing with the specific case of DTC-M-M-PSK, let us first consider some of the similar variations that have been reported in the literature. We are particularly interested in how these deviations affect the code distance properties associated with the original TC-2M-PSK code.

We start by reviewing the distance properties for TC-16-PSK. Figure 3.1 highlights all the basic TCM parameters for a trellis code using a 16-PSK constellation. Because of trellis symmetry and constellation symmetry, it is possible to specify the shortest error path for the trellis in terms of the squares of these distances.

The minimum distance between points from a pair of C-level subsets is determined by the B-level subset they have in common. This is because each point in a C-level subset has a nearest neighbour from each of the other C-level subsets which make up the other B-level subset. Consequently the distance is the same as that between B-level subsets.

This property does not hold at the D-level when using a PSK rather than QAM constellation. D-level subsets have only two nearest neighbour subsets from the other B-level subset. Consequently the distances to the other two D-level subsets must be greater than Δ_0. In the case of 8-PSK, these D-level subsets are individual constellation points.

Ungerboeck [1] has observed that there is typically no advantage to partitioning large constellations more than two or three times since the Δ_i values quickly exceed the best conceivable value for d_{free}. As a result it has generally been sufficient to consider all subsets of type B1 to have a distance Δ_0 from the all-zero correct path.

Now consider the effect when the phase offset between the $B0$ and $B1$ subsets is modified. Let ϕ' be defined as $\phi/(\frac{\pi}{M})$ where ϕ is the smallest phase spacing between a $B0$ point and a $B1$ point. Consequently ϕ' can be adjusted over the range from 0 to 1. The minimum spacing between C-level subsets is also modified when the phase relationship between $B0$ and $B1$ is adjusted. In the case of 8-PSK, as ϕ' is reduced from the usual 2M-PSK value of 0.5, the $C0$ subset becomes closer to the $C1$ subset and further from the $C3$ subset. In effect, two distances which we used to define as Δ_0 for a 2M-PSK constellation, must

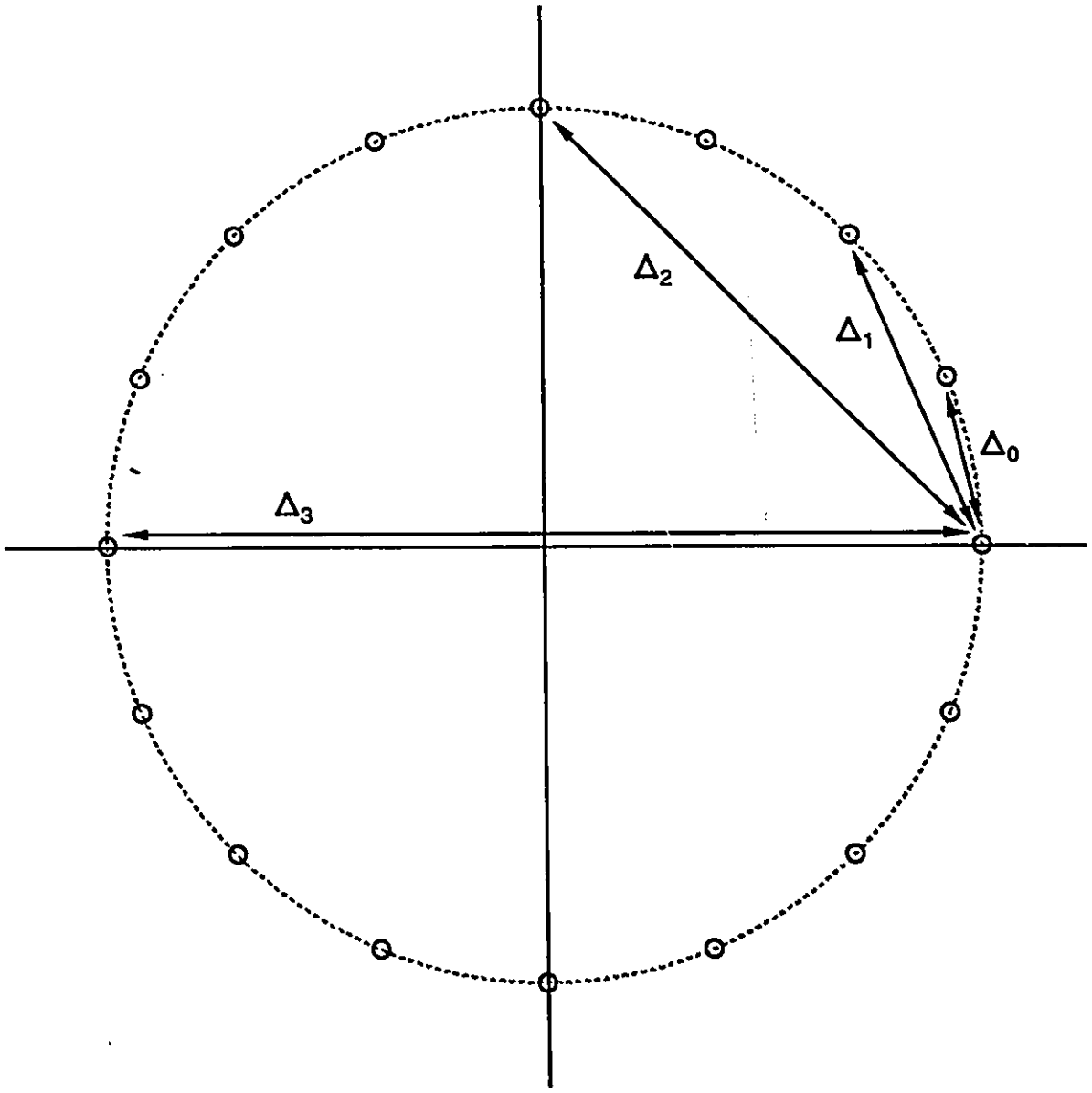

Figure 3.1: Distance Parameters for TC-16-PSK

now be specified individually as Δ_{C0-C1} and Δ_{C0-C3}. This is also evident in the work of Divsalar et al [10] with respect to coherent TC-2M-PSK with phase asymmetries.

Padovani and Wolfe [30] have explored techniques for combining both phase and frequency modulation using trellis coding. They have recognized that such deviations from the standard Ungerboeck constellation subsets alter the method used to evaluate trellis free distances. In their case, it was no longer possible to consider only the weights of potential error paths – namely their distance from an all-zero correct path. Because the code was no longer linear in Euclidean space, it was necessary to determine the minimum error path on the basis of all possible correct paths.

Chalid et al [19] have considered the case of coherent trellis coding with non-uniform phase spacing between PSK constellation points. In particular for an 8-point constellation, they varied the "twisted angle" between the $B0$ and $B1$ subsets as well as the angles, θ_1 and θ_2, between the C-level subsets within each of these B-level subsets. As with Padovani and Wolfe, they found that the codes were no longer linear in Euclidean space and it was necessary to consider a wider variety of possible correct paths. In their case it was necessary to consider both the all-zero and the all-one correct paths when evaluating trellis free distances with $\theta_1 \neq \theta_2$.

This "twisted angle" between B-level subsets is identical to the phase asymmetry angle cited by Divsalar and Simon [9] [31] with regard to trellis coded coherent PSK. It is also the same as the angle ϕ discussed in this thesis in the context of differentially coherent M-M-PSK codes.

Divsalar et al [31] also discuss the need to take into account the non-linearity of their asymmetric TC-2M-PSK codes and to collaborate analyses which use an all-zero correct path with tests using all other possible correct paths. Consequently the DTC-M-M-PSK analysis described later in this Chapter will be substantiated using simulation results.

3.3 Rationale for the M-M-PSK Constellation Format

Differential trellis-coded M-M-PSK is a logical next step to the use of trellis coding with PSK constellations and differential detection. It retains the advantages of trellis coding and differential detection while adjusting the transmit constellation to achieve better per-

formance with a specific alphabet size and encoder trellis.

The progression from DTC-2M-PSK to DTC-M-M-PSK does increase the number of product constellation points from $2M$ to $3M$. Usually it is desirable to minimize the number of points which must be processed by the Viterbi decoder. However, it is typically the Accumulate-Compare-Select portion of a Viterbi decoder which limits maximum receiver data rate [5]. Additional product space points have little impact on the Viterbi processing provided they do not result in an increase in the number of trellis states or branches.

Differentially coherent trellis-coded M-M-PSK does retain the many other advantages associated with PSK constellations. It can be implemented with a low peak-to-average energy ratio and can be differentially detected with a receiver that is marginally more complex than that required for DTC-2M-PSK.

It is precisely for these reasons that only one of many possible degrees of freedom are utilized when deviating from the PSK constellation format. Although an amplitude offset is permitted between the B-level subsets, DTC-M-M-PSK does not permit such amplitude deviations between lower level constellation subsets.

Divsalar and Simon [9] [31] have analysed the performance of coherent TC-2M-PSK when the angle between B-level subsets is adjusted. However they have not evaluated the combined use of differentially coherent detection and subset dilation. Instead their work has been restricted solely to using that one degree of freedom which does not lead to an increase in average constellation energy.

The chief advantage in using a PSK constellation is that it is closed under multiplication. This is strictly true only if the points lie on the unit circle in the complex plane and the point nearest the real axis has a phase of 0 or $\pi/(2M)$.

However even if these conditions are not met, the constellation still has the desirable property that if one set of $2M$ points is multiplied by another constellation set of $2M$ points, the result is a product constellation which is also PSK and contains only $2M$ points. As a result the overall effect of differential encoding and decoding has not increased the number of points in the constellation which the receiver uses to make decisions – the product constellation. If phase difference encoding is used, it has not altered the relative distances between pairs of constellation subsets. Consequently differential TC-2M-PSK can employ

a Viterbi decoder trellis that is identical in structure to its coherent counterpart. This will not be true for DTC-M-M-PSK.

The DTC-2M-PSK differential demodulator acts on up to $(2M)^2$ combinations of transmit symbol pairs. However, because many of the product points overlap, the resultant $(2M)^2$ point product constellation consists of sets of $2M$ points at each of $2M$ distinct locations. To achieve this desirable result it is only necessary to ensure that the $2M$ points in the transmit constellation are all at the same amplitude and are uniformly spaced in phase.

The objective in deviating from the PSK transmit constellation is to achieve better error path distances in the receiver's Viterbi decoder trellis by exploiting the structure of the encoder trellis. However the desire to utilize a similar trellis structure in both the encoder and Viterbi decoder does place some restrictions on the transmit constellation points. We will now consider the advantage in restricting these deviations from PSK to the overall 16-point constellation only, and not to the lower level subsets.

Consider first the individual constellation points for trellis-coded 16-PSK. These would correspond to E-level subsets if the trellis code required subset partitioning to that level. The product of any pair of E-level subsets would result in a product constellation subset containing but one point. If the previous symbols E-level subset was known, the current TCM point could be uniquely identified for any given state in the trellis.

Consider next the D-level in the subset partitioning tree for trellis-coded 16-PSK. Each of these D-level subsets contains two points. For differential TCM it is desirable to ensure that these pairs of points have the same amplitude and a phase separation of π radians. If this rule is observed, the multiplication of any two subsets at this level will result in a product space subset which also contains but two points. Figure 3.2 illustrates this principle by showing the resultant product constellation subsets for the various combinations of amplitude and phase offsets. In cases where either the amplitude or phase are modified, the result will be product space D-level subsets which contain at least 3 points. Only imposing the PSK restriction can prevent the product space subsets from having more points than the original TCM subsets.

Now if the Viterbi decoder can determine via the receive trellis that a specific subset

BEFORE DIFFERENTIAL DEMODULATION

AFTER DIFFERENTIAL DEMODULATION

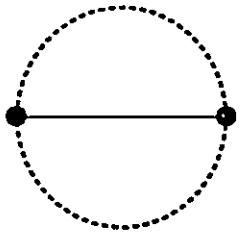

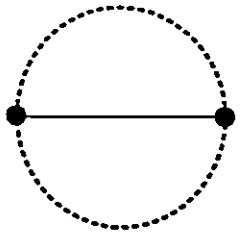

a) No Offsets

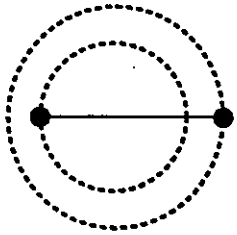

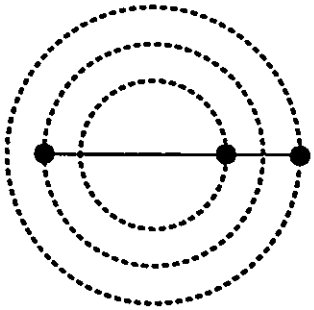

b) Amplitude Offset Only

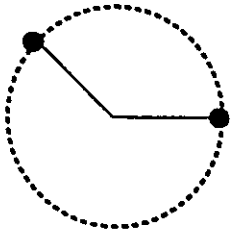

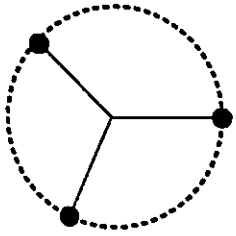

c) Phase Offset Only

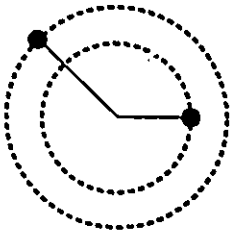

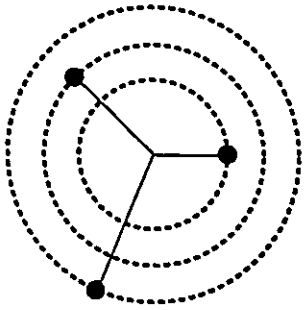

d) Amplitude and Phase Offset

Figure 3.2: Effect of Amplitude and Phase Offsets on D-level Subsets

preceded the current subset, it will only be necessary to evaluate one branch metric for each point in the current TCM subset. For trellis paths for which the previous subset is different, it will have to evaluate a different set of branch metrics, but in all cases the number of branch metrics will equal the number of points in the current TCM subset.

The point being emphasized is that it is necessary to impose the PSK restriction on TCM subsets at this level to ensure that the receiver's Viterbi decoder trellis will not require more trellis branches per state than does the Viterbi decoder trellis used for coherent detection. If we can maintain the same number of trellis branches we will not cause an increase in the complexity of the receiver.

Consider the next higher level of constellation subsets. Once again the points in these C-level should all have equal amplitude and uniform phase spacing. Consequently if the subsets of this level form parallel branches in the trellis, the differential encoding/decoding will not have increased the number of branches that must be evaluated.

These reasons for maintaining PSK-type subset constellations are valid at all levels at which the subsets contain M points or less. Thus it applies to all levels up to and including the B-level.

However the PSK restriction is not necessary at the highest level because for any given state in the trellis, the preceding symbol is restricted to a subset containing at most M points. Since this preceding subset is PSK-type, multiplying it by the current subset will produce a product subset which is another PSK ring with the same number of points as the current subset.

In the case of rate m/(m+1) trellis coding – used almost exclusively -- the major $B0$ and $B1$ subsets are required to be M-PSK. However we are free to alter the amplitude relationship between these major subsets without forcing an increase in the number of branches per state in the trellis. Consequently we have retained a degree of freedom which can be used to optimize the transmit constellation for a specific alphabet size and trellis.

For the rare cases in which trellis coding is used with rate $m/(m+2)$, these subset dilation techniques could be used on C-level subsets in a constellation with $4M$ points. However in product space this could lead to $20M$ points at up to 10 different amplitudes. Consequently all further discussion will be restricted to the more practical m/(m+1) case.

It is important to note that altering the amplitude ratio between $B0$ and $B1$ will affect the average energy of the constellation. As a result, any gains in trellis squared free distance must be large enough to compensate for increases in constellation energy. By contrast the free distance can be adjusted by changing the phase offset between $B0$ and $B1$ with no impact on the constellation energy.

It is worth noting that designing constellations for communication systems employing sequence estimation – or coded systems in general – many of the design criteria used with symbol-by-symbol detection are no longer appropriate.

For example, for constellations with greater than 4 points, MPSK in no longer optimum in terms of minimum distance and average constellation energy. However in terms of free distance for trellis codes the minimum distance, Δ_0^2, is only one of several parameters which must be jointly optimized. In general the techniques of Foschini et al [27], Forney et al [11], and Melvil et al [29], optimize the quantity Δ_0^2/E_{ave} but greatly attenuate other normalized TCM parameters such as Δ_1^2/E_{ave} and Δ_2^2/E_{ave}. These latter quantities are typically much larger than Δ_0^2/E_{ave} and have a much greater effect on TCM code distance properties.

Because with TCM, coding and modulation are no longer uncoupled, it is necessary to instead use techniques such as those described by Divsalar et al [9] [31], Chalid et al [19], and Padovani and Wolfe [30] to determine overall code performance for various changes in modulation format.

3.4 Differential Encoding

The above analysis determined that for differential TCM the optimum constellations are those in which each of the two B-level subsets form M-PSK constellations. It was not possible for the general case to specify the optimum amplitude relationship between these B-level subsets because that is dependent on the constellation size, M, the encoder trellis and the specific differential encoding strategy. In this section we will determine how the differential encoding strategy affects the TCM distance parameters in the product space constellation that will be used by the receiver's Viterbi decoder. For the purposes of this exercise we will use an 8-8-PSK constellation.

The advantages in using differential encoding and detection on mobile channels has

been discussed earlier. Our additional objective in selecting a specific differential encoding strategy is to control the locations at which a specific TCM symbol can appear in the product constellation. In general we wish to minimize the number of locations at which a specific TCM symbol can appear in product space since this will mean less processing for the Viterbi decoder. However it will be demonstrated that there are other free distance considerations that would favour multiple representation of TCM symbols for a specific constellation and trellis. For M-M-PSK, the product constellation uses $3M$ points to represent $2M$ symbols. Consequently some TCM symbols will of necessity have two possible locations in the product constellation.

We will now consider how these product space representations affect the distance properties of the trellis code. We will consider only the phase difference encoding technique described for PSK in Chapter 2 and we will determine the effects on the product constellation and receive trellis.

Phase Difference Encoding

Consider the case of the 8-8-PSK constellation whose transmit and product space constellations are shown in Figure 3.3. This constellation is 8-8-PSK with $r_B = 1.638$. For these specific parameters, the diagram shows TCM symbol assignments that would give good distance parameters for most trellises. These correspond to a phase difference encoding strategy similar to that commonly used for 2M-PSK.

The subset partitioning tree for the TCM constellation – before differential encoding – was shown earlier in Figure 2.5. Because part of the signal constellation has been dilated, the subset partitioning for the transmit constellation is as shown in Figure 3.4. Subset labels are not shown for the various sub-constellations because any TCM constellation subset could be mapped into any of the transmit constellation subsets. For example, the $D0$ TCM subset could map into any of the D-level subsets in the transmit constellation, depending on which transmit constellation symbol preceded it. This would suggest that performance will be limited by the intra-subset distance of the smaller D-level sub-constellations on the left side of the partitioning tree. It would appear, from this diagram, that the only distance increase achieved by subset dilation is the increase in Δ_0 – the distance between the $B0$ subset and

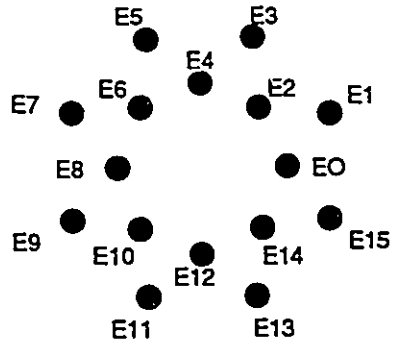

a) TCM Constellation (before differential encoding)

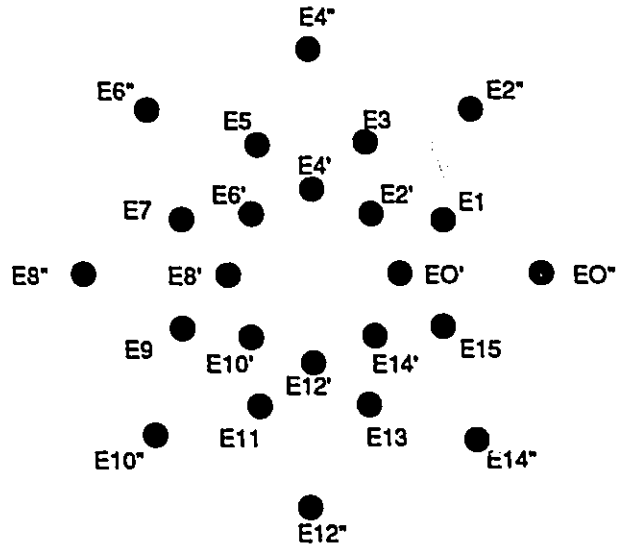

b) Product Constellation (after differential encoding)

Figure 3.3: Effect of Phase-Difference Encoding on the DTC-8-8-PSK Product Constellation

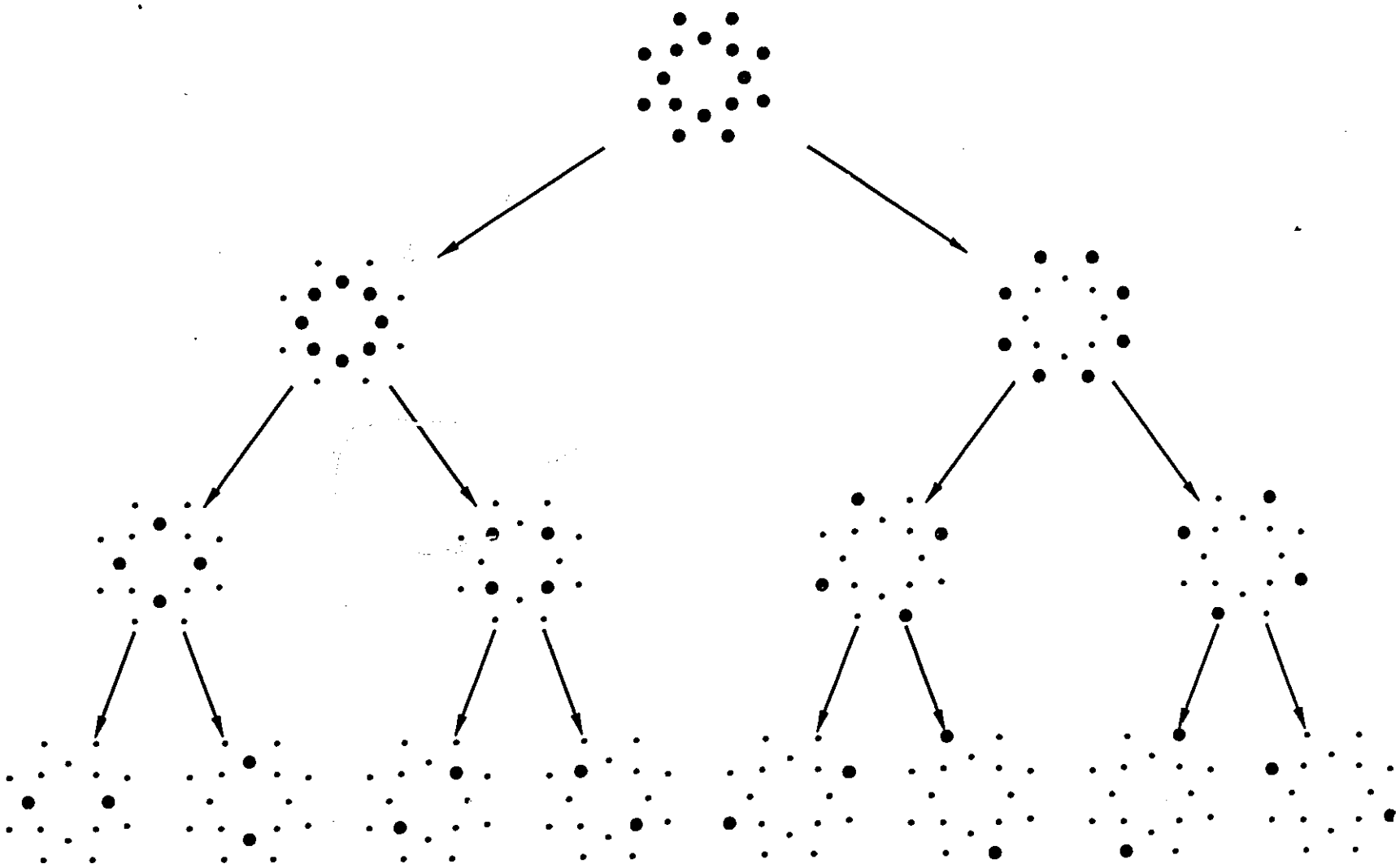

Figure 3.4: Subset Partitioning Tree for the 8-8-PSK Transmit Constellation

the dilated $B1$ subset. However the differential encoding and decoding process ensures that additional distance increases are possible.

After differential decoding, all of the TCM constellation subsets have rotated back to their original phase locations. This is shown in Figure 3.5 However, because of subset dilation, an amplitude ambiguity exists in each of the subsets on the $B0$ side of the partitioning tree. For each of these $B0$-type subsets we define a "prime" subset and a "double-prime" subset. The inner points in a $B0$-type product constellation subset are defined as the "prime" subset – the outer points are defined as the "double-prime" subset.

Our objective is to relate these multiple representations to the TCM trellis such that the Viterbi decoder need only consider points from either the $B0'$ subset or the $B0''$ subset but not both. By isolating the $B0'$ and $B0''$ subsets in the Viterbi decoder trellis we can exploit the larger distances associated with the $B0''$ subset rather than being limited to the smaller distances associated with the $B0'$ subset.

Assuming for the moment that a Viterbi decoder trellis achieving this objective does exist, let us consider how this would affect the intra-subset distances for the trellis code. The TCM distance parameters for this product constellation are highlighted in Figure 3.6. It can be seen that, for any value of r_B, the weight properties of paths which only use $B0'$ will remain unchanged from their values for the corresponding 2M-PSK constellation. Paths which use only $B1$ points will have weights that increase with r_B and the weights for paths which use only $B0''$ points will increase with $r_B{}^2$. All other paths of a given length will have a weight that is larger than in the corresponding 2M-PSK constellation and this weight will have been increased by a factor of less than $r_B{}^2$.

For trellises in which parallel paths exist it is the all-$B0'$ paths – the ones for which the sequence of symbols are all from the $B0'$ subset – that will have the closest parallel paths.

This suggests that an all-$B0'$ path would make a good reference path when determining which single-symbol-error paths will limit code performance.

In view of the symmetry in the product constellation about the B-circle, it can be readily shown that any specific trellis path will be closer to an all-$D0'$ path than would the corresponding all-$D0''$ path. Consider, for example the points referenced to $D0'$ in Figure 3.6. If these constitute a transmitted symbol sequence, the sum of the squares of

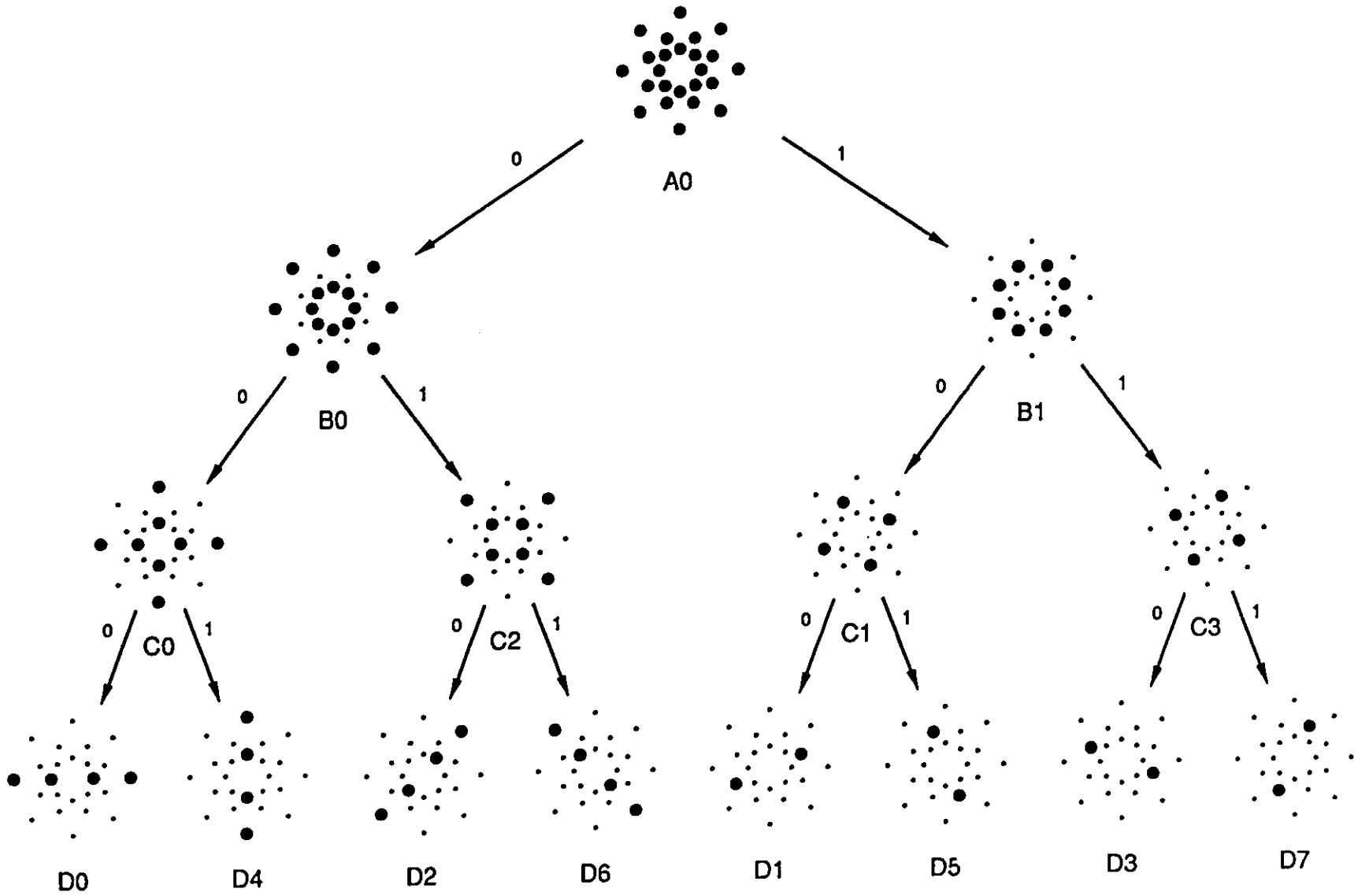

Figure 3.5: Subset Partitioning Tree for the 8-8-PSK Product Constellation

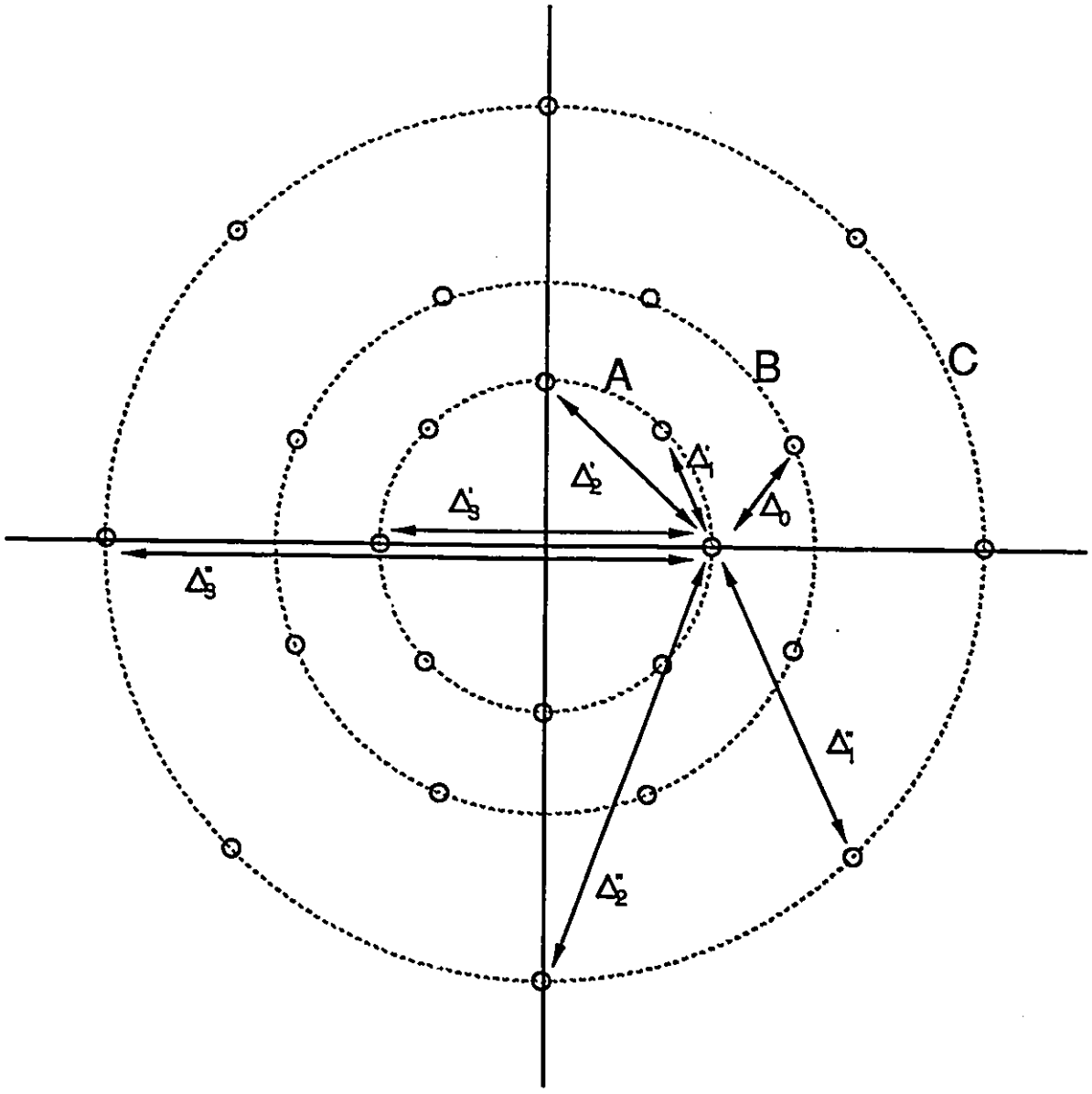

Figure 3.6: TCM Intrasubset Distances for DTC-8-8-PSK

these distances is the paths' squared distance from the all-$D0'$ path. If the ends of these distance vectors are moved from $D0'$ to $D0''$, each of these distance components will increase. The same would be true with respect to any other $B0$ point.

Consider now the case of an all-$B1$ correct path. Paths involving $B1$ points and $B0'$ points will always be closer to an all-$B1$ path than would the corresponding paths which use points from $B1$ and $B0''$. Thus, for an all-$B1$ correct path only error paths of type $B1 - B0'$ need to be considered.

Consider now the general case of an all-$B0''$ correct path. Distances from a $B0''$ point to a $B1$ point are always larger than between a $B0'$ point and a $B1$ point. Consequently any choice of an all-$B0'$ correct path will result in error path weights lower than for the corresponding all-$B0''$ path. Thus the use of an all-$D0'$ correct path will yield the lowest weight for an error path relative to any all-$B0'$ or all-$B0''$ path.

Consider now the general case of an all-$B1$ correct path. Any error path that involves $B0''$ points will definitely be closer to an all-B1 correct path than to an all-$B0'$ correct path. This remains true even if the error path includes both $B0'$ and $B0''$ points. When the error path includes only $B1$ and $B0'$ points either an all-$B0'$ or an all-$B1$ correct path will yield the same weight for the shortest error path.

Finally consider the general case of a $B0' - B1 - B0''$ correct path. Error paths will be closer to a $B0' - B1$ correct path than to a $B0'' - B1$ correct path. The distance from an all-$B0'$ or all-$B1$ error path to a $B0' - B1$ correct path cannot be lower than for a $B0' - B1$ error path and an all-$B0'$ correct path.

Now consider the effect of changes in r_B and ϕ' on the intra-subset distance parameters that will be used in the path weight expressions for a specific trellis code. These were highlighted in Figure 3.6 for the 8-8-PSK product constellation. This drawing depicts a ϕ' value of 0.5 with the points from the $B1$ subset falling on phase lines that are midway between those for points in the $B0$ subset.

For this arrangement of TCM symbols in product space, it is immediately obvious that $\phi' = 0.5$ is the optimum phase spacing between the $B0$ and $B1$ subsets. Any deviation from $\phi' = 0.5$ would lead to a reduction in all TCM intra-subset distances except those for the $B0'$ subsets. Thus although a change in phase spacing would not alter the constellation

energy, it would reduce the weight of all trellis paths except the all-$B0'$ paths. Unless the code is limited by an all-$B0'$ parallel path, this would also cause an undesirable reduction in the free distance of the trellis code.

The chief advantage for this encoding strategy is that $B0'$ and $B0''$ points fall on the same phase lines in the product constellation – provided ϕ' is kept at a value of 0.5. As a result most $B0''$ points are further away from the all-$D0'$ correct path than are their $B0'$ counterparts. Consequently the weight of $B0''$-type branch segments are always larger than they would be in the reference 2M-PSK constellation.

The most dramatic increases in squared free distance for 4-4-PSK occurs for the $D4$ point. For M-M-PSK this $\Delta^2_{\frac{M}{4}}$ value is $(1+r_B)^2$ compared to 4 for the reference constellation. Unfortunately Δ_2^2 is seldom one of the terms in a path weight expression that affects the code free distance. It is usually the Δ_1^2 and Δ_0^2 parameters that are of significance. For 4-4-PSK, Δ_2^2 has a weight of $(1+r_B{}^2)$ compared to 2 for the reference 8-PSK constellation. Table 3.1 contains algebraic expressions for each TCM parameter and highlights their values for various M-M-PSK constellations at $r_B = 1$ and $r_B = \sqrt{2}$. All of these parameters are based on the optimum ϕ' of 0.5. These two values for r_B correspond to average constellation energies of 1 and 1.5 respectively.

It is readily apparent from the table that as M increases a change from 2M-PSK to M-M-PSK with $r_B = \sqrt{2}$ will lead to a rather dramatic increase in Δ_0^2. This term appears in all error paths; however the effect on code free distances is not as dramatic since it must be weighted by a noise correction factor.

The chief disadvantage of the above differential encoding strategy is that the $B0'$ subset cannot uniquely identify the current TCM symbol after a $B0 - B0$ type state or a state of type $B1 - B0$; the same is true for the $B0''$ subset. As a result, in an N-state receive trellis the $B0'$ and $B0''$ branches always appear in parallel and the larger distance properties associated with the $B0''$ subset cannot be utilized. It is only the increases in Δ_0^2 that can be used to increase the weight of the shortest error path. However since Δ_0^2 is the smallest term in the path weight expression, a fairly large r_B value is required to achieve this effect and consequently the average constellation energy is much larger than in the reference constellation.

Symbol	Expression	4-4-PSK		8-8-PSK		16-16-PSK		32-32-PSK	
		r_B = 1.000	r_B = 1.414	r_B = 1.000	r_B = 1.414	r_B = 1.000	r_B = 1.414	r_B = 1.000	r_B = 1.414
Δ_0^2	$1 + r_B^2 - 2r_B \cdot \cos(\frac{\pi}{M})$	0.5858	1.0000	0.1522	0.3869	0.0384	0.2259	0.0096	0.1652
$\Delta_1^{\prime 2}$	$4\sin^2(\frac{\pi}{M})$	2.0000	2.0000	0.5858	0.5858	0.1522	0.1522	0.0384	0.0384
$\Delta_1^{\prime\prime 2}$	$1 + r_B^4 - 2r_B^2 \cdot \cos(\frac{2\pi}{M})$	2.0000	3.0000	0.5858	1.0000	0.1522	0.3869	0.0384	0.2259
$\Delta_2^{\prime 2}$	$4\sin^2(\frac{2\pi}{M})$	4.0000	4.0000	2.0000	2.0000	0.5858	0.5858	0.1522	0.1522
$\Delta_2^{\prime\prime 2}$	$1 + r_B^4 - 2r_B^2 \cdot \cos(\frac{4\pi}{M})$	4.0000	5.8284	2.0000	3.0000	0.5858	1.0000	0.1522	0.3869
$\Delta_3^{\prime 2}$	$4\sin^2(\frac{4\pi}{M})$			4.0000	4.0000	2.0000	2.0000	0.5858	0.5858
$\Delta_3^{\prime\prime 2}$	$1 + r_B^4 - 2r_B^2 \cdot \cos(\frac{8\pi}{M})$			4.0000	5.8284	2.0000	3.0000	0.5858	1.0000
$\Delta_4^{\prime 2}$	$4\sin^2(\frac{8\pi}{M})$					4.0000	4.0000	2.0000	2.0000
$\Delta_4^{\prime\prime 2}$	$1 + r_B^4 - 2r_B^2 \cdot \cos(\frac{16\pi}{M})$					4.0000	5.8284	2.0000	3.0000
$\Delta_5^{\prime 2}$	$4\sin^2(\frac{16\pi}{M})$							4.0000	4.0000
$\Delta_5^{\prime\prime 2}$	$1 + r_B^4 - 2r_B^2 \cdot \cos(\frac{32\pi}{M})$							4.0000	5.8284

Table 3.1: Optimum TCM Intrasubset Distances for M-M-PSK using Phase Difference Encoding

Better results are possible if the receiver's Viterbi decoder uses a trellis which contains more states and is able to prevent $B0'$ and $B0''$ from appearing on parallel branches. This would ensure that the larger distance parameters associated with the $B0''$-type subsets can in fact be utilized.

3.5 DTC-M-M-PSK Noise Model

3.5.1 Differential Demodulation

The analysis provided earlier in section 2.4.1 was sufficiently general that it can be readily applied to the case of DTC-M-M-PSK.

For PSK the modulating functions for the in-phase and quadrature baseband signals were defined in equations (2.21) and (2.22). These expressions also apply to M-M-PSK except that the value for r_m is equal to $r_A = 1$ for the even-numbered constellation points and is another larger value, r_B, for the odd-numbered constellation points.

The final expression for the product constellation point given by equation (2.31) includes the envelope parameters r_n and r_{n-1}. Consequently this general expression is also valid for M-M-PSK. It is repeated here for convenience.

$$\begin{aligned} p_n &= r_n \cdot r_{n-1}[\cos(\theta_n - \theta_{n-1}) + \mathrm{j} \cdot \sin(\theta_n - \theta_{n-1})] \\ &= D_n \cdot D_{n-1}^* \\ &= E_n \end{aligned} \tag{3.1}$$

In the case of 2M-PSK the product constellation points, E_n had a direct correspondence to original TCM constellation points, C_n. This is no longer true with M-M-PSK. Although the original $2M$ constellation points are present in the product constellation, there is also a new set of M points. There is effectively an amplitude ambiguity in the product constellation representation of the points from the $B0$ subset. They occur at the same phase angles as in the original TCM constellation, but at an amplitude of either r_A or r_B^2.

The DTC-M-M-PSK Viterbi decoder must compare each differentially demodulated symbol with each of these $3M$ constellation points. In order to determine an optimal set of branch metrics to use with this new constellation we must first consider how the noise at

the output of the differential detector is affected by the fact that not all transmit symbols have the same amplitude.

3.5.2 Effects of Noise

In this section we develop a model for the noise that will be present in M-M-PSK product space. The objective is to define the assumptions which are necessary to easily evaluate the effects of subset dilation on path distances in a modified Viterbi decoder trellis.

For DTC-M-M-PSK we may use the general expression for the noise in product space that was shown earlier in equation (2.38). It is repeated here for convenience.

$$n_{P_n} = D_n \cdot n^*_{R_{n-1}} + D^*_{n-1} \cdot n_{R_n} + n_{R_n} \cdot n^*_{R_{n-1}} \tag{3.2}$$

where D_n and D^*_{n-1} are the transmit constellation points. Since we are now dealing with M-M-PSK constellations, each of these complex values have an amplitude of $r_A = 1$ or r_B depending on whether the points are from the A (inner) or B (outer) PSK ring in the transmit constellation.

For DTC-M-M-PSK we obtain the same expression for the variance of the noise in product space. It is repeated here for convenience.

$$\sigma^2_{N_P} = \sigma^2_N[|D_n|^2 + |D_{n-1}|^2 + \sigma^2_N] \tag{3.3}$$

However, as noted earlier, the values for $|D_n|$ and $|D_{n-1}|$ are no longer restricted to a value of 1 as they were for DTC-2M-PSK

Application to Trellis Metrics

Before applying the above results to trellis branch metrics we will make one further assumption. Our objective is to determine how the branch metrics for the DTC-2M-PSK Viterbi decoder of Chapter 2 must be modified to work with DTC-M-M-PSK. This assumption will permit DTC-M-M-PSK to use scaled versions of the branch metrics used in the DTC-2M-PSK Viterbi decoder.

This assumption will also facilitate the evaluation of trellis free distances for a variety of M-M-PSK constellations and trellises. It permits the calculation of asymptotic coding

gains which can be used to compare DTC-M-M-PSK codes with other codes reported in the literature.

These results will then be used to select a candidate constellation and trellis whose performance will be simulated over the entire range of practical SNR values.

Once again, for this high SNR case we discount the Noise × Noise term in equation (2.38) and approximate n_P as follows:

$$n_P \approx D_n n_{n-1}^* + D_{n-1}^* n_n \tag{3.4}$$

This simplifies equation (2.41) to produce the following noise variance:

$$\begin{aligned} \sigma_{N_P}^2 &\approx \sigma_N^2[|D_n|^2 + |D_{n-1}|^2] \\ &\approx \sigma_N^2[r_n^2 + r_{n-1}^2] \end{aligned} \tag{3.5}$$

This instead can be expressed as,

$$\sigma_{N_P}^2 = \frac{1}{w_k} \cdot \sigma_N^2 \tag{3.6}$$

where $w_k = \{w_A, w_B, w_C\}$ depending on whether the product constellation point, E_n, is on ring A, B or C in the product constellation shown earlier in Figure 3.6. These noise-correction factors are defined as

$$w_A = \frac{1}{2} \tag{3.7}$$

$$w_B = \frac{1}{1 + r_B^2} \tag{3.8}$$

$$w_C = \frac{1}{2r_B^2} \tag{3.9}$$

Now we will consider how this variety of noise weightings affects the assignment of branch metrics in the Viterbi decoder. For symbol by symbol detection this unequal distribution in noise weights would cause a re-alignment of decision thresholds in the receiver constellation. Decision thresholds would be moved further away from constellation points that have a high noise weighting and would be moved closer to constellation points that have a lower noise weighting. The objective would be to obtain a uniform maximum probability that a noisy

symbol would remain within its correct decision boundaries regardless of which symbol was sent.

The objective in a Viterbi decoder is similar but must take into account the special characteristics of the MLSE detection algorithm. An MLSE detector does not simply place a decision threshold between the correct constellation point and its nearest neighbours. Because the actual decision must be deferred, it instead obtains the necessary information to make optimum pairwise decisions between any possible pair of constellation points.

Consequently the branch metrics used by the Viterbi decoder must be adjusted such that they correspond to the optimum decision threshold between any two pairs of product constellation points. For a uniform noise weighting, the decision thresholds are straight lines perpendicular to the line joining each pair of points. For unequal noise weights, the decision threshold is a hyperbola with the two constellation points as foci. This is depicted in Figure 3.7. A receive signal whose vector falls on this line must have an equal probability of having been generated by either transmit signal.

Now the Viterbi algorithm stores a branch metric for each constellation point that will be used later to determine if in fact that constellation point was the most likely point to have been transmitted. It is clear that these branch metrics can no longer be a simple Euclidean distance measure between the receive vector and the appropriate constellation point vector. These Euclidean distances must be divided by the constellations points' noise weighting to obtain the optimum metric.

When the branch metrics are compensated for the noise weighting, a comparison of any two branch metrics will always show that they are equal for receive vectors that lie on the pairwise decision threshold. If the receive vector lies to one side of the pairwise decision threshold, the branch metric for the constellation point on that side of the threshold will always be lower.

In summary, for M-M-PSK the optimum metrics in the Viterbi decoder will be calculated as follows:

$$\mu_{E_n} = d^2(E_n, p_n) \cdot w_n \tag{3.10}$$

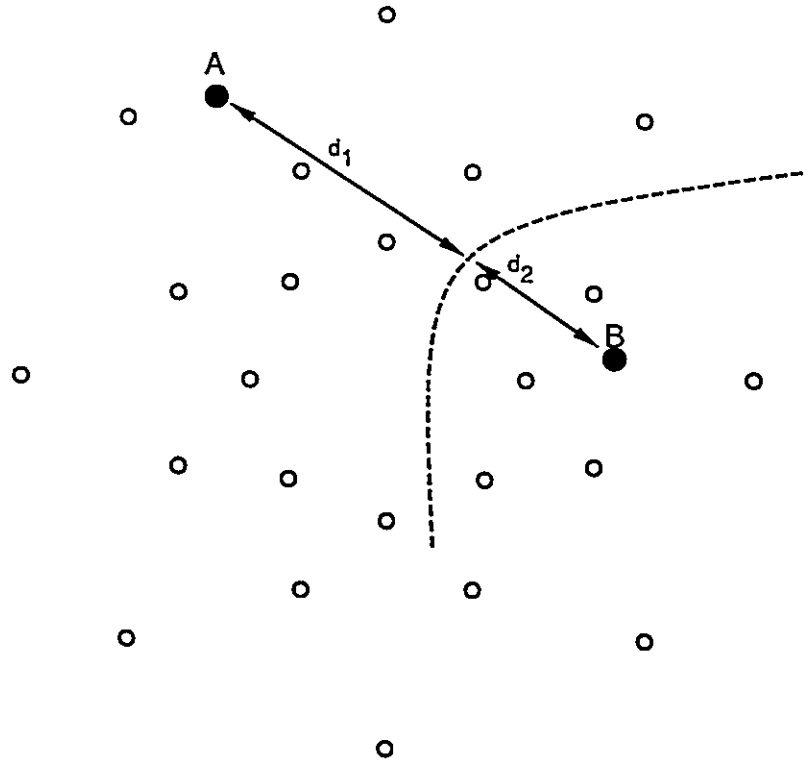

a) Decision threshold for two points, A and B, with different noise weightings

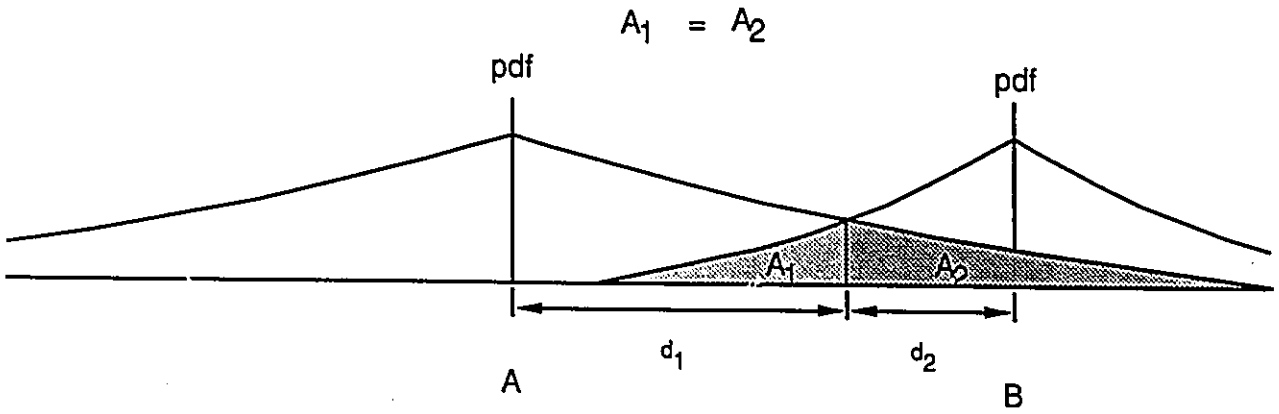

a) Noise pdf cross-section for points A and B

Figure 3.7: Determination of Pairwise Decision Thresholds

This expression was used to provide branch metric weighting factors for DTC-M-M-PSK simulations that will be discussed in Chapter 4.

3.6 Modified Viterbi Decoder Trellis Structure

As highlighted earlier in section 3.5.1, subset dilation introduces an amplitude ambiguity in the product constellation – the constellation that is used by the Viterbi decoder.

We could use the same trellis structure for both the convolutional encoder and the Viterbi decoder. However, as shown earlier in Figure 3.5, all the even-numbered D-level subsets in the product constellation contain twice as many constellation points as their counterparts in the TCM constellation shown in Figure 2.5. This effectively doubles the number of parallel branches in each branch set for an even-numbered D-level subset.

Because the A-level and C-level versions of these subsets are grouped together we cannot yet take advantage of the larger distance parameters associated with the double-prime subsets. The minimum distance between the correct path and the overall D-level subset will always be limited to the single-prime distance parameters.

Consequently, if the original N-state Viterbi decoder trellis is used, the only free distance improvement that would be realized is that associated with the larger Δ_0 parameter – the distance between the $B0'$ subset and the dilated $B1$ subset. In view of the fact that subset dilation increases the average energy of the constellation, the net effect is likely to be a reduction in performance when compared on an average energy basis – if the original N-state Viterbi decoder trellis is used.

To fully realize the free distance increases associated with subset dilation it is necessary to create a modified trellis structure for which subsets of type $B0'$ and type $B0''$ do not appear on parallel branches. The superstate diagrams shown in Figure 3.8 are helpful in identifying the appropriate trellis structure.

The upper portion of the figure shows the superstate diagram for trellis-coded PSK – either coherent or differentially coherent. Only two types of states need be considered – those which produce symbols from the $B0$ subset and those which produce symbols from the $B1$ subset. The two sets of trellis states are grouped into superstates $B0$ and $B1$ respectively. Each superstate produces symbols only from the appropriate B-level subset.

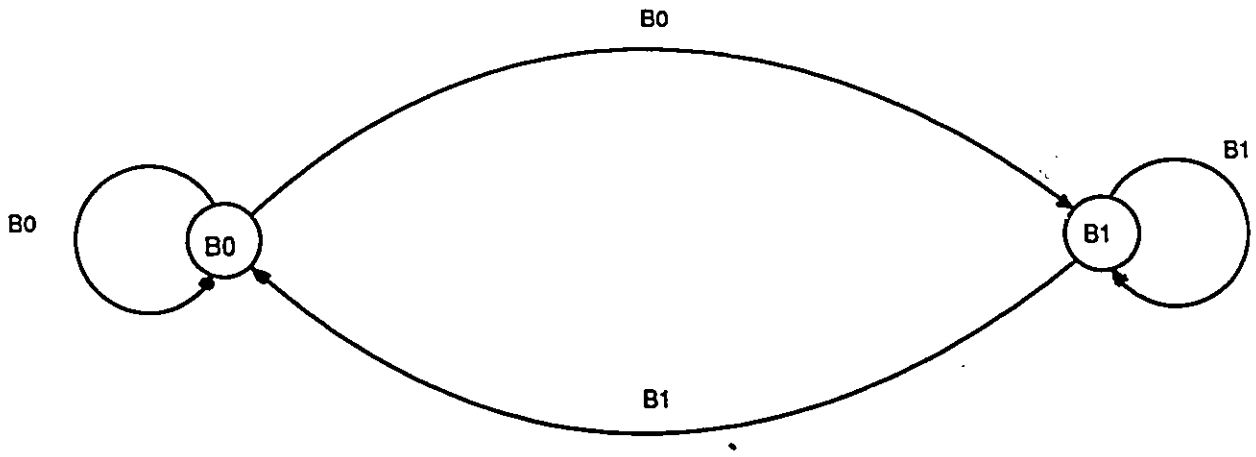

a) Superstate Diagram for Trellis-coded PSK

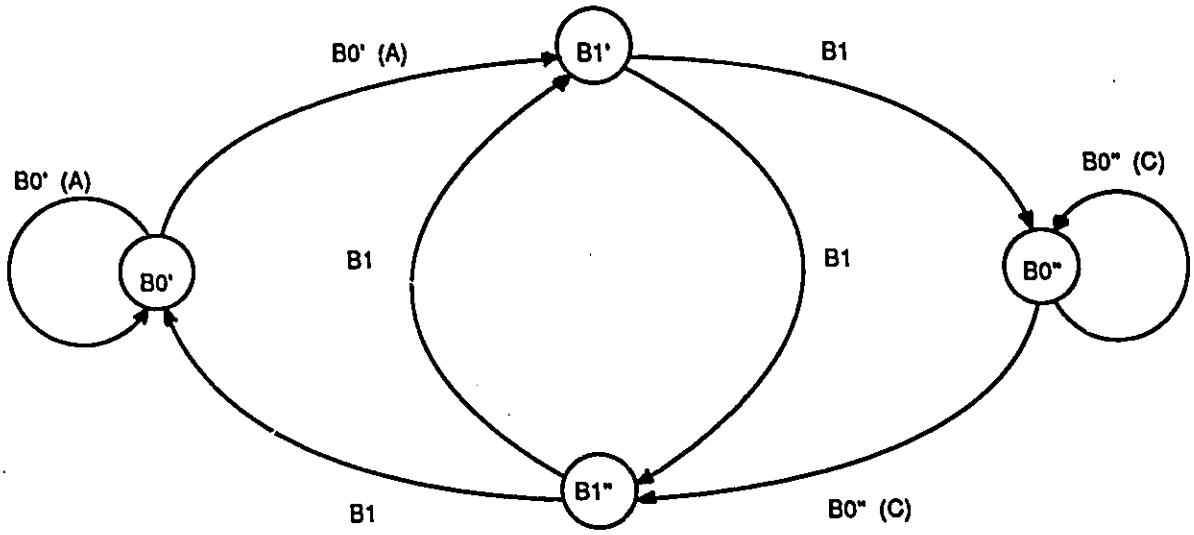

b) Superstate Diagram for Differentially Coherent Trellis-coded M-M-PSK

Figure 3.8: Superstate Diagrams for DTC-2M-PSK and DTC-M-M-PSK

However, in so doing, it may either return to the same superstate or make a transition to the other superstate.

The superstate diagram for M-M-PSK is shown in the lower portion of Figure 3.8. By contrast it contains four superstates. The use of two superstates of type $B0$ – labelled $B0'$ and $B0''$ – permits branches associated with the $B0'$ and $B0''$ subsets to be isolated. $B0'$ points which appear on the A-ring in the product constellation, can only occur when leaving the $B0'$ superstate. Similarly, the $B0''$ symbols which appear on the C-ring in the product constellation, can only occur when leaving the $B0''$ superstate.

To explain the need for two superstates of type $B1$, we must consider the correlation between occurrences of $B0'$ and $B0''$ symbols in the product constellation. A closer examination of the differential encoding and decoding process reveals that the amplitude of a $B0$ point in the product constellation depends on the number of $B1$ symbols which followed the previous $B0$ symbol. If the two $B0$ symbols are separated by an even number of $B1$ symbols there will be no amplitude change. However if they are separated by an odd number of $B1$ symbols, there will be an amplitude change.

The superstate diagram shown in the lower portion of Figure 3.8 meets this requirement. However, to achieve this objective, it was necessary to introduce a second set of states of type $B1$. Consequently we have superstates $B1'$ and $B1''$ which occur at different places in the superstate diagram, yet both produce symbols from the $B1$ subset.

We will now make use of this superstate diagram to produce a trellis diagram that is similar to our encoder trellis yet permits isolation of the $B0'$ and $B0''$ subsets.

The number of states associated with each superstate is the same for both the diagrams in Figure 3.8. This follows from the fact that any $B0$ branch in the encoder trellis could result in either a $B0'$ or $B0''$ symbol in the Viterbi decoder.

Because the M-M-PSK diagram has twice as may superstates as does the 2M-PSK diagram, the M-M-PSK Viterbi decoder trellis must have twice as many states. In both superstate diagrams each superstate has two departing branches – one returning to the same superstate and one producing a transition to another type of superstate. This is also true for the original 2M-PSK superstate diagram. As a result, the M-M-PSK Viterbi decoder can use a trellis structure that is very similar to the original encoder trellis but introduces

a "single-prime" substate and a "double-prime" substate for each of the original states.

Although the state-to-state transitions remain the same as in the original trellis, there are restrictions imposed on the originating and terminating substates. From the superstate diagram we can see that a branch from a $B1$-type state must cause a transition from one type of substate to the other type of substate. By contrast, a branch leaving $B0$-type state must preserve the type of the substate. The resultant Viterbi decoder trellis for the DTC-(8,4)-M-M-PSK codes is shown in Figure 3.9.

It is important to note that this modified trellis does not affect the length of the various error paths discussed earlier. It merely permits an increase in the weight of some error paths by facilitating the isolation of the $B0'$ and $B0''$ subsets.

An error path is still defined on the basis of the original encoder trellis state sequence. Although substates are used to differentiate between $B0'$ and $B0''$ subsets during Viterbi decoding, the substate information is discarded after a state decision has been made. Only information concerning the encoder state sequence is retained for use by the convolutional decoder. In effect, the decoder has discarded the amplitude information and retained sufficient information to determine the sequence of symbols from the original TCM constellation.

The amplitude encoding inherent in M-M-PSK is used to increase the error path distances associated with the Viterbi decoder and thereby improve performance. Once this function has been fulfilled, the amplitude information is truncated when the substate is discarded.

3.7 Asymptotic Coding Gain

The objective of DTC-M-M-PSK is to bring about an increase in the minimum weight error path in the differential receive trellis. This is achieved by increasing the amplitude of the $B1$ subset transmit symbols. However this also increases the average energy of the signal constellation. Consequently the increase in the trellis free distance must exceed the increase in the constellation energy if a coding advantage is to be obtained over the DTC-2M-PSK case.

We will consider the case of 4-, 8- and 16-state trellises.

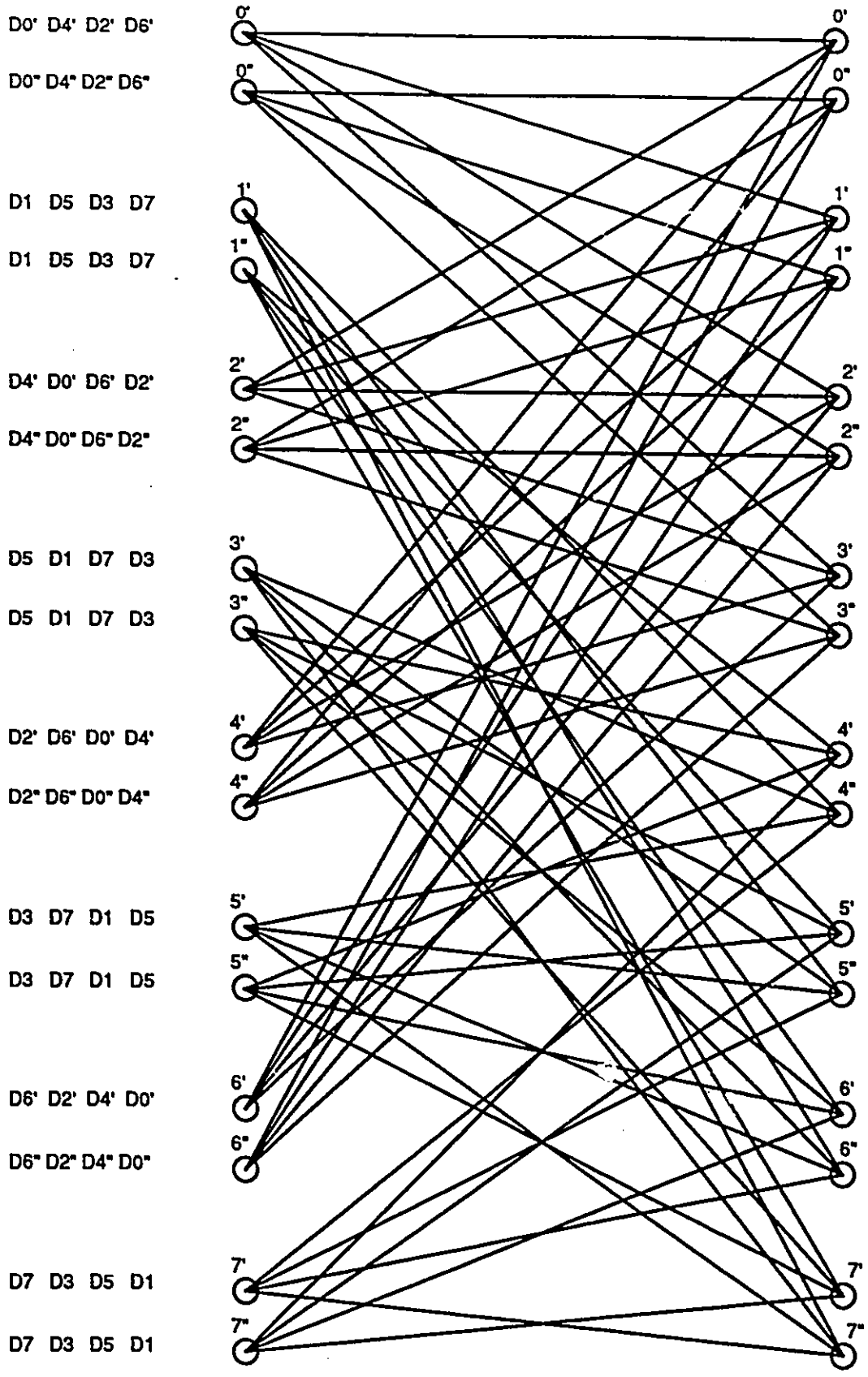

Figure 3.9: Viterbi Decoder Trellis for DTC-(8,4)-M-M-PSK

3.7.1 4-state Trellis

Figure 3.10 shows the standard Ungerboeck 4-state trellis with labels showing which C-level subset is associated with each state-to-state transition. This is referred to as the (4,2)-trellis because it has 4 states and 2 sets of branches per state. Figure 3.11 shows the differential trellis which must be used to receive the above code after differential demodulation. The branches are labelled with C-level 'prime' and 'double prime' subsets found in the product constellation. Because there are two representations for $B0$ subset points in product space, it is necessary for the trellis to have 2 substates for each of the 4 original states.

All of the error paths highlighted in Figure 3.10 will still be valid error paths in the expanded Viterbi decoder trellis. This is true because the substate has no significance when decoding the trellis state sequence into an estimate for the sequence of transmit symbols. It is only the sequence of original 4 states which determines the estimate of the transmit symbols.

Table 3.2 highlights the path weights for potential error paths up to length 6 in the (4,2)-trellis. These are referenced to the all-$D0'$ correct path. The column labelled $r_B = 1$, represents the 8-PSK case. No subset dilation has been introduced as yet.

The minimum weight path is shown to be the length 1 parallel path which uses the other symbol from the $C0$ subset – namely $D4$. For differential demodulation and the noise model described in Section 3.5.1, the minimum weight is shown to be 2. This is exactly half the weight determined by Ungerboeck [1] for the case of coherent detection.

The other columns in Table 3.2 show the effect on trellis paths when the amplitude of the $B1$ transmission subset is increased. All the paths except the parallel path increase in weight as the $B1$ transmission subset is dilated. However, for this code, the trellis free distance is obtained from the parallel path and consequently does not change. Since the constellation energy is minimum for $r_B = 1$, this is the (4,2)-4-4-PSK code which yields the best coding gain.

In summary, for an 8-point constellation with the (4,2)-trellis there is no coding advantage to be obtained by dilating the $B1$ transmission subset – 8-PSK is the optimum M-M-PSK constellation.

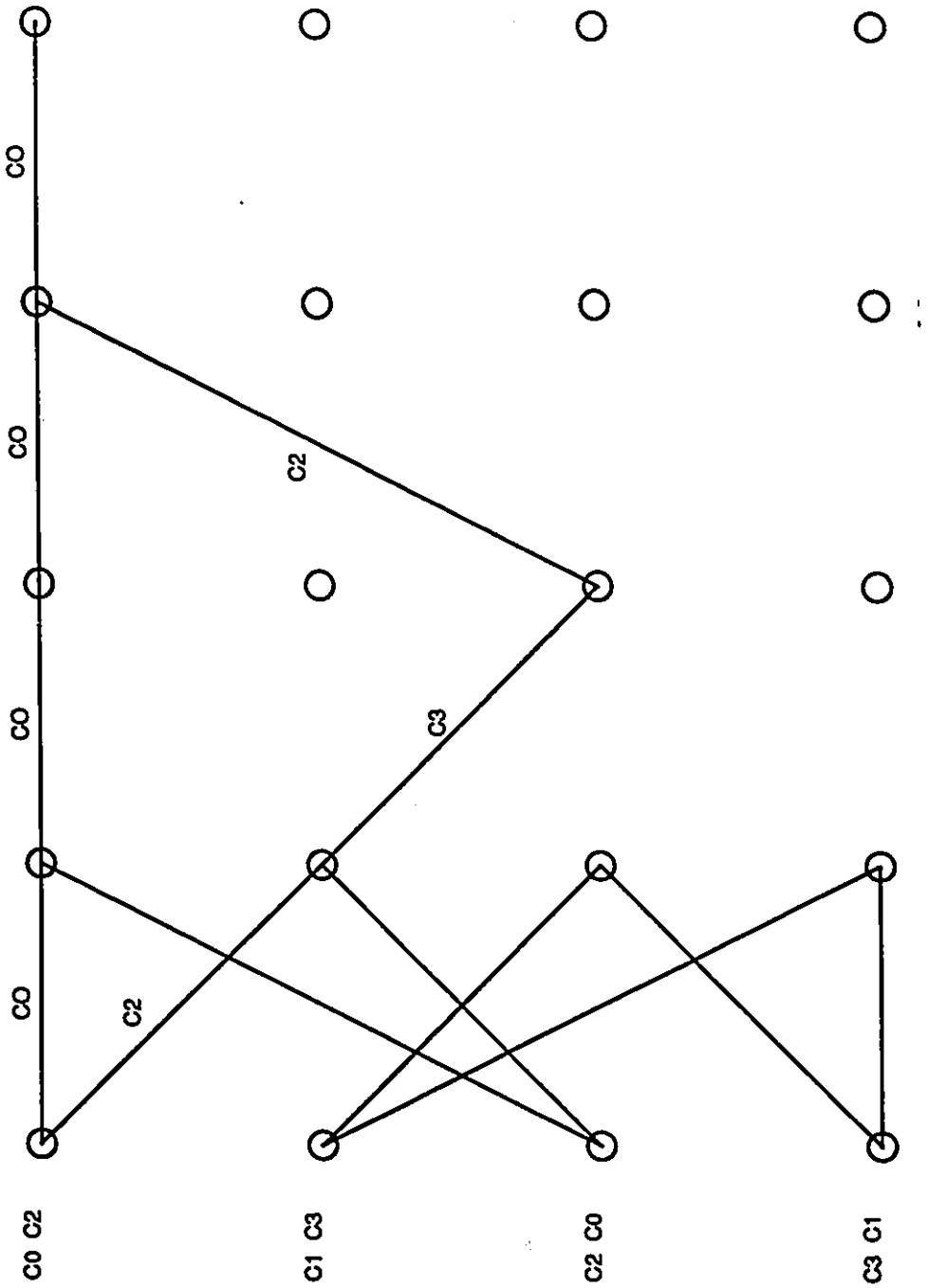

Figure 3.10: Standard (4,2)-trellis

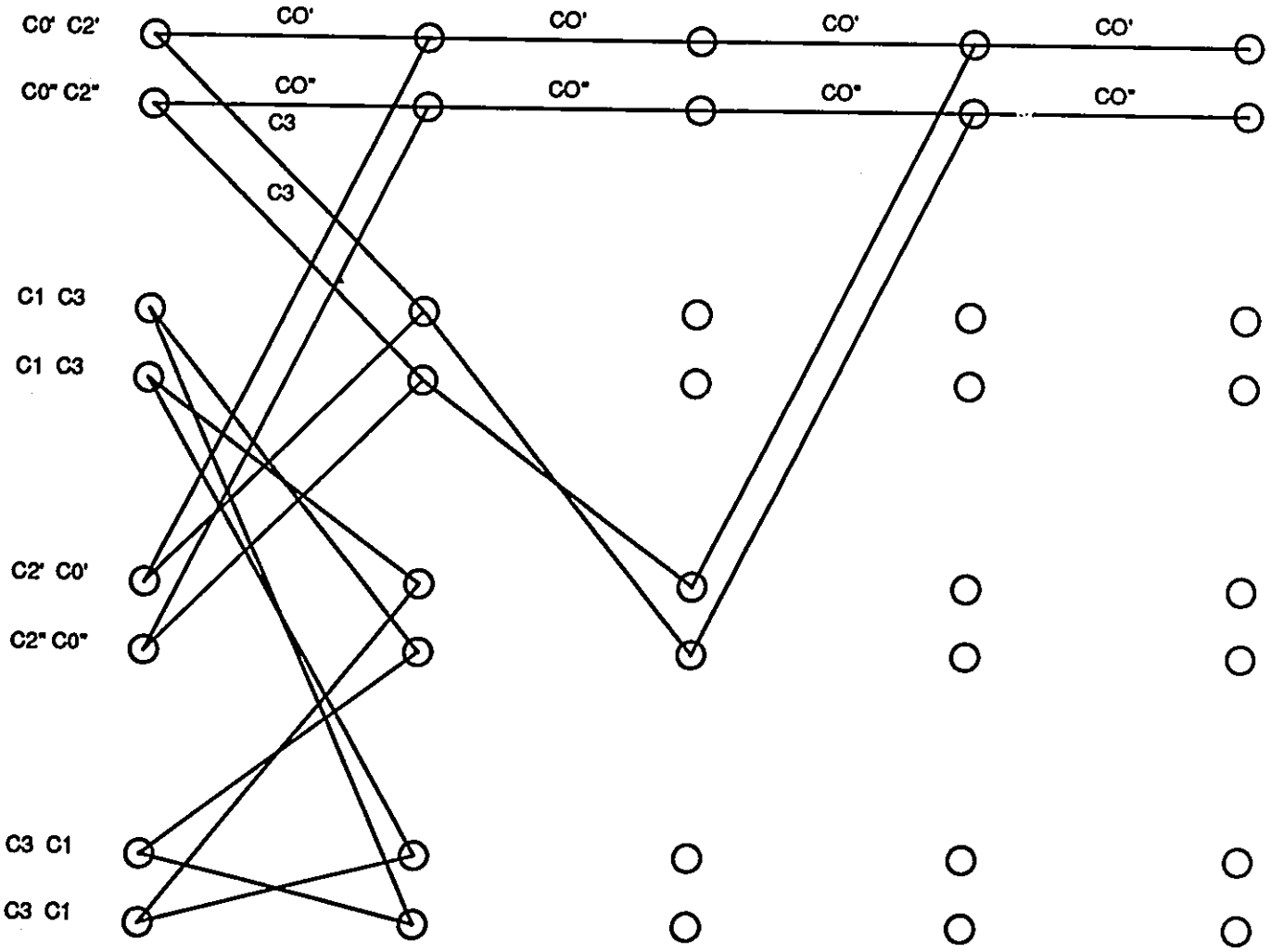

Figure 3.11: Viterbi Decoder Trellis used with DTC-(4,2)-M-M-PSK

Path No.	Path Length	Path	Path Weight					
M			4	4	4	4	4	4
r_B			1.0000	1.1000	1.2000	1.3000	1.4000	1.5000
1	1	C0	2.0000	2.0000	2.0000	2.0000	2.0000	2.0000
2	3	C2-C1-C2	2.2929	2.3143	2.3717	2.4574	2.5662	2.6945
3	4	C2-C3-C3-C2	2.5858	2.5922	2.6090	2.6331	2.6622	2.6946
4	5	C2-C3-C1-C3-C2	2.8787	2.9065	2.9807	3.0905	3.2284	3.3891
5	5	C2-C1-C0-C1-C2	2.5858	2.5922	2.6090	2.6331	2.6622	2.6946
6	6	C2-C3-C3-C0-C1-C2	2.8787	2.9065	2.9807	3.0905	3.2284	3.3891
7	6	C2-C1-C0-C3-C3-C2	2.8787	2.9065	2.9807	3.0905	3.2284	3.3891

M	4	4	4	4	4	4
r_B	1.0000	1.1000	1.2000	1.3000	1.4000	1.5000
Min. Weight	2.0000	2.0000	2.0000	2.0000	2.0000	2.0000
Energy Penalty	1.0000	1.1050	1.2200	1.3450	1.4800	1.6250
(dB)	0.00	0.43	0.86	1.29	1.70	2.11
Coding Gain over M-PSK	1.0000	0.9050	0.8197	0.7435	0.6757	0.6154
(dB)	0.00	-0.43	-0.86	-1.29	-1.70	-2.11
Coding Gain over TC-2M-PSK	0.5000	0.4525	0.4098	0.3717	0.3378	0.3077
(dB)	-3.01	-3.44	-3.87	-4.30	-4.71	-5.12
Coding Gain over DTC-2M-PSK	1.0000	0.9050	0.8197	0.7435	0.6757	0.6154
(dB)	0.00	-0.43	-0.86	-1.29	-1.70	-2.11
Peak-to-Average Energy Ratio	1.00	1.10	1.18	1.26	1.32	1.38

Table 3.2: Contender Path Weights for DTC-(4,2)-4-4-PSK at various values of r_B

Table 3.3 shows the optimum 16-16-PSK constellation for the (4,2) trellis. For this constellation ($M = 16$) the coding gain over coherent uncoded M-PSK can be increased from 0.52dB to 1.18dB by increasing r_B from 1 to 1.391.

In this case it was a length 3 path of type C2-C1-C2 which had limited the free distance for the 32-PSK constellation. However for values of r_B beyond 1.1, this path is no longer the minimum weight path. At this point a length 4 path of type C2-C3-C3-C2, with a weaker dependence on r_B becomes the minimum weight path at this point. However at $r_B = 1.391$ even this path exceeds the weight of the parallel path which has not changed at all with r_B.

Because the parallel path only uses symbols from the $B0$ transmission subset, its weight is not affected by r_B. The dependence of the other two contender paths on r_B is shown in the following equations:

$$W_{C2-C3-C2} = \Delta_1^2 \cdot w_A + \Delta_0^2 \cdot w_B + \Delta_1''^2 \cdot w_C \tag{3.11}$$

$$W_{C2-C3-C3-C2} = 2\,\Delta_1^2 \cdot w_A + 2\,\Delta_0^2 \cdot w_B \tag{3.12}$$

These two equations highlight the advantage of DTC-M-M-PSK. The length 3 path consists of two $B0$ symbols separated by a single symbol of type $B1$. In such a case, the two $C2$ symbols cannot occur at the same amplitude in the product constellation. One will be at amplitude r_A and the other at amplitude $r_C = r_B^2$. Consequently Δ_1' applies to one of these symbols and the larger Δ_1'' applies to the other. It is generally paths with Δ_1'' in their weight expression which show dramatic increases as the $B1$ subset is dilated.

By contrast, for the length 4 path, the two $C2$ symbols (type $B0$) are separated by an even number of symbols of type $B1$. In this case the two $C2$ symbols will of necessity appear at the same amplitude in the product constellation. Since either amplitude is equally likely, the one which produces the lower error path weight will dominate code performance. Consequently the weight of the length 4 path is based on the lower Δ_1' value only. Paths of this type must depend on the meagre increases in Δ_0 as the $B1$ subset is dilated.

Asymptotic results for the best M-M-PSK codes are shown in Table 3.4 for values of M from 4 to 64. Although they cannot be considered practical constellations, the results for $M = 16, 32$, and 64 show improvements of 0.66dB, 1.66dB and 2.12dB, respectively, over their DTC-(4,2)-2M-PSK counterparts.

Path No.	Path Length	Path	Path Weight					
M			16	16	16	16	16	16
r_B			1.0000	1.1000	1.2000	1.3000	1.3500	1.3910
1	1	C0	0.2929	0.2929	0.2929	0.2929	0.2929	0.2929
2	3	C2-C1-C2	0.1715	0.1941	0.2548	0.3451	0.3996	0.4484
3	4	C2-C3-C3-C2	0.1907	0.1995	0.2228	0.2563	0.2758	0.2929
4	5	C2-C3-C1-C3-C2	0.2099	0.2414	0.3253	0.4492	0.5232	0.5890
5	5	C2-C1-C0-C1-C2	0.1907	0.2020	0.2306	0.2742	0.3012	0.3257
6	6	C2-C3-C3-C0-C1-C2	0.2099	0.2414	0.3253	0.4492	0.5232	0.5890
7	6	C2-C1-C0-C3-C3-C2	0.2099	0.2414	0.3253	0.4492	0.5232	0.5890
8								
9								
10								
11								
12								
13								
14								

M		16	16	16	16	16	16
r_B		1.0000	1.1000	1.2000	1.3000	1.3500	1.3910
Min. Weight		0.1715	0.1941	0.2228	0.2563	0.2758	0.2929
Energy Penalty		1.0000	1.1050	1.2200	1.3450	1.4113	1.4674
	(dB)	0.00	0.43	0.86	1.29	1.50	1.67
Coding Gain	over M-PSK	1.1262	1.1539	1.1997	1.2517	1.2837	1.3109
	(dB)	0.52	0.62	0.79	0.97	1.08	1.18
Coding Gain	over TC-2M-PSK	0.5000	0.5123	0.5326	0.5557	0.5699	0.5820
	(dB)	-3.01	-2.90	-2.74	-2.55	-2.44	-2.35
Coding Gain	over DTC-2M-PSK	1.0000	1.0246	1.0653	1.1114	1.1398	1.1639
	(dB)	0.00	0.11	0.27	0.46	0.57	0.66
Peak-to-Average Energy Ratio		1.00	1.10	1.18	1.26	1.29	1.32

Table 3.3: Contender Path Weights for DTC-(4,2)-16-16-PSK at various values of r_B

Path No.	Path Length	Path	Path Weight				
M			4	8	16	32	64
r_B			1.0000	1.0000	1.3910	1.1840	1.0886
1	1	C0	2.0000	1.0000	0.2929	0.0761	0.0192
2	3	C2-C1-C2	2.2929	0.6619	0.4484	0.1149	0.0289
3	4	C2-C3-C3-C2	2.5858	0.7380	0.2929	0.0761	0.0192
4	5	C2-C3-C1-C3-C2	2.8787	0.8141	0.5890	0.1526	0.0385
5	5	C2-C1-C0-C1-C2	2.5858	0.7380	0.3257	0.0799	0.0197
6	6	C2-C3-C3-C0-C1-C2	2.8787	0.8141	0.5890	0.1526	0.0385
7	6	C2-C1-C0-C3-C3-C2	2.8787	0.8141	0.5890	0.1526	0.0385

M	4	8	16	32	64
r_B	1.0000	1.0000	1.3910	1.1840	1.0886
Min. Weight	2.0000	0.6619	0.2929	0.0761	0.0192
Energy Penalty	1.0000	1.0000	1.4674	1.2009	1.0925
(dB)	0.00	0.00	1.67	0.80	0.38
Coding Gain over M-PSK	1.0000	1.1299	1.3109	1.6493	1.8262
(dB)	0.00	0.53	1.18	2.17	2.62
Coding Gain over TC-2M-PSK	0.5000	0.5000	0.5820	0.7327	0.8105
(dB)	-3.01	-3.01	-2.35	-1.35	-0.91
Coding Gain over DTC-2M-PSK	1.0000	1.0000	1.1636	1.4671	1.6285
(dB)	0.00	0.00	0.66	1.66	2.12
Peak-to-Average Energy Ratio	1.00	1.00	1.32	1.17	1.08

Table 3\4: Contender Path Weights for DTC-(4,2)-M-M-PSK at optimum values of r_B

However these codes require an expanded Viterbi decoder trellis with twice as many states as the encoder trellis. Consequently they should be compared with the best DTC-2M-PSK codes using an 8-state trellis. Even on this basis, they yield improvements of 0.20dB, 1.20dB and 1.65dB.

3.7.2 8-state Trellises

Now let us consider the case of an 8-state trellis. Two possible trellis structures will be considered. The first employs 2-sets-of-($\frac{M}{2}$) branching; the second uses 4-sets-of-($\frac{M}{4}$) branching. These will be referred to as the (8,2)-trellis and the (8,4)-trellis, respectively.

The (8,4)-trellis is the one attributed to Ungerboeck [1]. The (8,2)-trellis achieves a better free distance for 2M-PSK codes on a AWGN channel and is found in Ungerboeck's Table II [3]. Its performance with 2M-PSK has been further explored by Wilson et al [13].

The optimum DTC-(8,2)-M-M-PSK codes are identified in Table 3.5 for the cases of M from 4 to 64. Although PSK constellations above 32 points are generally not feasible, they are included in the tables to identify trends in DTC-2M-PSK performance with respect to the constellation size.

Once again DTC-(8,2)-2M-PSK constellations are optimum for 8 points ($M = 4$), 16 points ($M = 8$) and 32 points ($M = 16$). It is only for the unrealistic cases of $M = 32$ and $M = 64$ that M-M-PSK can achieve coding gains beyond those realizable with a 2M-PSK constellation.

However it is interesting to note that for 32-32-PSK with the (8,2)-trellis the coding gain is 0.68 dB higher than for DTC-64-PSK using the (16,2)-trellis. Since DTC-M-M-PSK requires a 2N-state receive trellis it is appropriate to compare its performance with that of a 16-state DTC-2M-PSK code. The one cited above is the 16-state code which yields the best performance.

Similarly DTC-(8,2)-64-64-PSK outperforms the best 16-state code, DTC-(16,2)-128-PSK by 1.21 dB. Although these coding gains are for unrealistic constellations at high SNR, the results do suggest that possible advantages may exist for using DTC-M-M-PSK with smaller constellations. It remains to be seen if a constellation with 16 points or less can achieve an improvement using DTC-M-M-PSK over DTC-2M-PSK.

Path No.	Path Length	Path	Path Weight				
M			4	8	16	32	64
r_B			1.0000	1.0000	1.0000	1.2090	1.0940
1	1	C0	2.0000	1.0000	0.2929	0.0761	0.0192
2	4	C2-C1-C2-C2	3.2929	0.9548	0.2476	0.1530	0.0359
3	5	C2-C3-C3-C0-C2	2.5858	0.7380	0.1907	0.0762	0.0192
4	6	C2-C1-C0-C3-C2-C2	3.5858	1.0309	0.2668	0.1026	0.0249
5	6	C2-C3-C1-C1-C0-C2	2.8787	0.8141	0.2099	0.1788	0.0415
6	7	C2-C1-C2-C0-C1-C2-C2	2.8787	0.8141	0.2099	0.1788	0.0415
7	7	C2-C3-C3-C2-C3-C2-C2	2.8787	0.8141	0.2099	0.1788	0.0415
8	7	C2-C1-C0-C1-C3-C0-C2	2.8787	0.8141	0.2099	0.1788	0.0415
9	7	C2-C3-C1-C3-C1-C0-C2	2.8787	0.8141	0.2099	0.1059	0.0253
10	8	C2-C3-C3-C0-C0-C1-C2-C2	3.8787	1.1070	0.2860	0.1980	0.0463
11	8	C2-C1-C0-C3-C0-C3-C2-C2	3.8787	1.1070	0.2860	0.1980	0.0463
12	8	C2-C3-C1-C1-C2-C3-C2-C2	5.1716	1.4761	0.3813	0.3126	0.0725
13	8	C2-C1-C2-C0-C3-C3-C2-C2	4.8787	1.3999	0.3621	0.2172	0.0511
14	8	C2-C3-C3-C2-C1-C3-C2-C2	5.1716	1.4761	0.3813	0.1668	0.0401
15	8	C2-C1-C0-C1-C1-C1-C0-C2	3.1716	0.8903	0.2291	0.1283	0.0305
16	8	C2-C3-C1-C3-C3-C1-C0-C2	3.4645	0.9664	0.2483	0.2237	0.0519

M	4	8	16	32	64
r_B	1.0000	1.0000	1.0000	1.2090	1.0940
Min. Weight	2.0000	0.7380	0.1907	0.0761	0.0192
Energy Penalty	1.0000	1.0000	1.0000	1.2308	1.0984
(dB)	0.00	0.00	0.00	0.90	0.41
Coding Gain over M-PSK	1.0000	1.2599	1.2524	1.6093	1.8161
(dB)	0.00	1.00	0.98	2.07	2.59
Coding Gain over TC-2M-PSK	0.5000	0.5000	0.5001	0.6435	0.7257
(dB)	-3.01	-3.01	-3.01	-1.91	-1.39
Coding Gain over DTC-2M-PSK	1.0000	1.0000	0.9998	1.2857	1.4575
(dB)	0.00	0.00	0.00	1.09	1.64
Peak-to-Average Energy Ratio	1.00	1.00	1.00	1.19	1.09

Table 3.5: Contender Path Weights for DTC-(8,2)-M-M-PSK at optimum values of r_B

At a constellation size of 16 points, 16-QAM has a 4dB advantage over 16-PSK when compared on an average energy basis. The use of 16-PSK can still be justified on non-linear channels because of its other desirable properties. However the 32-CROSS constellation has an 8dB advantage over 32-PSK. A satellite channel backed off into the linear region using 32-CROSS can in all likelihood outperform a system using 32-PSK in the saturation region.

On the basis of coded constellations 32-QASK would have an even greater advantage over 32-PSK. In general the Δ-values for QASK increase faster than for PSK. This is related to the fact that QASK is truly two-dimensional whereas PSK can be regarded as quasi-one-dimensional. With the introduction of M-M-PSK we are increasing both the dimensionality and the average energy of the constellation.

Now let us consider the results for Ungerboeck's (8,4)-trellis as summarized in Table 3.6. Once again 8-PSK is the optimum 8-point constellation. However a 0.25dB improvement can be obtained if a 16-PSK constellation is modified to become 8-8-PSK with $r_B = 1.636$. An 8-8-PSK constellation definitely qualifies as being practical. This is based on the continued discussion in the literature about whether 16-PSK or 16-QASK is best for satellite applications [6] [13].

DTC-(8,4)-8-8-PSK shows a 0.78dB improvement over uncoded D8PSK. The 16-state DTC-(16,4)-16-PSK code shows an improvement of only 0.53dB over coherent uncoded 8PSK. Consequently DTC-(8,4)-8-8-PSK is superior to DTC-(16,4)-16-PSK by 0.25dB.

However when compared with DTC-(8,2)-16-PSK it has a lower performance. DTC-(8,2)-16-PSK has a gain of 1.00dB over uncoded 8-PSK. By contrast, DTC-(8,4)-8-8-PSK has a gain of only 0.78dB. It is also worth noting that DTC-(8,4)-8-8-PSK is 0.65dB worse than the best 16-state, 16-point code – DTC-(16,2)-16-PSK. This is consistent with the observation by Wilson et al [13] that for trellis codes with less than 128 states, a 2-sets-of-$(\frac{M}{2})$ branching technique yields the best performance for 2M-PSK on the AWGN channel.

However the simulation results of Lee et al [24] and McLane et al [25] indicate that on fading channels PSK and DPSK constellations perform better using trellises with more than 2 sets of branches per state. These promising results have been attributed to the increased diversity of such codes which permits them to better combat the effects of fading.

Thus, when considered in the context of a fading environment, DTC-(8,4)-8-8-PSK

Path No.	Path Length	Path	Path Weight				
M			4	8	16	32	64
r_B			1.0000	1.6380	1.3226	1.1545	1.0754
1	1	D0		4.0000	2.0000	0.5858	0.1522
2	2	D2-D4	3.0000	1.2929	0.3690	0.0953	0.0240
3	3	D2-D6-D4	4.0000	1.5858	0.4451	0.1145	0.0288
4	3	D6-D5-D2	2.2929	1.2919	0.3691	0.0950	0.0241
5	3	D6-D7-D6	2.2929	1.2919	0.3691	0.0950	0.0241
6	3	D4-D1-D2	3.2929	1.9990	0.5858	0.1519	0.0385
7	3	D4-D3-D6	3.2929	1.9990	0.5858	0.1519	0.0385
8	4	D4-D1-D0-D4	4.2929	2.1782	0.6421	0.1672	0.0423
9	4	D4-D5-D3-D2	3.5858	1.6493	0.4817	0.1253	0.0317
10	4	D4-D5-D1-D6	3.5858	1.6493	0.4817	0.1253	0.0317
11	4	D4-D3-D4-D4	6.2929	3.7061	1.0955	0.2849	0.0721
12	4	D4-D7-D7-D2	3.5858	1.6493	0.4817	0.1253	0.0317
13	4	D4-D7-D5-D6	3.5858	1.6493	0.4817	0.1253	0.0317
14	4	D4-D6-D6-D4	6.0000	2.5858	0.7380	0.1907	0.0481

M	4	8	16	32	64
r_B	1.0000	1.6380	1.3226	1.1545	1.0754
Min. Weight	2.2929	1.2919	0.3690	0.0950	0.0240
Energy Penalty	1.0000	1.8415	1.3746	1.1864	1.0782
(dB)	0.00	2.65	1.38	0.67	0.33
Coding Gain over M-PSK	1.1464	1.1976	1.7633	2.1192	2.3141
(dB)	0.59	0.78	2.46	3.26	3.64
Coding Gain over TC-2M-PSK	0.5000	0.5299	0.7829	0.9415	1.0270
(dB)	-3.01	-2.76	-1.06	-0.26	0.12
Coding Gain over DTC-2M-PSK	1.0000	1.0599	1.5653	1.8852	2.0635
(dB)	0.00	0.25	1.95	2.75	3.15
Peak-to-Average Energy Ratio	1.00	1.46	1.27	1.14	1.07

Table 3.6: Contender Path Weights for DTC-(8,4)-M-M-PSK at optimum values of r_B

shows considerable promise. The use of differential demodulation is also more prevalent on fading channels because of its more graceful degradation during fades compared with coherent systems [9] [15].

However it is beyond the scope of the present research to simulate the performance of DTC-(8,4)-8-8-PSK on a fading channel. Instead we seek to validate these asymptotic results for DTC-M-M-PSK by obtaining comparable simulation results for the AWGN channel.

If we now consider the remaining "impractical" constellations of Table 3.6 we see that even larger improvements are obtained by modifying the 32-, 64- and 128-point constellations to obtain optimum M-M-PSK constellations. These three codes outperform the corresponding 16-state 2M-PSK codes by 1.07dB, 1.88dB and 2.27dB respectively. However these improvements cannot compete with the advantages of using coherent detection on trellis coded non-PSK constellations which have a lower average constellation energy.

3.7.3 16-state Trellises

Asymptotic results were also obtained for the (16,2)-trellis cited by Wilson et al [13] and Ungerboeck [3] and the (16,4)-trellis that was discussed in Ungerboeck's earlier paper [1]. These results are shown in Tables 3.7 and 3.8, respectively.

For 8 points and 16 points, the 2M-PSK constellations are still optimum for these trellises. Consistent with our results for the smaller trellises, M-M-PSK constellations perform better than 2M-PSK for the impractical constellations with more than 32 points.

Results were not calculated for a (16,8)-trellis. No references to a specific (16,8)-trellis were found in the literature. It was also readily determined that there are 53 possible error paths of length 4 or less. In view of the non-linear nature of DTC-M-M-PSK, it would be prudent to consider the effects of subset dilation on all of these path weights before forming conclusions regarding the improvement achievable using DTC-M-M-PSK.

3.7.4 Summary

The above analysis of DTC-M-M-PSK asymptotic performance highlighted a practical 16-point code which achieved a modest 0.25dB improvement over the DTC-2M-PSK code using

Path No.	Path Length	Path	Path Weight				
M			4	8	16	32	64
r_B			1.0000	1.0000	1.1190	1.1810	1.0883
1	1	C0	2.0000	1.0000	0.2029	0.0761	0.0192
2	5	C2-C2-C0-C1-C2	3.2929	0.9548	0.2537	0.0761	0.0192
3	6	C2-C0-C2-C1-C3-C2	5.0000	1.4645	0.3889	0.1456	0.0376
4	7	C2-C2-C2-C3-C2-C1-C2	5.5858	1.6167	0.4566	0.1888	0.0480
5	7	C2-C0-C0-C3-C3-C3-C2	2.8787	0.8141	0.2538	0.1496	0.0383
6	8	C2-C0-C2-C3-C1-C2-C1-C2	4.8787	1.3999	0.4060	0.1880	0.0479
7	8	C2-C0-C0-C1-C1-C3-C3-C2	3.1716	0.8903	0.2538	0.1121	0.0287
8	8	C2-C2-C2-C1-C0-C1-C3-C2	4.8787	1.3999	0.4060	0.1880	0.0479
9	8	C2-C2-C0-C3-C0-C0-C1-C2	3.5858	1.0309	0.2791	0.0945	0.0240

M	4	8	16	32	64
r_B	1.0000	1.0000	1.1190	1.1810	1.0883
Min. Weight	2.0000	0.8141	0.2537	0.0761	0.0192
Energy Penalty	1.0000	1.0000	1.1261	1.1974	1.0922
(dB)	0.00	0.00	0.52	0.78	0.38
Coding Gain over M-PSK	1.0000	1.3898	1.4801	1.6533	1.8268
(dB)	0.00	1.43	1.70	2.18	2.62
Coding Gain over TC-2M-PSK	0.5000	0.5000	0.5368	0.6005	0.6639
(dB)	-3.01	-3.01	-2.70	-2.21	-1.78
Coding Gain over DTC-2M-PSK	1.0000	1.0001	1.0735	1.2010	1.3328
(dB)	0.00	0.00	0.31	0.80	1.25
Peak-to-Average Energy Ratio	1.00	1.00	1.11	1.16	1.08

Table 3.7: Contender Path Weights for DTC-(16,2)-M-M-PSK at optimum values of r_B

Path No.	Path Length	Path	Path Weight				
M			4	8	16	32	64
r B			1.0000	1.0000	1.7150	1.3000	1.1391
1	1	D0		4.0000	2.0000	0.5858	0.1522
2	3	D4-D1-D2	3.2929	1.3690	1.1561	0.2743	0.0678
3	3	D2-D4-D4	5.0000	2.2929	0.6619	0.1715	0.0432
4	3	D6-D5-D6	2.2929	0.6619	0.9393	0.2174	0.0534
5	4	D4-D3-D3-D2	3.5858	1.4451	1.3025	0.3124	0.0774
6	4	D2-D0-D5-D2	2.2929	0.6619	0.9393	0.2174	0.0534
7	4	D6-D1-D7-D2	2.5858	0.7380	0.4451	0.1147	0.0289
8	4	D4-D3-D6-D4	4.2929	1.6619	1.2322	0.2935	0.0726
9	4	D2-D6-D0-D4	4.0000	1.5858	0.4451	0.1145	0.0288
10	4	D6-D7-D2-D4	4.2929	1.6619	1.2322	0.2935	0.0726
11	4	D4-D7-D6-D6	4.2929	1.6619	1.8728	0.4344	0.1067
12	4	D2-D2-D1-D6	3.2929	0.9546	1.6560	0.3775	0.0923
13	4	D6-D3-D3-D6	2.5858	0.7380	0.4451	0.1147	0.0289

M	4	8	16	32	64
r B	1.0000	1.0000	1.7150	1.3000	1.1391
Min. Weight	2.2929	0.6619	0.4451	0.1145	0.0288
Energy Penalty	1.0000	1.0000	1.9706	1.3450	1.1488
(dB)	0.00	0.00	2.95	1.29	0.60
Coding Gain over M-PSK	1.1464	1.1299	1.4837	2.2162	2.8073
(dB)	0.59	0.53	1.71	3.46	4.16
Coding Gain over TC-2M-PSK	0.5000	0.5000	0.6587	0.9846	1.1571
(dB)	-3.01	-3.01	-1.81	-0.07	0.63
Coding Gain over DTC-2M-PSK	1.0000	1.0000	1.3170	1.9715	2.3250
(dB)	0.00	0.00	1.20	2.95	3.66
Peak-to-Average Energy Ratio	1.00	1.00	1.49	1.26	1.13

Table 3.8: Contender Path Weights for DTC-(16,4)-M-M-PSK at optimum values of r_B

the same transmit trellis.

Although this code – DTC-(8,4)-8-8-PSK – outperforms DTC-(16,4)-16-PSK by 0.25dB, it yields worse results on an AWGN channel than DTC-(16,2)-16-PSK. However the (8,4) and (16,4) codes are of greater importance on fading channels because of their diversity advantage over the (16,2) codes.

On the basis of its potential importance for fading channel applications, the analytical results for DTC-(8,4)-8-8-PSK at high SNR will be compared with simulation results for a variety of SNR values. These simulations will be restricted to the case of an AWGN channel.

Chapter 4

DTC-M-M-PSK Simulation Results

4.1 Introduction

This chapter provides simulation results for the DTC-(8,4)-8-8-PSK code identified in Chapter 3. The analytical predictions were for the case of asymptotically high SNR. The simulations however cover the appropriate SNR range for reasonable bit error rates in practical communication systems.

The simulation software is described briefly to establish the conditions under which the simulations were performed. The simulation package was designed to handle a wide variety of TCM-related modulation formats – including DTC-M-M-PSK. It was written in C and executed on an IBM PC.

The analytical calculations from Chapter 3 predicted a 0.25 dB coding gain over DTC-(8,4)-16-PSK. The simulations demonstrate that at low SNR the DTC-(8,4)-8-8-PSK code outperforms DTC-(8,4)-16-PSK by even more than 0.25 dB. Extremely long simulation runs would be required to confirm the predicted coding gain for high SNR. However the error curves that have been obtained are consistent with this prediction.

Additional simulation runs were performed to validate the simulation package and to provide reference curves against which DTC-(8,4)-8-8-PSK could be compared. These results are provided for uncoded D8PSK, DTC-(8,4)-16-PSK and DTC-(16,4)-16-PSK.

In view of its excellent performance at low SNR, additional simulations were performed for DTC-(8,4)-8-8-PSK with different dilation factors, r_B. The results confirm a degradation

in overall performance as r_B is increased beyond the predicted optimum of 1.638. They also demonstrate that – at practical bit error rates – a trade-off exists between the Peak-to-Average-Energy ratio and the coding gain.

Tabular results from these simulation runs can be found in Appendix A.

4.2 Simulation Software

This section provides a brief description of the conditions under which the simulations were performed.

The simulation package was specifically developed to handle a wide variety of TCM formats – including DTC-M-M-PSK. Figure 4.1 shows how it is organized. The "parameter" routine is used to establish the model for the modulation format. The other routines correspond to their hardware equivalents as shown in Figures 2.1 and 2.9.

4.2.1 Data Sequence Generator

This routine produces a pseudo-random sequence of uncoded bits based on a maximal length shift register code shown in Figure 4.2 The generator uses a 32-bit shift register with feedback taps at positions 1,11,31 and 32. This code with a period of greater than 4 Gigabits, was obtained from Proakis [14].

4.2.2 Convolutional Encoder

This routine implements a specific convolutional encoder based on the previously established model. For these simulations the input symbols contain 3 bits. For all but the D8PSK case, the output symbols contain 4 bits.

4.2.3 Differential Encoder

This routine implements standard phase-difference coding combined with subset dilation. The phase of the transmit symbol is equal to the phase difference of the current TCM symbol and the previous transmit symbol. However transmit constellation points whose phase is an odd multiple of $\frac{\pi}{M}$ have a higher amplitude. In effect, one of the major subsets in the transmit constellation has been dilated after phase difference encoding.

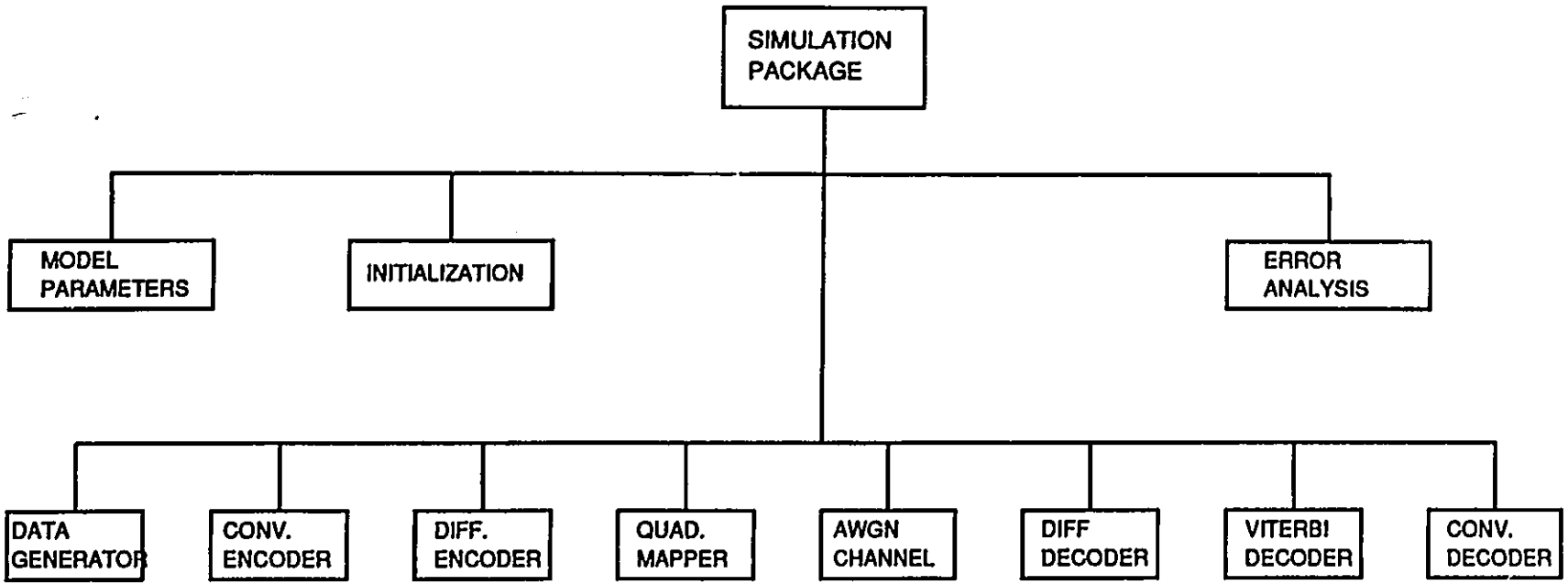

Figure 4.1: Organization of the Simulation Software

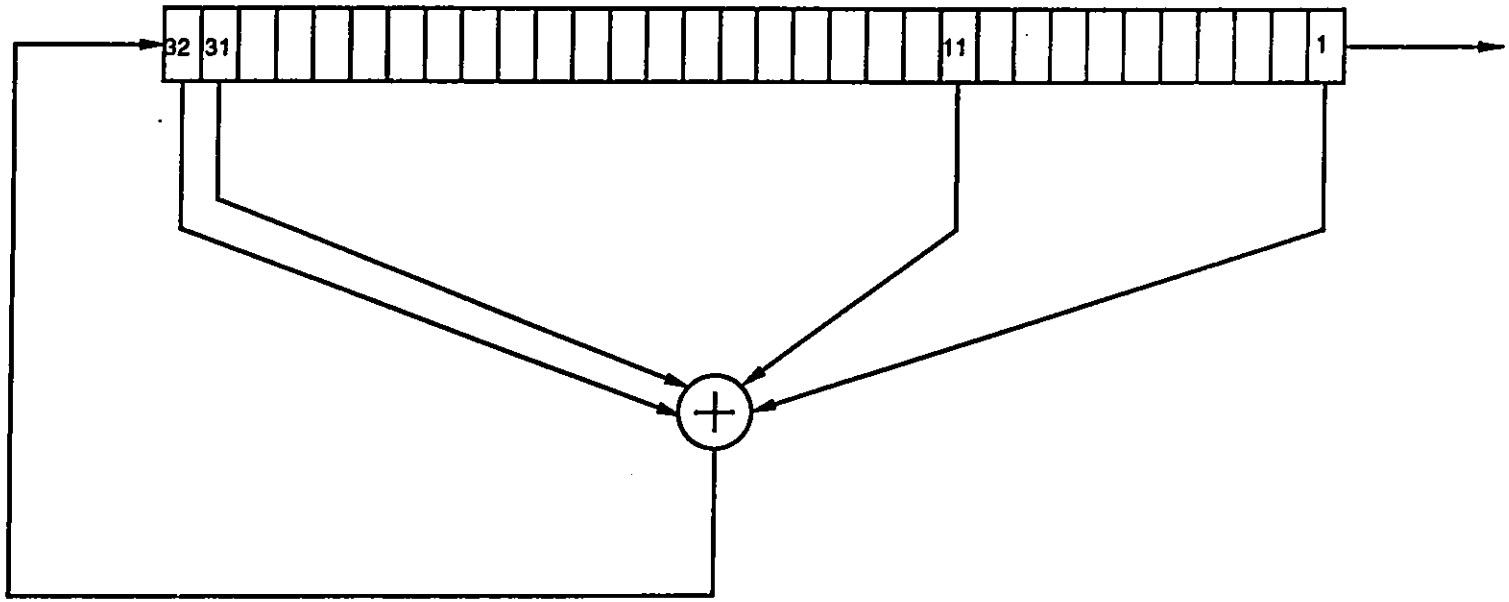

Figure 4.2: Random Data Sequence Generator

4.2.4 Signal Mapper

This routine implements the TCM mapping function by table lookup. The result is the equivalent baseband complex representation for the transmit constellation symbols.

The in-phase and quadrature components consist of integer values with 15 bits of dynamic range. They have been scaled such that the outer points in the product constellation will span the set of integers from 4000_{16} to $C000_{16}$. These values correspond to points on the product constellation C-ring of radius $r_C = r_B^2$.

4.2.5 AWGN Channel

This routine adds values from a Gaussian noise file to the channel symbols.

The noise file consists of 2048 pairs of in-phase and quadrature noise samples. Each complex noise sample has a variance of 2. Before the noise samples are added to the complex channel symbols, they are scaled to achieve the desired value for E_b/N_0. The samples are used repetitively in sequence until the simulation run is completed.

4.2.6 Differential Demodulator

This routine performs a complex floating point multiply on the noisy channel symbols.

4.2.7 Viterbi Decoder

This routine implements a Viterbi decoder in a number of stages similar to those that would be found in a practical receiver. The structure of the Viterbi decoder trellis is based on the previously defined model.

For these simulations the branch metrics and path metrics had a dynamic range of 10 bits and 30 bits respectively. During each symbol period the lowest path metric was identified and then subtracted from the entire set of path metrics. Any path metrics which exceeded 30 bits had their high order bits truncated to prevent eventual overflow.

In the case of DTC-M-M-PSK, the branch metric weights are implemented in integer arithmetic with 10 bits of precision. The use of floating point arithmetic would have greatly increased the simulation run time. These branch metric weighting factors were implemented based on equations (3.7) – (3.9) from Chapter 3.

The decoding depth for all simulation runs was 16 bits. This is considered to be more than adequate for a trellis code with a constraint length of 3. During each symbol period the Viterbi decoder determines the best current path metric and traces that path back through the trellis for 16 symbol periods. The last two states from this traceback are used to estimate the channel symbol.

4.2.8 Convolutional Decoder

This routine implements the convolutional decoder based on the previously defined model. The data estimates could have been obtained directly from the Viterbi Algorithm. However the use of a separate convolutional decoder stage permits end-to-end tests to be performed separately on the coder/decoder and modulator/demodulator segments of the simulated communication system. This is consistent with practical hardware implementations.

4.2.9 Error Analysis

This routine compares the original random data sequence with the output of the convolutional decoder and evaluates the Symbol Error Rate (SER) and the Bit Error Rate (BER). SER and BER are calculated separately; no assumptions are required concerning the relative importance of single-bit and multi-bit errors.

4.3 Simulation Results

We will now consider the results obtained by using this simulation package on a variety of DTC-M-M-PSK constellations.

When a Monte Carlo simulation is performed for an uncoded transmission system with no ISI, the errors have a binomial distribution [8]. The standard deviation for such an error distribution is given by the following equation:

$$\sigma_P = \sqrt{\frac{P_e(1-P_e)}{N}} \tag{4.1}$$

where N is the number of samples in the simulation.

In general we seek to have σ_P an order of magnitude lower than the probability of error itself. For $P_e << 1$ this leads to a requirement for $N \geq 100/P_e$. However, we are dealing

with coded systems using differential detection. Such systems tend to have burst errors rather than random errors [18]. Consequently we usually continue the simulation runs until several hundred bit errors occur.

4.3.1 Differentially Coherent Uncoded 8-PSK (D8PSK)

The simulation of D8PSK served two purposes. It permitted the simulation software to be checked against well established theoretical results. No such data is easily obtainable for trellis coded error performance curves. In addition, the D8PSK curves provide an uncoded reference for all simulations which follow.

Results for D8PSK were obtained using the same simulation software as for all other trellis coded simulations. However, in this case, the model was configured for a rate 1/1 convolutional code and a trivial one-state trellis with 8 "parallel" branches as shown in Figure 4.3.

The 8-PSK constellation is shown in Figure 4.4. The results for D8PSK are shown in Figure 4.5. The theoretical curve is obtained from tables produced by Lindsey and Simon [45] for the D8PSK error rate as described by the following equation taken from Lucky, Saltz and Weldon [32]:

$$P_e = 2[1 - \int_{-\pi}^{\frac{\pi}{8}} p(\theta)d\theta] \tag{4.2}$$

where

$$p(\theta) = \frac{1}{2\pi} e^{-\rho\cos\theta}[1 + \sqrt{4\pi\rho}\cos\theta e^{\rho\cos^2\theta} Q(\sqrt{2\pi}\cos\theta)] \tag{4.3}$$

where ρ is the signal-to-noise ratio, $\theta = 22.5^o$ is the angle between constellation points and $Q(\cdot)$ is the Gaussian error function defined earlier in equation (2.7). The theoretical bit error rate was calculated by dividing the symbol error rate values by 3. This assumes the use of Grey coding with the result that the overwhelming majority of symbol errors correspond to single bit errors.

4.3.2 DTC-(8,4)-16-PSK

The simulation runs for DTC-(8,4)-16-PSK implement Ungerboeck's 8-state trellis as shown in Figure 4.6.

The corresponding convolutional encoder is shown in Figure 4.7.

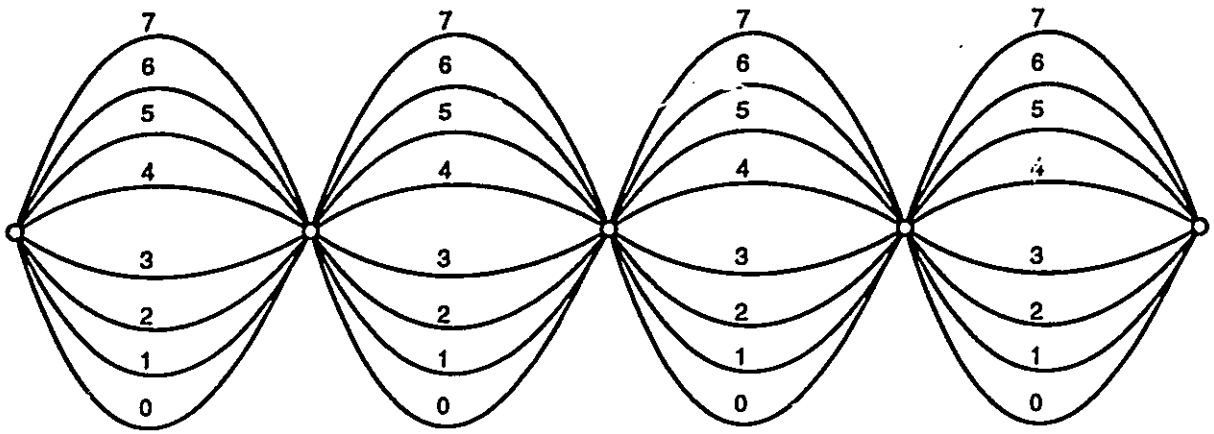

Figure 4.3: Trellis for D8PSK

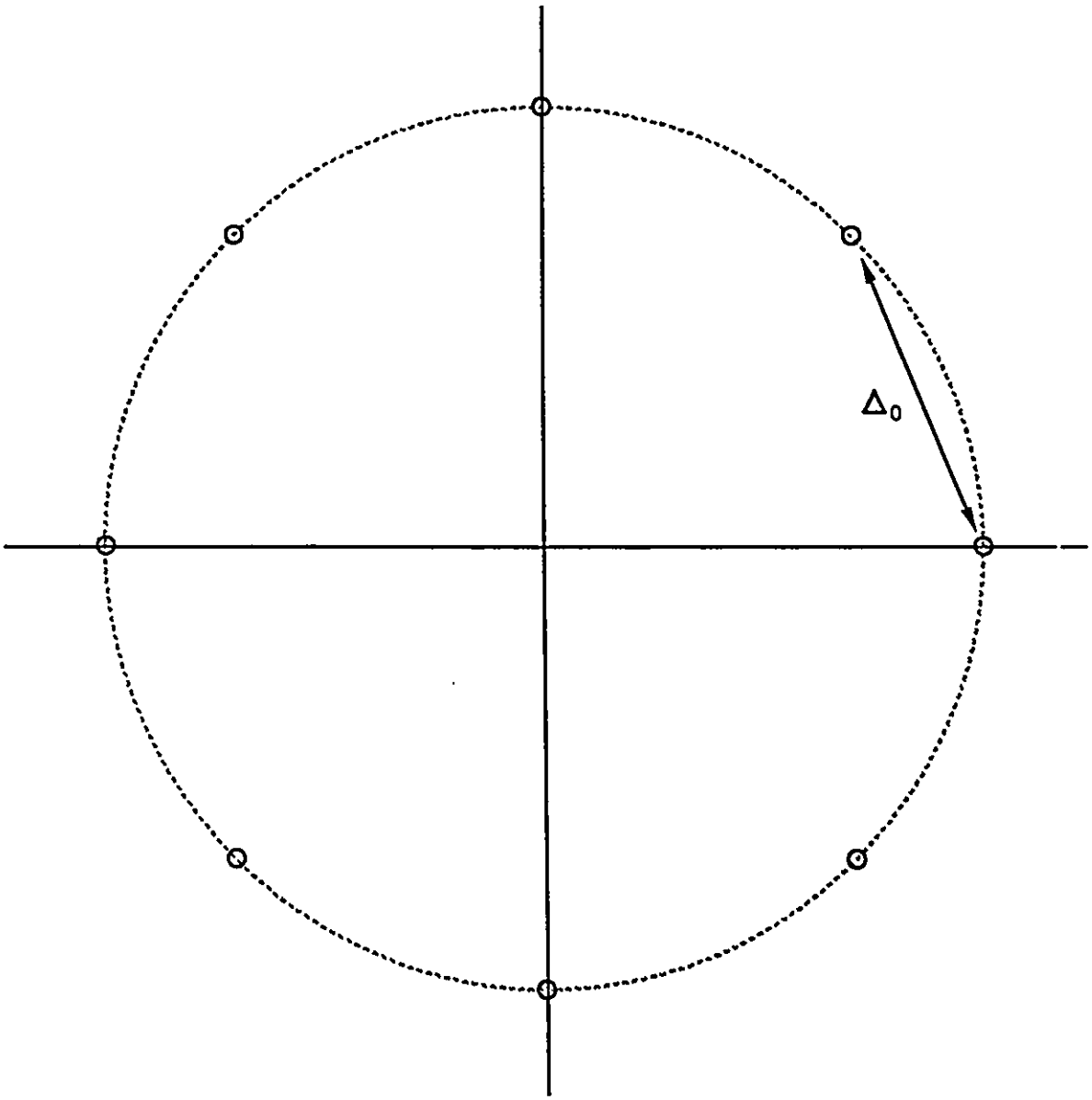

Figure 4.4: Constellation for D8PSK

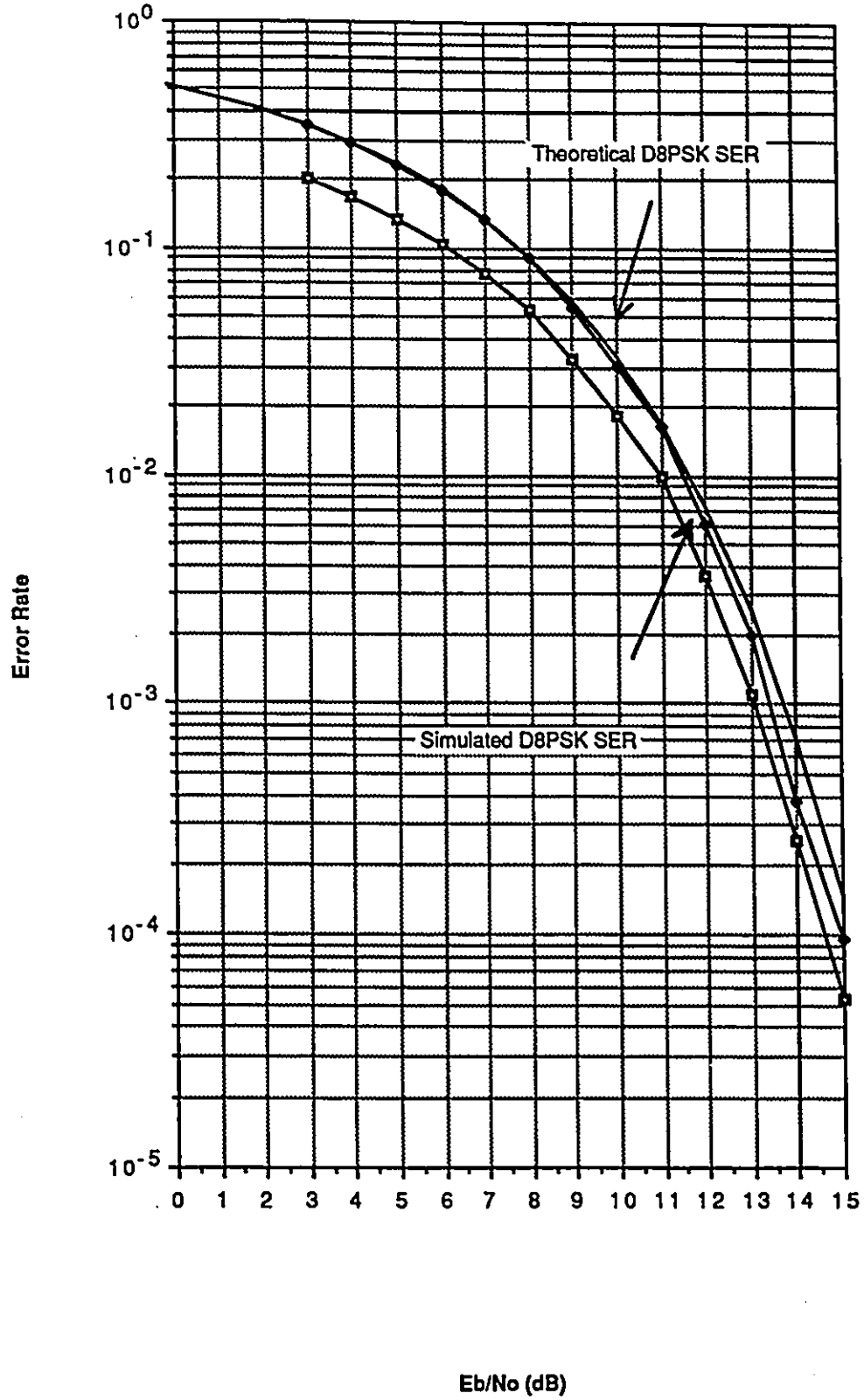

Figure 4.5: Simulation results for D8PSK

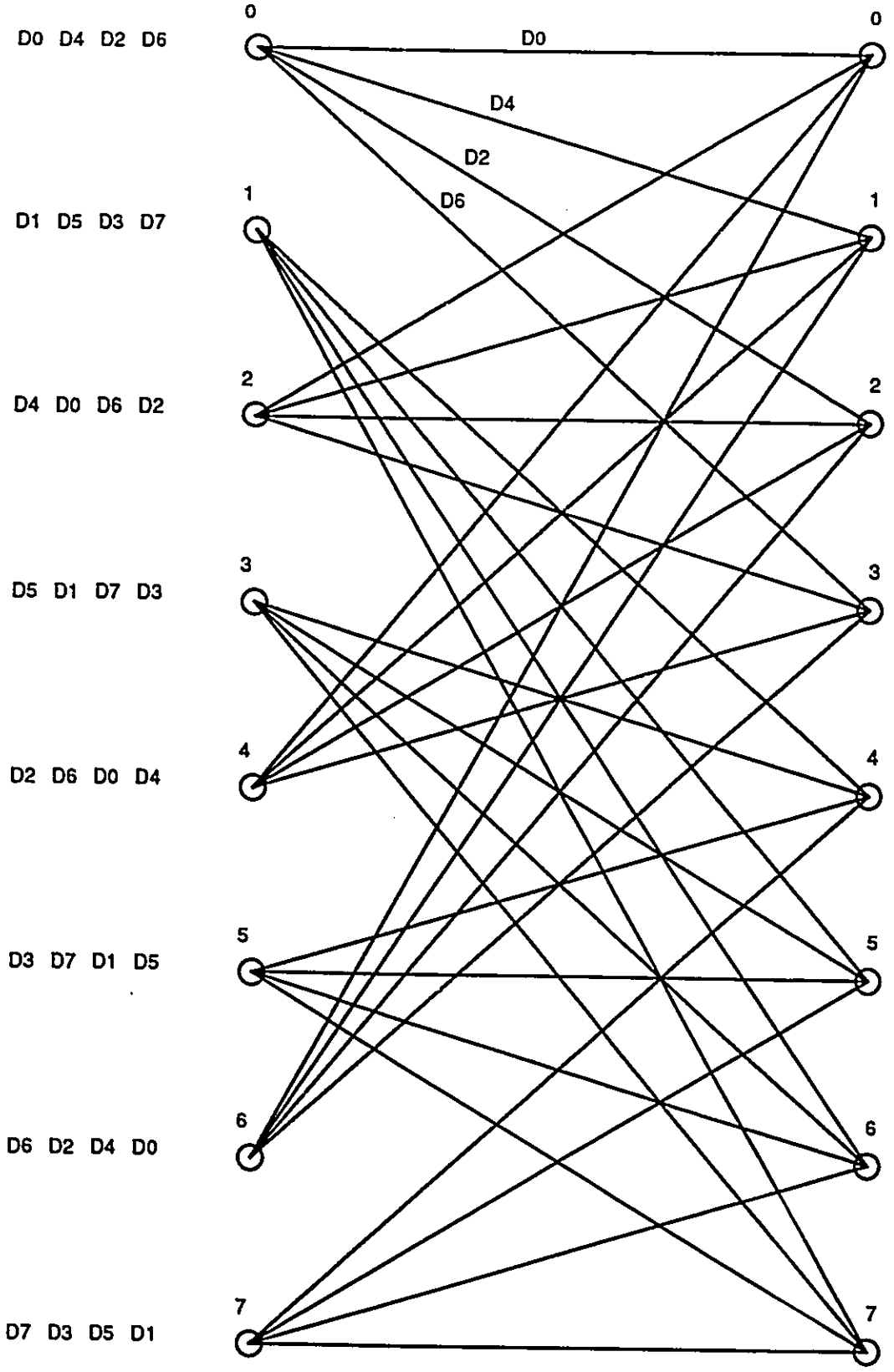

Figure 4.6: Transmit trellis for all Type-(8,4) Trellis Codes

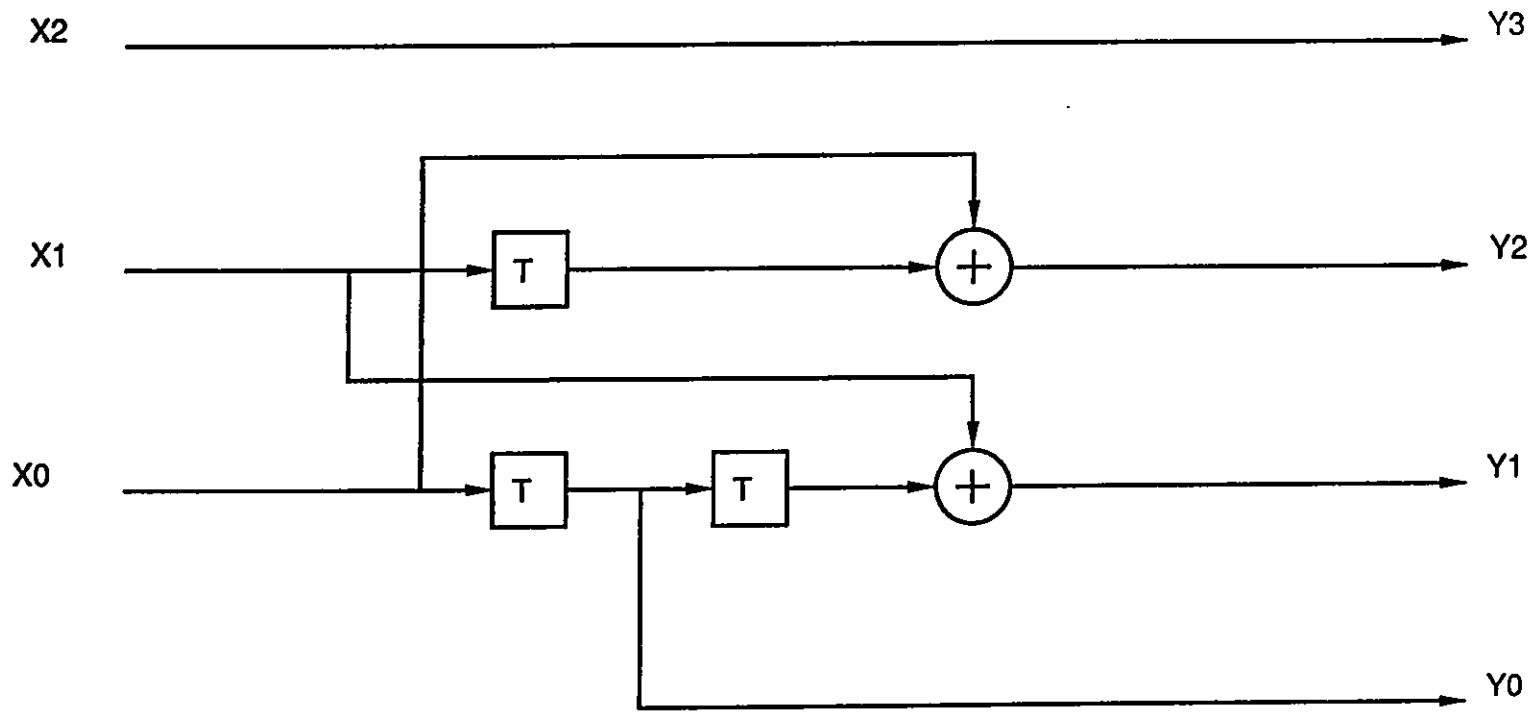

Figure 4.7: Convolutional Encoder for all Type-(8,4) Trellis Codes

The resultant coded symbols are mapped to a 16-PSK constellation in a counterclockwise fashion as shown in Figure 4.8.

After differential demodulation an 8-state Viterbi decoder uses the trellis shown in Figure 4.6 to estimate the sequence of transmitted TCM symbols. Then a convolutional decoder implements the reverse operation for the convolutional encoder shown earlier in Figure 4.7. The results for DTC-(8,4)-16-PSK are given in Figure 4.9.

4.3.3 DTC-(16,4)-16-PSK

The results for DTC-(16,4)-16-PSK are given in Figure 4.10. Performance is actually worse than for the DTC-(8,4)-16-PSK code for the range of E_b/N_0 values used in the simulation.

It is quite common with differential detection for more complex codes to exhibit worse performance at low bit error rates. However in most cases they yield a performance improvement at high SNR. In the case of this trellis code there is no performance improvement because the free distance of the (16,4) trellis is the same as that for the (8,4) trellis.

This is significant in that for most trellis codes an asymptotic improvement of about 0.4 dB can be obtained by using a trellis with twice as many states. DTC-(8,4)-8-8-PSK requires a receive trellis with 16 states rather than the 8 states used in the encoder. Consequently this code should be compared against a code requiring a receiver of comparable complexity – a 16-state 16-PSK code. However in this case, comparing DTC-(8,4)-8-8-PSK against the original DTC-(8,4)-16-PSK is equally valid since it has better performance than the 16-state 16-PSK code.

4.3.4 DTC-(8,4)-8-8-PSK

DTC-(8,4)-8-8-PSK uses the convolutional encoder shown in Figure 4.7 above. It also uses the same transmit trellis as for DTC-(8,4)-16-PSK. This is shown in Figure 4.6.

However the differentially coded TCM symbols are mapped into the constellation of Figure 4.11 rather than the 16-PSK constellation used for DTC-(8,4)-16-PSK.

For this transmit constellation, the resultant constellation after differential demodulation – the product constellation – is as shown in Figure 4.12. To obtain the estimates of the transmitted TCM symbols, the Viterbi decoder must implement the expanded trellis

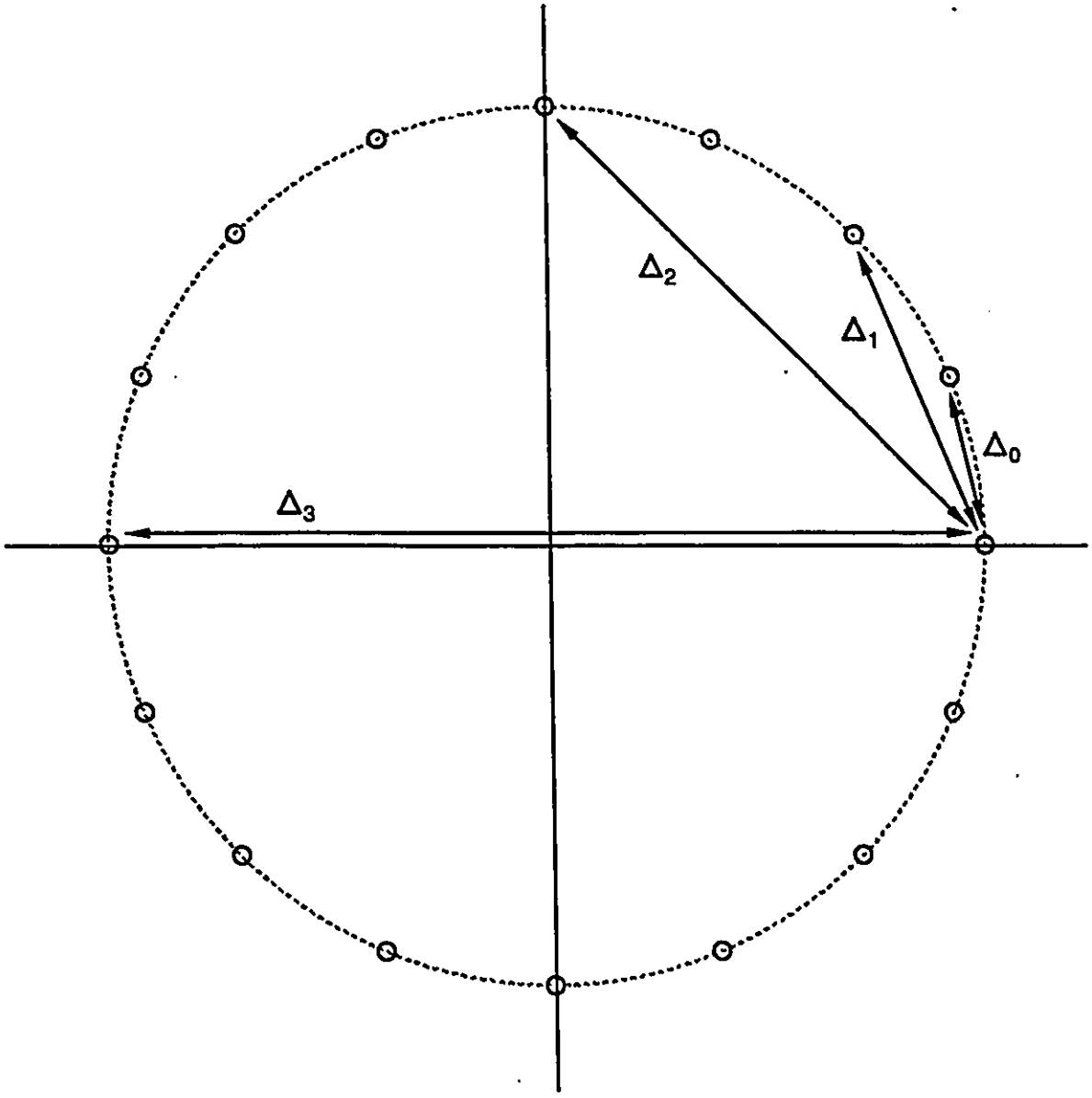

Figure 4.8: Transmit Constellation for DTC-(8,4)-16-PSK

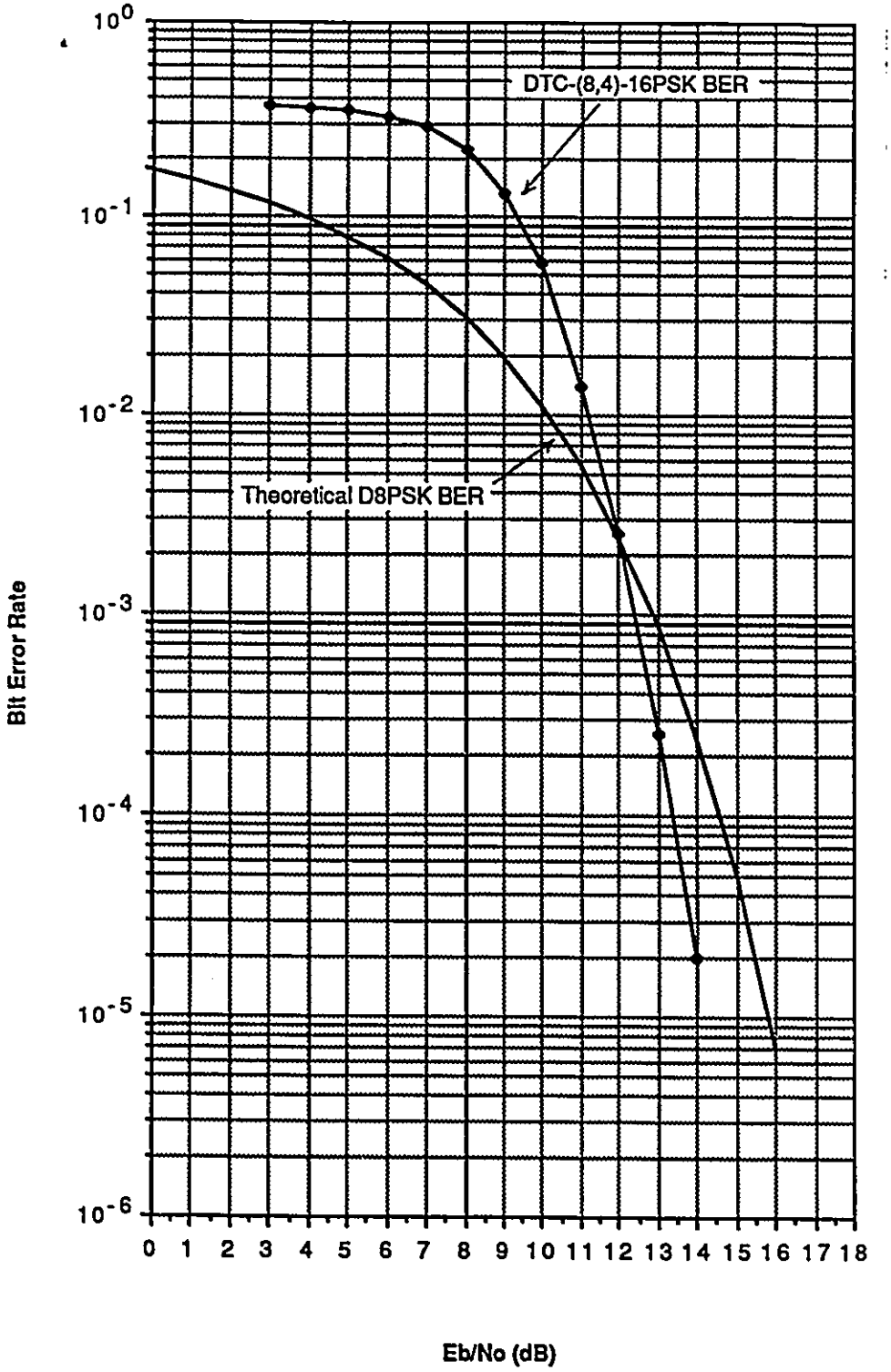

Figure 4.9: Simulation results for DTC-(8,4)-16-PSK

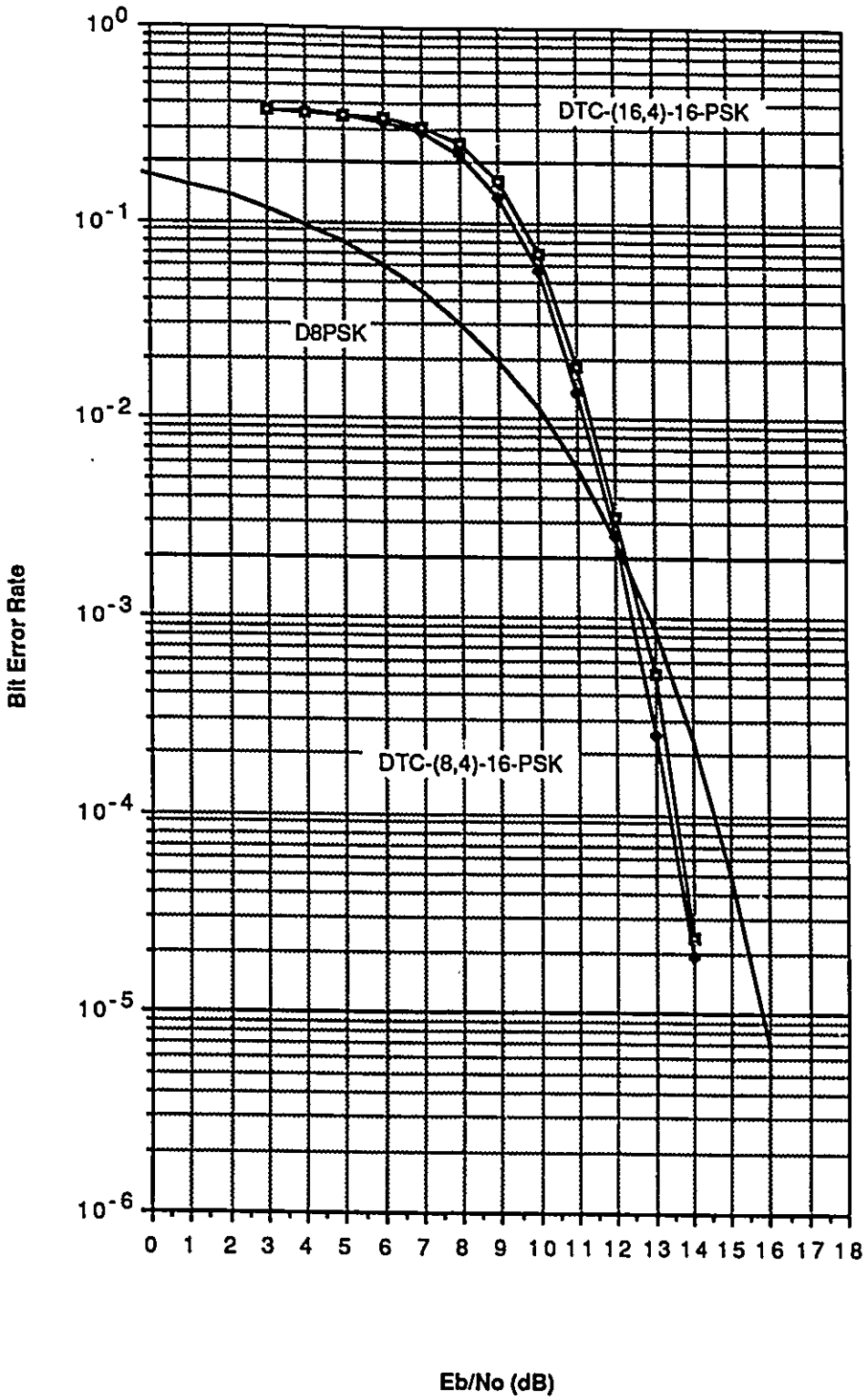

Figure 4.10: Simulation results for DTC-(16,4)-16-PSK

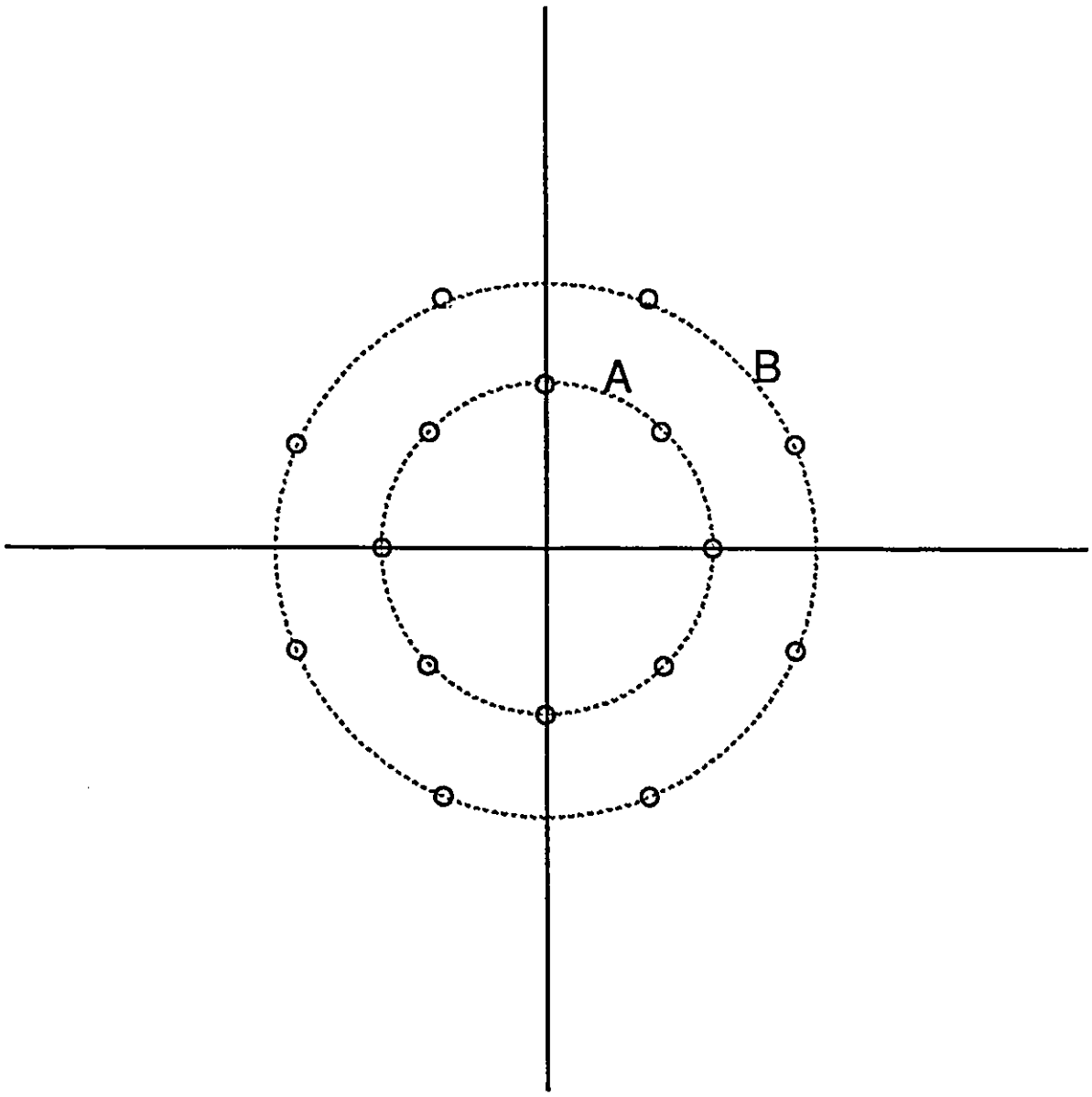

Figure 4.11: Transmit Constellation for DTC-(8,4)-8-8-PSK

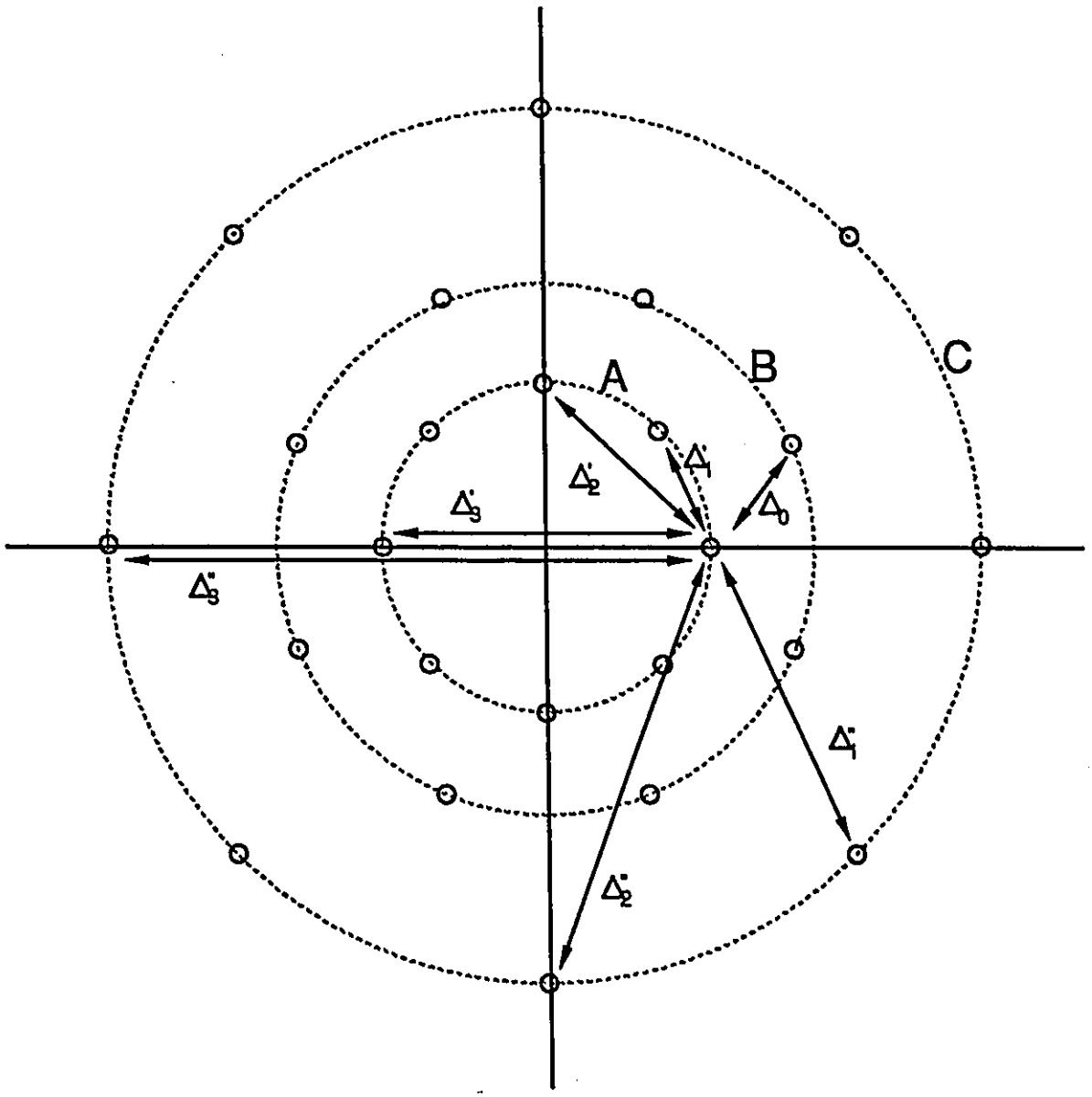

Figure 4.12: Product Constellation for DTC-(8,4)-8-8-PSK

shown in Figure 4.13.

The results for DTC-(8,4)-8-8-PSK are given in Figure 4.14. At $P_b = 10^{-4}$ this code outperforms DTC-(8,4)-16-PSK by 0.6dB. The analysis in Chapter 3 predicted a coding gain of 0.25dB at asymptotically high SNR. It is clear from the simulation results that at high SNR the coding gain will be a value lower than 0.6 dB.

What is more significant however is that at low SNR the coding gain is much larger than 0.25 dB. At $P_b = 10^{-3}$ it has a gain of 1.3dB over DTC-(8,4)-16-PSK and 1.8dB over D8PSK. In effect M-M-PSK has doubled the trellis coding gain over D8PSK for an error rate which is acceptable for many practical communication systems.

In view of these promising results, additional simulation runs were performed for dilation factors other than the predicted optimum of $r_B = 1.638$. As shown in Figures 4.15 and 4.16, any value for r_B between 1.0 and 1.638 yields a coding gain over DTC-(8,4)-16-PSK at low SNR as well as the asymptotic case. Increasing r_B beyond 1.638 yields little improvement in coding gain at low SNR and results in worse performance than DTC-(8,4)-16-PSK at high SNR. This is consistent with the analytical prediction that $r_B = 1.638$ would yield the optimum asymptotic result.

4.4 Summary

These simulation results have confirmed that DTC-M-M-PSK can indeed achieve coding gains over standard trellis codes using differentially coherent 2M-PSK.

They have also shown that at low and moderate value of E_b/N_0, DTC-M-M-PSK exceeds the predicted coding gains which were based on the asymptotic case of high SNR.

At a practical bit error rate of 10^{-3}, DTC-(8,4)-8-8-PSK more than doubled the coding gain that had been previously achieved by its 2M-PSK counterpart. This is based on a comparison with differentially coherent uncoded 8-PSK.

It was also confirmed that for dilation factors, r_B, below the optimum value of 1.638, it is possible to reduce the Peak-to-Average-Energy ratio of the Transmit constellation while still retaining most of the M-M-PSK coding gain.

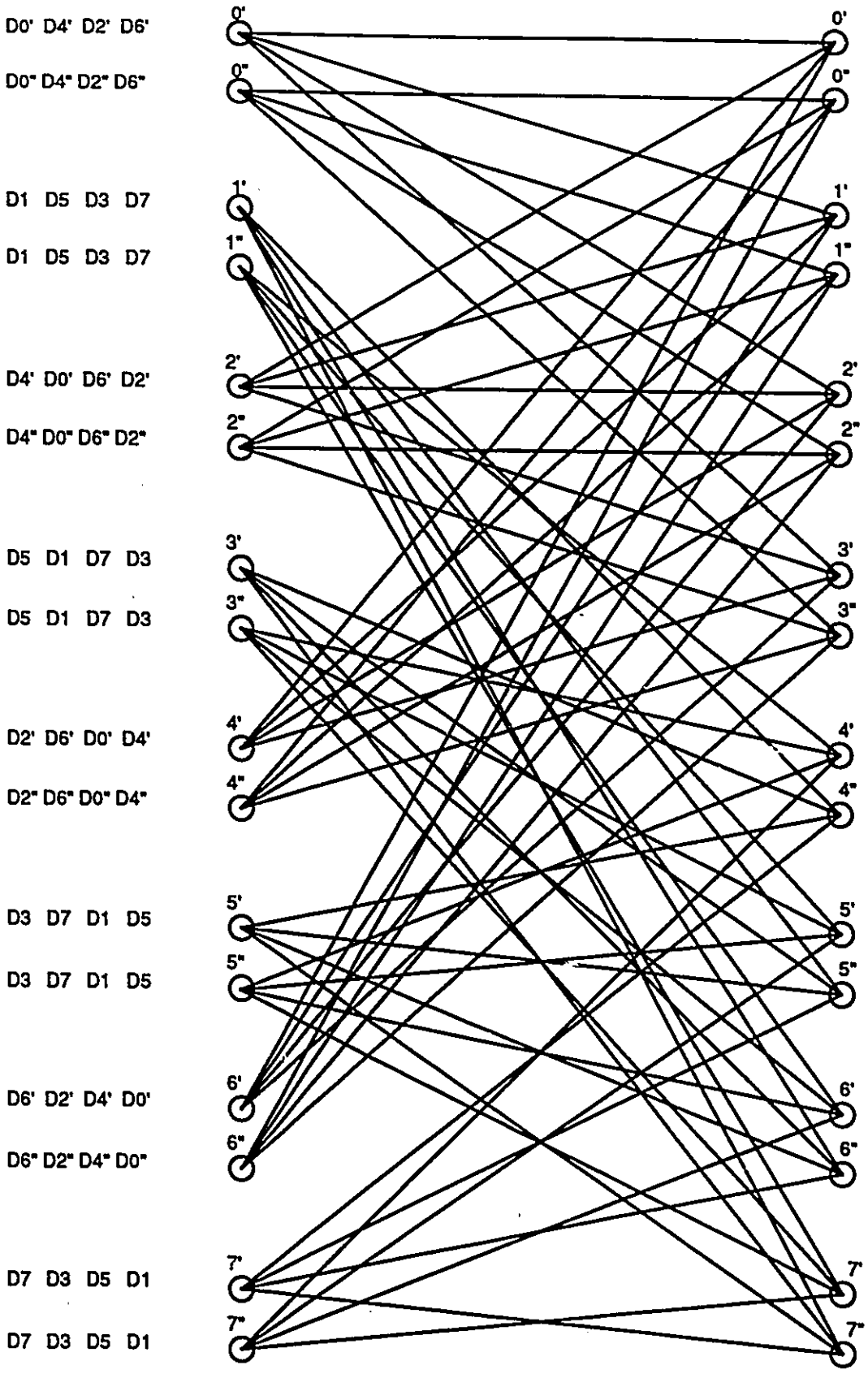

Figure 4.13: Viterbi decoder trellis for DTC-(8,4)-8-8-PSK

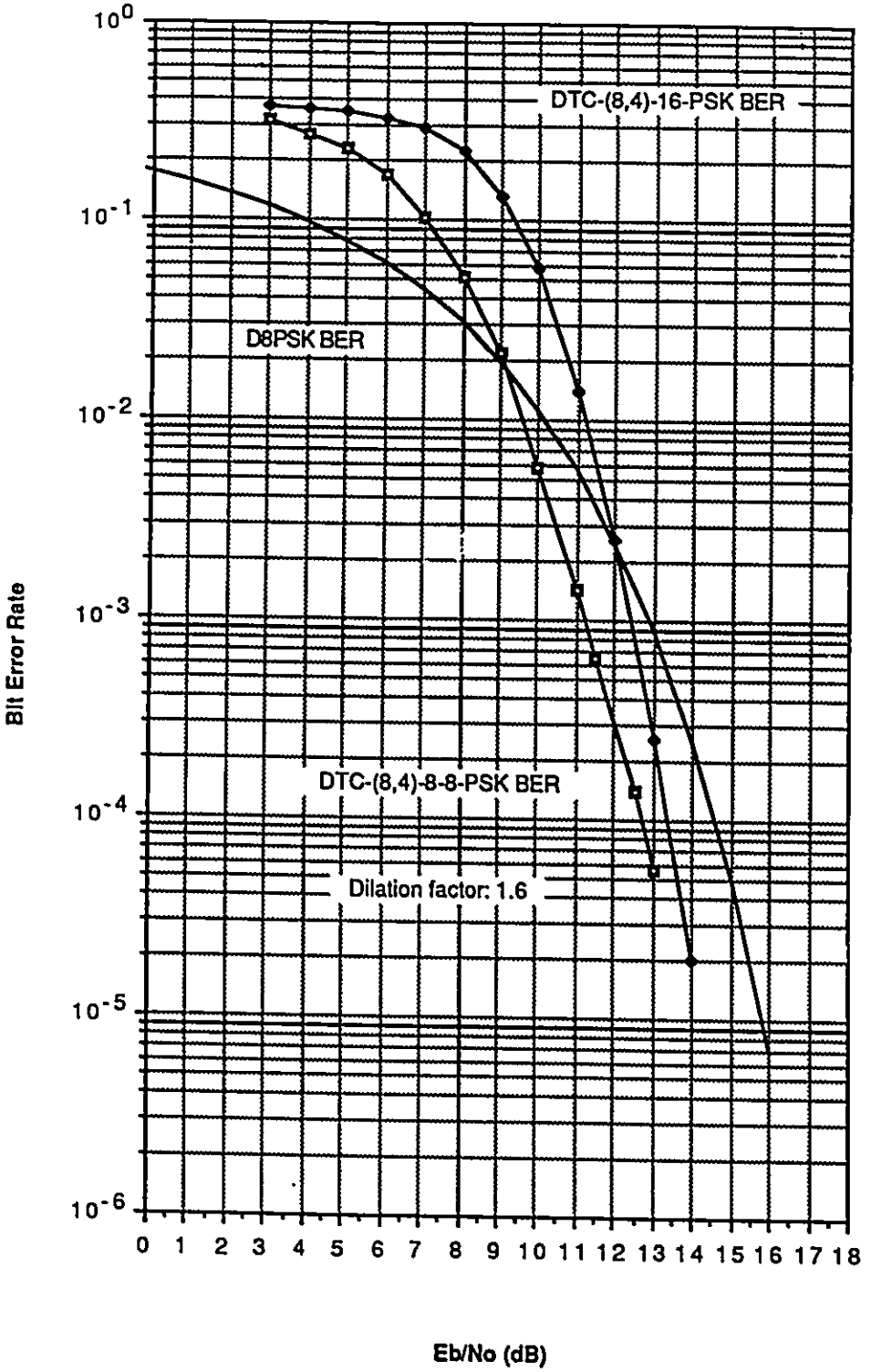

Figure 4.14: Simulation results for DTC-(8,4)-8-8-PSK

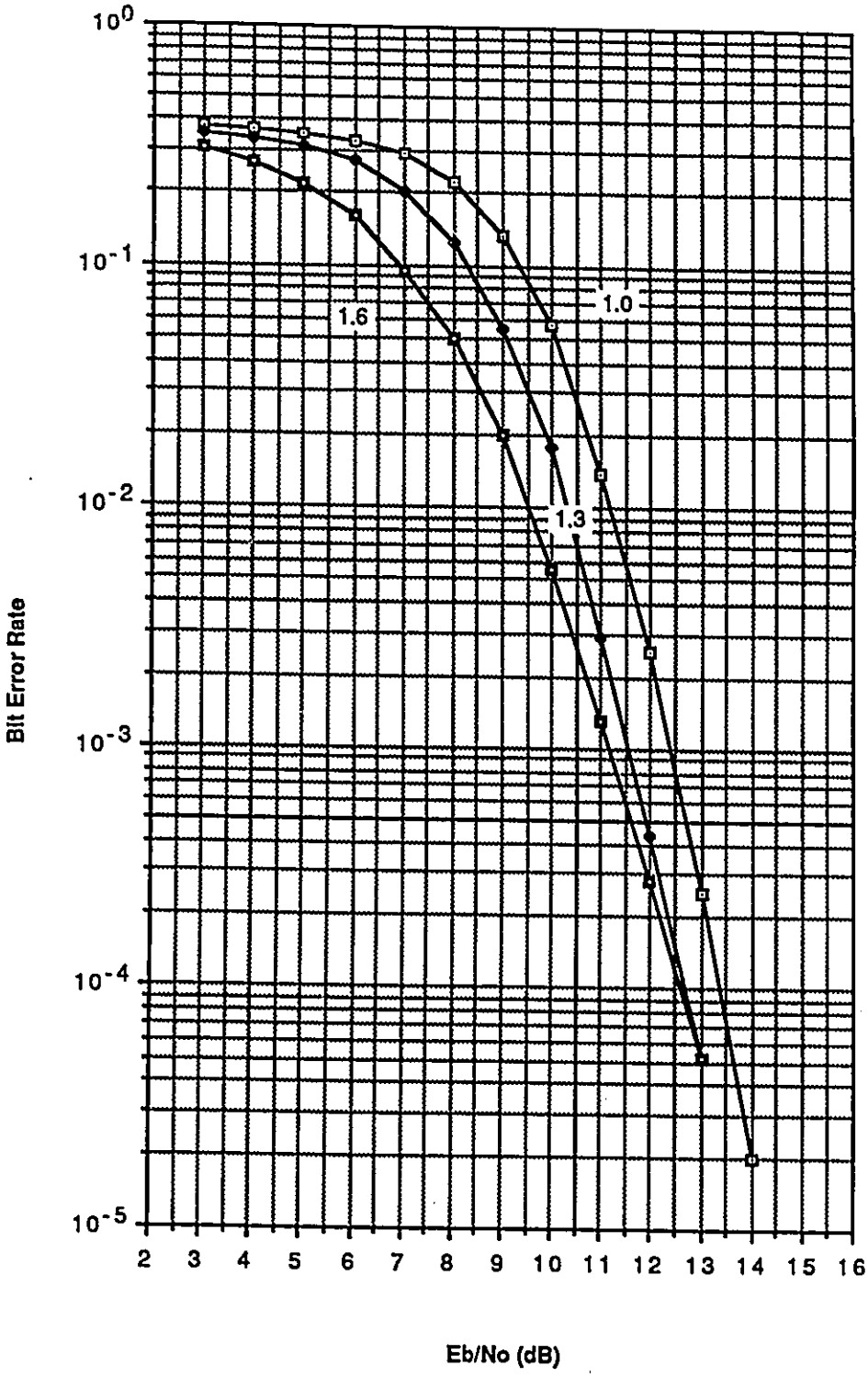

Figure 4.15: Simulation of DTC-(8,4)-8-8-PSK for $r_B \leq 1.638$

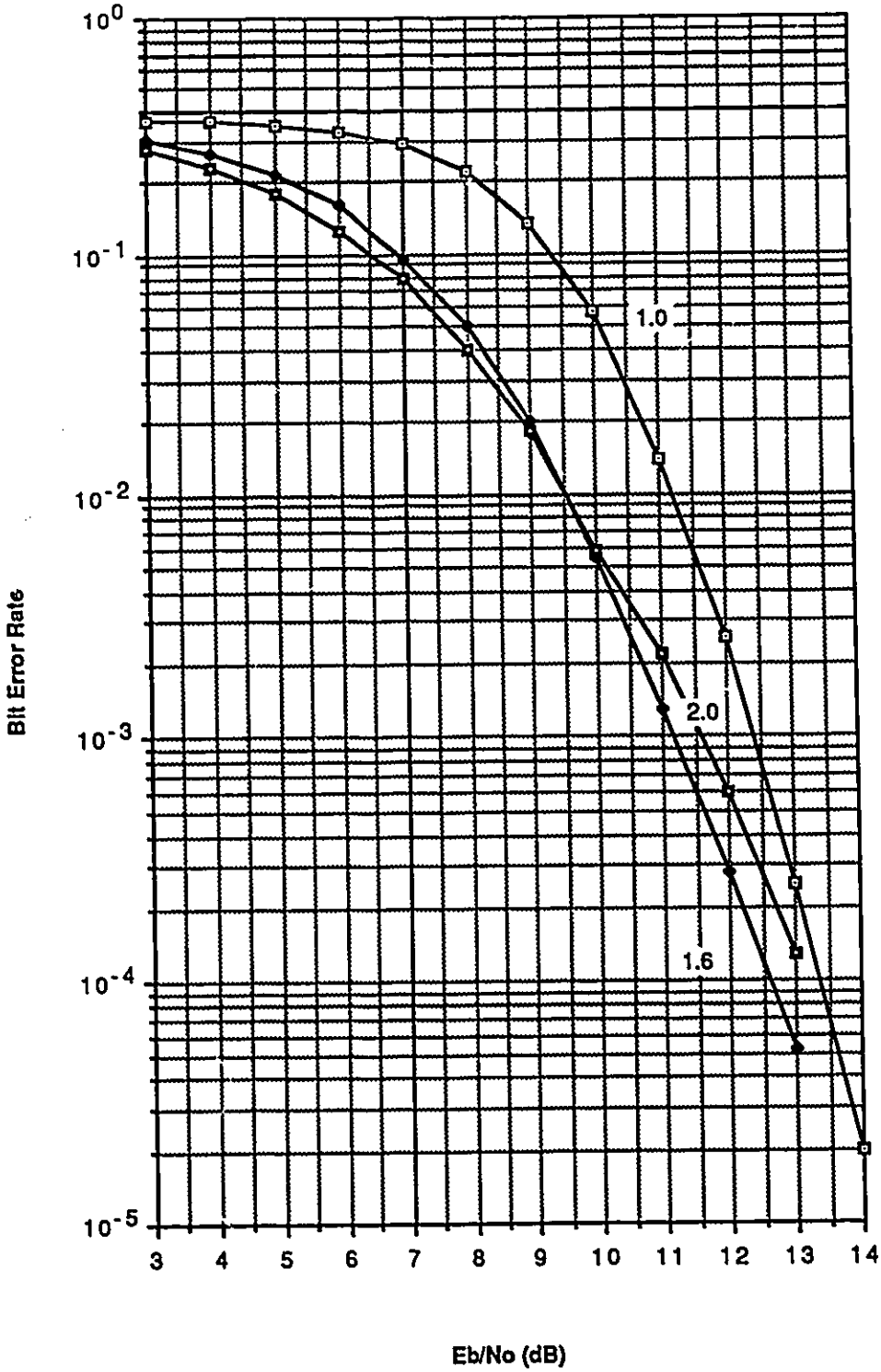

Figure 4.16: Simulation of DTC-(8,4)-8-8-PSK for $r_B \geq 1.638$

Chapter 5

Conclusions and Recommendations

5.1 Summary

This chapter will briefly review the analysis and results described in earlier chapters. Conclusions obtained from both analysis and simulation will be summarized. There are many interesting aspects of subset dilation which could not be fully explored in the context of this thesis. These will be enumerated with suggestions for their development.

The material in this thesis is based on the combined use of trellis-coding and differentially coherent detection. It began with the premise that further coding gains should be possible by deviating from the usual PSK transmit constellation in a manner which exploits the structure of the trellis code. The simulation results from Chapter 4 indicate that this objective has been achieved.

Chapter 2 presented the material for the current use of differentially coherent trellis-coded PSK and introduced the idea of showing all TCM intrasubset distances on a single constellation diagram. This assists in determining distance increases which would result from various changes in the constellation points. A noise model was developed which demonstrated that the same Viterbi decoder trellis and branch metrics are optimum for both coherent and differentially coherent trellis-coded PSK. We then proceeded to discuss the limitations of PSK constellations as constellation sizes increase.

Chapter 3 described some of the deviations from trellis-coded PSK which have been reported in the literature. We then proceeded to demonstrate the advantages in using two

PSK constellations of different amplitude for the B0 and B1 subsets in the overall TCM constellation. The noise model of Chapter 2 was expanded to handle these codes and to determine the appropriate changes in the Viterbi decoder trellis structure and branch metrics. A modest coding gain was predicted for DTC-(8,4)-8-8-PSK on the basis of asymptotically high SNR.

Chapter 4 described the Monte Carlo simulation software that was used to test this prediction. It also documented the constellations and convolutional encoder used to perform these tests.

The next section will summarize the conclusions derived from the above research.

5.2 Conclusions for DTC-M-M-PSK

The analytical and simulation results provided in this thesis demonstrate that the use of subset dilation can improve the performance of traditional differentially coherent trellis-coded PSK. It also demonstrates the advantages in considering non-PSK constellations for use with differentially coherent demodulation. The DTC-M-M-PSK codes described in this thesis provide more efficient use of the two-dimensional transmit constellation based on optimization criteria appropriate for trellis-coded modulation.

Simulation results for a specific code – DTC-(3,4)-8-8-PSK – indicate that at a bit error rate of 10^{-3}, subset dilation can provide a 1.3dB coding gain over the corresponding differentially coherent PSK code using the same encoder trellis. This used a dilation factor of $r_B = 1.638$ based on an analysis which predicted a 0.25dB coding gain for the asymptotic case of high SNR.

Additional simulations demonstrated that at a bit error rate of 10^{-3}, most of this coding gain can still be achieved using a smaller dilation factor. In particular a gain of 0.9dB was obtained for $r_B = 1.3$. This corresponds to a lower Peak-to-Average energy ratio such as would be desirable in peak-energy constrained systems. Consequently the DTC-M-M-PSK dilation factor,r_B, is shown to be a design parameter which can be adjusted to obtain the best tradeoff between Peak-to-Average-Energy ratio and the coding gain for a particular system implementation.

5.3 Recommendations for Further Research

The results obtained for DTC-M-M-PSK leave many profitable areas for continued research. A few are described below.

In view of the significant coding gains at low and moderate SNR for the DTC-(8,4)-8-8-PSK code, there is good reason to believe that similar results can be obtained for other DTC-M-M-PSK codes using simpler transmit trellises and smaller M-M-PSK constellations. The analysis in Chapter 3 implies that such codes would have little or no coding gain for asymptotically high SNR. However the simulation results suggest that, in general, most DTC-M-M-PSK codes would outperform their DTC-2M-PSK counterparts at low and moderate SNR.

There would also be merit in exploring the combination of the subset dilation as described in this research, and the phase asymmetries described in the work of Divsalar, Simon and Yuen [31]. This may provide further increases in trellis free distance at a lower average constellation energy – and lower Peak-to-Average-Energy ratio.

The results in this thesis clearly demonstrate a need for further analysis of DTC-M-M-PSK at low SNR. This would require consideration of the effects of $Noise \times Noise$ terms that were discounted in our high SNR analyses in Sections 2.4.1 and 3.5.1. It would also require a more detailed evaluation of the effects of other error paths whose weights are greater than the minimum error path. Subset dilation increases the weight of most error paths with the exception of those for symbol sequences that use only the $B0$ constellation points. Transfer functions for specific DTC-M-M-PSK codes could be obtained using signal flow graph techniques such as those described by Clark and Cain [40] and applied by Galko [42] and Zehavi and Wolfe [17].

With the traditional constraints now lifted from differentially coherent encoding techniques, the use of encoding schemes other than Phase-Difference encoding deserves further investigation. It would be particularly useful to find pre-coding and decoding operators that would permit the receiver to use a Viterbi decoder trellis with as few states as that used in the transmitter's convolutional encoder. However deviation from phase-difference encoding is likely to alter the noise statistics in product space.

Appendix A

Tabulated Simulation Results

This appendix provides more detail on the simulation measurements used for the performance graphs in Chapter 4.

	DATE	γ_B	SYMBOL COUNT	E_b/N_0	SYMBOL ERRORS	BIT ERRORS	SYMBOL ERROR RATE	BIT ERROR RATE	σ_S	σ_B
1	Feb 11/89	1.0000	11,000	3.0	8539	12,238	0.7762727	0.3708485	3.97×10^{-3}	2.66×10^{-3}
2			11,000	4.0	8493	12,093	0.7720909	0.3664545	4.00×10^{-3}	2.65×10^{-3}
3			10^4	5.0	7531	10,589	0.7531	0.35296667	4.31×10^{-3}	2.76×10^{-3}
4			10^4	6.0	7,038	9,781	0.7038	0.3260333	4.57×10^{-3}	2.71×10^{-3}
5			10^4	7.0	6,254	8,600	0.6254	0.2866667	4.84×10^{-3}	2.61×10^{-3}
6			10^4	8.0	4,899	6,666	0.4899	0.2222	5.00×10^{-3}	2.40×10^{-3}
7			10^4	9.0	2,997	4,021	0.2997	0.1340333	4.58×10^{-3}	1.97×10^{-3}
8			20,000	10.0	2,404	3,244	0.1202	0.05406667	2.30×10^{-3}	9.23×10^{-4}
9			25,000	11.0	898	1,235	0.03592	0.01646667	1.18×10^{-3}	4.65×10^{-4}
10			36,000	12.0	200	266	0.005555556	0.002462963	3.92×10^{-4}	1.51×10^{-4}
11	↓	↓	2,357,000	13.0	1,351	1,862	0.0005731863	0.0002633291	1.56×10^{-5}	6.10×10^{-6}
12										
13										
14										
15										
16										
17										
18										
19										
20										

17H18M

TRELLIS: DTC-(8,4) (N)

P-N START VALUE: B9725361 16

BRANCH METRIC BITS: 10

PATH METRIC BITS: 32

BRANCH METRIC WEIGHT BITS: 10

DECODING DEPTH: 16

DIFFERENTIAL/COHERENT: DIFF

BITS PER UNCODED SYMBOL: 3

Table A.1: Simulation Data for DTC-(8,4)-16-PSK

	DATE	γ_{R_1}	SYMBOL COUNT	E_b/N_0	SYMBOL ERRORS	BIT ERRORS	SYMBOL ERROR RATE	BIT ERROR RATE	δ_S	δ_B	
1	Feb24/89	1.000	215,000	3.0	166,455	237,798	0.7742093	0.3686791	9.02×10^{-4}	6.01×10^{-4}	
2	Feb24/89	1.000	70,000	4.0	53,602	76,000	0.7657429	0.3619048	1.60×10^{-3}	1.05×10^{-3}	
3	Feb23/89	1.000	20,000	5.0	15,...	21,233	0.7568	0.3538835	3.03×10^{-3}	1.95×10^{-3}	18M
4	Feb24/89	1.000	40,000	6.0	29,225	40,717	0.7306250	0.3393083	2.22×10^{-3}	1.37×10^{-3}	25M
5	Feb24/89	1.000	30,000	7.0	13,391	18,430	0.66955	0.3071667	3.33×10^{-3}	1.88×10^{-3}	14M
6	Feb24/89	1.000	20,000	8.0	11,072	15,083	0.5536	0.2513833	3.51×10^{-3}	1.77×10^{-3}	
7	Feb24/89	1.000	20,000	9.0	7,207	9,734	0.3602	0.1622333	3.39×10^{-3}	1.51×10^{-3}	
8	Feb23/89	1.000	50,000	10.0	7,622	10,287	0.15244	0.06858	1.61×10^{-3}	6.53×10^{-4}	42M
9	Feb24/89	1.000	300,000	11.0	12,464	16,744	0.04154667	0.01860444	3.64×10^{-4}	1.62×10^{-4}	2H 53.
10	Feb23/89	1.000	263,000	12.0	1,873	2,486	0.007121673	0.003150823	1.64×10^{-4}	6.31×10^{-5}	10H
11	Feb28/89	1.000	2,801,000	13.0	3,403	4,297	0.001214923	0.000511365	2.08×10^{-3}	7.80×10^{-6}	
12	Feb26/89	1.000	1,770,000	14.0	1,154	1,353	0.0006519774	0.0002548023	1.92×10^{-5}	693×10^{-6}	
13											
14											
15											
16											
17											
18											
19											
20											

TRELLIS: N-(16,4)

P-N START VALUE: $B972536_{16}$

BRANCH METRIC BITS: 10

PATH METRIC BITS: 30

BRANCH METRIC WEIGHT BITS: 10

DECODING DEPTH: 16

DIFFERENTIAL/COHERENT: DIFF

BITS PSK UNCODED SYMBOL: 3

Table A.2: Simulation Data for DTC-(16,4)-16-PSK

	DATE	r_B	SYMBOL COUNT	E_b/N_0	SYMBOL ERRORS	BIT ERRORS	SYMBOL ERROR RATE	BIT ERROR RATE	δ_S	δ_B	
1	FEB 15/89	1.3000	10^4	3.0	7333	10971	0.7333	0.3490333	4.42×10^{-3}	2.75×10^{-3}	
2	FEB 15/89	1.3000	10^4	4.0	7150	10072	0.7150	0.3357333	4.51×10^{-3}	2.73×10^{-3}	
3	FEB 15/89	1.3000	10^4	5.0	6692	9431	0.6692	0.3143667	4.71×10^{-3}	2.68×10^{-3}	
4	Feb 16/89	1.3000	10^4	6.0	5774	8078	0.5774	0.2692667	4.94×10^{-3}	2.56×10^{-3}	
5	Feb 16/89	1.3000	10^4	7.0	4,329	6,082	0.4329	0.2027333	4.95×10^{-3}	2.32×10^{-3}	
6	FEB 15/89	1.3000	10^4	8.0	2709	3748	0.2709	0.1249333	4.99×10^{-3}	1.91×10^{-3}	
7	Feb 16/89	1.3000	10^4	9.0	1,185	1,632	0.1185	0.0544	3.23×10^{-3}	1.31×10^{-3}	
8	Feb 16/89	1.3000	10^4	10.0	372	529	0.0372	0.01763333	1.94×10^{-3}	7.60×10^{-4}	
9	Feb 16/89	1.3000	60,000	11.0	375	527	0.00625	0.002927778	3.22×10^{-4}	1.27×10^{-4}	38M
10	FEB 15/89	1.3000	$1.05\times10^{+6}$	12.0	971	1389	0.0009247619	0.0004393651	2.97×10^{-5}	1.18×10^{-5}	10H 45M
11	Feb 20/89	1.300	3,383,000	13.0	353	528	0.0001043453	0.0000520283	5.55×10^{-6}	2.26×10^{-6}	30H 37M
12											
13											
14											
15											
16											
17											
18											
19											
20											

TRELLIS: DTC-(8,4) (2N)

P-N START VALUE: $B9725361_{16}$

BRANCH METRIC BITS: 10

PATH METRIC BITS: 32

BRANCH METRIC WEIGHT BITS: 10

DECODING DEPTH: 16

DIFFERENTIAL/COHERENT: DIFF

BITS PER UNCODED SYMBOL: 3

Table A.3: Simulation Data for DTC-(8,4)-8-8-PSK at $r_B = 1.3$

	DATE	r_B	SYMBOL COUNT	E_b/N_0	SYMBOL ERRORS	BIT ERRORS	SYMBOL ERROR RATE	BIT ERROR RATE	σ_S	σ_B
1	Feb10/89	1.638	32,000	3.0	20,802	30,007	0.6500625	0.3125729	2.67×10^{-3}	1.50×10^{-3}
2	Feb10/89	1.638	10^4	4.0	5,704	8,126	0.5704	0.2708667	4.95×10^{-3}	2.57×10^{-3}
3	Feb10/89	1.638	10^4	5.0	4,768	6,766	0.9768	0.2255333	4.99×10^{-3}	2.41×10^{-3}
4	Feb10/89	1.638	10^4	6.0	3,542	1,997	0.3542	0.1665667	4.78×10^{-3}	2.15×10^{-3}
5	Feb10/89	1.638	10^4	7.0	2,208	3,110	0.2208	0.1036667	4.15×10^{-3}	1.76×10^{-3}
6	Feb10/89	1.638	10^4	8.0	1,100	1,568	0.1100	0.05226667	3.13×10^{-3}	1.29×10^{-3}
7	Feb10/89	1.638	10^4	9.0	449	641	0.0449	0.02136667	2.07×10^{-3}	8.35×10^{-3}
8	Feb10/89	1.638	26,000	10.0	248	351	0.0124	0.00585	7.83×10^{-3}	3.11×10^{-4}
9	Feb10/89	1.638	670,000	11.0	2,010	2,869	0.003	0.001429876	6.68×10^{-5}	2.66×10^{-5}
10	Feb10/89	1.638	100,000	11.5	133	195	0.00133	0.00065	1.15×10^{-4}	4.65×10^{-5}
11	Feb10/89	1.638	1,485,000	12.5	427	617	0.0002875421	0.0001384961	1.39×10^{-5}	5.58×10^{-6}
12	Feb17/89	1.638	5,280,000	13.0	618	898	0.0001166496	0.0000568118	4.70×10^{-6}	1.89×10^{-6}
13										
14										
15										
16										
17										
18										
19										
20										

50 2% HIOM

TRELLIS: 2N-(8,4)

P-N START VALUE: B9725361 16

BRANCH METRIC BITS: 10

PATH METRIC BITS: 32

BRANCH METRIC WEIGHT BITS: 10

DECODING DEPTH: 16

DIFFERENTIAL/COHERENT: DIFF

BITS PER UNCODED SYMBOL: 3

Table A.4: Simulation Data for DTC-(8,4)-8-8-PSK at $r_B = 1.6$

	DATE	r_B	SYMBOL COUNT	E_b/N_0	SYMBOL ERRORS	BIT ERRORS	SYMBOL ERROR RATE	BIT ERROR RATE	σ_S	σ_B
1	Feb 16/89	2.000	10^4	3.0	5,764	8,287	0.5764	0.27623333	4.94×10^{-3}	2.58×10^{-3}
2	Feb 16/89	2.000	10^4	4.0	4,901	6,969	0.4901	0.2323	5.00×10^{-3}	2.99×10^{-3}
3	Feb 16/89	2.000	10^4	5.0	3,856	5,430	0.3856	0.181	4.87×10^{-3}	2.22×10^{-3}
4	Feb 16/89	2.000	10^4	6.0	2,691	3,779	0.2691	0.1259667	4.43×10^{-3}	1.92×10^{-3}
5	Feb 16/89	2.000	10^4	7.0	1,696	2,377	0.1696	0.07923333	3.75×10^{-3}	1.56×10^{-3}
6	Feb 16/89	2.000	10^4	8.0	857	1,198	0.0857	0.03993333	2.80×10^{-3}	1.13×10^{-3}
7	Feb 16/89	2.000	10^4	9.0	407	548	0.0407	0.01826667	1.98×10^{-3}	7.73×10^{-4}
8	Feb 16/89	2.000	30,000	10.0	386	533	0.01286667	0.005922222	6.51×10^{-4}	2.56×10^{-4}
9	Feb 16/89	2.000	166,000	11.0	831	1,095	0.005006024	0.002198795	1.73×10^{-4}	6.64×10^{-5}
10	Feb 16/89	2.000	1,400,000	12.0	1907	2,403	0.001362143	0.000591905	3.12×10^{-5}	1.19×10^{-5}
11	Feb 16/89	2.000	4,000,000	13.0	301	387	0.0003015	0.000129	1.73×10^{-5}	6.56×10^{-6}
12										
13										
14										
15										
16										
17										
18										
19										
20										

TRELLIS: 2N-(8,4)

P-N START VALUE: B97253616

BRANCH METRIC BITS: 10

PATH METRIC BITS: 30

BRANCH METRIC WEIGHT BITS: 10

DECODING DEPTH: 16

DIFFERENTIAL/COHERENT: DIFF

BITS PER UNCODED SYMBOL: 3

Table A.5: Simulation Data for DTC-(8,4)-8-8-PSK at $r_B = 2.0$

Bibliography

[1] G. Ungerboeck, "Channel coding with multi-level/phase signals", *IEEE Trans. on Information Theory*, Vol. IT-28, No. 1, pp 55–67, January 1982.

[2] G. Ungerboeck, "Trellis coded modulation with redundant signal sets – Part I: Introduction", *IEEE Communications Magazine*, Vol. 25, No. 2, pp 5–11, February 1987.

[3] G. Ungerboeck, "Trellis coded modulation with redundant signal sets – Part II: State of the art", *IEEE Communications Magazine*, Vol. 25, No. 2, pp 12–21, February 1987.

[4] T. Fugino et al., "A 120Mbit/s 8PSK modem with soft-decision Viterbi decoder", In *Proc. 7th Int'l Conf. on Digital Satellite Communications*, pp 315–321, Munich, May 1986.

[5] R.J. Fang, "A coded 8PSK system for 140Mbits/s information rate transmission over 80-MHz nonlinear transponders", In *Proc. 7th Int'l Conf. on Digital Satellite Communications (ICDSC-7)*, pp 315–321, Munich, May 1986.

[6] M. T. Lyons et al., "16-QAM and trellis coded 16-QAM on non-linear channels", In *IEEE Int'l Conf. on Comm. (ICC-85)*, pp 493–498, 1985.

[7] G. Ungerboeck et al., "Coded 8-PSK experimental modem for the Intelsat SCPC system", In *Proc. 7th Int'l Conf. on Digital Satellite Communications (ICDSC-7)*, pp 315–321, Munich, May 1986.

[8] D. P. Taylor and H. C. Chan, "A simulation study of two bandwidth efficient modulation techniques", *IEEE Trans. on Comm.*, Vol. COM-29, No. 3, pp 267–275, March 1981.

[9] D. Divsalar and M. K. Simon, "Trellis coded modulation for 4800-9600 bits/s transmission over a fading satellite channel", *IEEE Journal on Sel. Areas in Comm.*, Vol. SAC-5, No. 2, pp 162–175, February 1987.

[10] D. Divsalar and M. K. Simon, "Multiple trellis coded modulation (MTCM)", In *Proc. Int'l Conf. on Global Telecommunications (GLOBECOM-86)*, pp 1088–1094, 1986.

[11] D. G. Forney Jr. et al., "Efficient modulation for bandlimited channels", *IEEE Journal on Sel. Areas in Comm.*, Vol. SAC-2, No. 5, pp 632–647, September 1984.

[12] J. Hui and R. J. Fang, "Convolutional code and signal waveform design for bandlimited satellite channels", In *Proc. Int'l Conf. on Communications (ICC-81)*, pp 47.5.1–47.5.10, 1981.

[13] S. G. Wilson et al., "Rate 3/4 convolutional coding of 16-PSK: Code design and performance study", *IEEE Trans. on Comm.*, Vol. COM-33, No. 12, pp 1308–1315, December 1984.

[14] J. G. Proakis, *Digital Communications*, pp 173–178. McGraw-Hill, Toronto, 1983.

[15] D. Makrakis, A. Yongacoglu, and K. Feher. "A sequential decoder for differential detection of trellis coded PSK signals", In *Proc. of the Int'l Conf. on Comm. (ICC-88)*, pp 1433–1438, June 1988.

[16] G. D. Forney Jr., "The Viterbi algorithm", *Proc. of the IEEE*, Vol. 61, No. 3, pp 268–278, March 1973.

[17] E. Zehavi and J. K. Wolfe, "On the performance evaluation of trellis codes", *IEEE Trans. on Info. Theory*, Vol. IT-33, No. 2, pp 196–202, March 1987.

[18] A. M. Michelson and A. H. Levesque, *Error Correction Coding*, Chapter 9, pp 229–336, John Wiley and Sons, 1985.

[19] A. Chalid et al., "Coded non-uniform phase/frequency modulation", In *Proc. Int'l Conf. on Comm. (ICC-88)*, pp 707–711, June 1988.

[20] A. Chouly and H. Sari, "Application of trellis coding to digital radio", In *Proc. Int'l Conf. on Comm.(ICC-88)*, pp 468–472, June 1988.

[21] D. Divsalar and M. K. Simon, "The design of trellis coded MPSK for fading channels: Performance criteria", *IEEE Trans. on Comm.*, Vol. COM-36, No. 9, pp 1004–1012, September 1988.

[22] D. Divsalar and M. K. Simon, "The design of trellis coded MPSK for fading channels: Set partitioning for optimum code design", *IEEE Trans. on Comm.*, Vol. COM-36, No. 9, pp 1013–1021, September 1988.

[23] C. L. B. Despins, *Trellis Coded Modulation Performance Evaluation over Faded Channels; Review and Analysis of Recent Results*, Technical Report 87-03, OCIEE, December 1987.

[24] A. Lee and P. J. McLane, *Convolutionally Interleaved PSK and DPSK for Fast Fading, Shadowed Mobile Satellite Communication Channels*, Technical Report , Queen's University, Kingston, 1988.

[25] P. J. McLane, P. H. Wittke, and C. Loo, *PSK and DPSK Trellis Codes for Fast Fading, Shadowed Mobile Satellite Communication Channels*, Technical Report, Queen's University, Kingston, 1988.

[26] J. P. Driscoll and N. Karia, "Detection processes for V32 modems using trellis coding", *IEE Proc.*, 135 Pt. F(2), pp 143–154, April 1988.

[27] G. J. Foschini et al., "Optimization of two-dimensional signal constellations in the presence of Gaussian noise", *IEEE Trans. on Comm.*, Vol. COM-22, No. 1, pp 28–38, January 1974.

[28] E. Biglieri, "High level modulation and coding for non-linear satellite channels", *IEEE Trans. on Comm.*, Vol. COM-32, No. 5, pp 616–626, May 1984.

[29] C. T. Melvil et al., "Digital amplitude-phase keying with M-ary alphabets", *IEEE Trans. on Comm.*, Vol. COM-22, No. 2, pp 168–179, February 1974.

[30] R. Padovani and J. K. Wolfe, "Coded phase/frequency modulation", *IEEE Trans. on Comm.*, Vol. COM-34, No. 5, pp 446–453, May 1986.

[31] D. Divsalar, M. K. Simon, and J H. Yuen, "Trellis coding with asymmetric modulations", *IEEE Trans. on Comm.*, Vol. COM-35, No. 2, pp 130–141, February 1987.

[32] R. W. Lucky, J. Saltz, and E. J. Weldon Jr., *Principles of Data Communication*, Chapter 9, pp 246–276, McGraw-Hill, 1968.

[33] J. H. Park Jr., "On binary DPSK detection", *IEEE Trans. on Comm.*, Vol. COM-36, No. 4, pp 484–486, April 1978.

[34] A. Grami, D. Makrakis, and S. Pasupathy, "Detection using a noise estimation-cancellation technique", *IEEE Trans. on Comm.*, Vol. COM-35, No. 8, pp 786–794, August 1987.

[35] M. K. Simon and D. Divsalar, "Doppler-corrected differential detection of MPSK", *IEEE Trans. on Comm.*, Vol. COM-37, No. 2, pp 99–109, February 1989.

[36] D. D. Falconer, P. Mohanraj, V. Joshi, and T. A. Kwasniewski, "Reduced complexity trellis coding/decoding for high bit rate digital subscriber loop transmission", In *Int'l Conf. on Comm. (ICC-89)*, pp 17.2.1–17.2.5, June 1989.

[37] V. Joshi and D. D. Falconer, "Reduced state sequence estimation techniques for digital subscriber loop application", In *Proc. Int'l Conf. on Global Comm. (GLOBECOM-88)*, pp 799–803, November 1988.

[38] CCITT, "Recommendation V.32: A Family of 2-wire, duplex modems operating at data signalling rates of up to 9600 bit/s for use on the general switched telephone network and on leased telephone-type circuits", In *CCITT Red Book*, Fascicile VIII.1, pp 221-238, Malaga-Torremolinos 1984.

[39] CCITT, "Draft Recommendation V.33: 14400 Bit per second modem standardized for use on point-to-point 4-wire leased telephone-type circuits", In *CCITT COM XVII-R 1-E Annex 1*, pp 38-57.

[40] G. C. Clark Jr. and J. B. Cain, *Error-Correction Coding for Digital Communications*, Chapter 6, pp 227–266, Plenum Press, New York, 1981.

[41] J. L. Massey, "Coding and Modulation in Digital Communications", *Proc. 1974 Int'l Zurich Seminar on Digital Comm.*, pp E2(1)–(4), Zurich, Switzerland, March 1974.

[42] P. Galko and S. Pasupathy, "Performance Evaluation of Generalized MSK", In *Proc. of the Int'l Conf. on Global Comm. (GLOBECOM-82)*, pp 344-348, Miami, December 1982.

[43] G. Ungerboeck and C. Csajka, "On improving data-link performance by increasing the channel alphabet and introducing sequence coding", In *1976 Int'l Symp. Info. Theory*, Ronneby, Sweden, June 1976.

[44] R. G. McKay, M. Shafi, and C. J. Carlisle, "Trellis-coded Modulation on Digital Microwave Radio Systems – Simulations for Multipath Fading Channels", In *Proc. Int'l Conf. on Global Comm. (GLOBECOM-88)*, pp 239–243, November 1988.

[45] W. C. Lindsey and M. K. Simon, *Telecommunication Systems Engineering*, pp 250–251, Prentice-Hall, 1973.